UNIVERSIDAD DE CÓRDOBA

DEPARTAMENTO DE AGRONOMÍA

Programa de Doctorado

Dinámica de flujos biogeoquímicos y su aplicación

TESIS DOCTORAL

Development of sediment tracers to study soil redistribution and sediment dynamic due to water erosion

Desarrollo de trazadores de suelo para el estudio del arrastre y redistribución de sedimentos debidos a la erosión hídrica

Autor

María Gema Guzmán Díaz

Dirigida por

Dr. Juan Vicente Giráldez Cervera

Dr. José Alfonso Gómez Calero

Córdoba, Noviembre 2011

TÍTULO: *Development of sediment tracers to study soil redistribution and sediment dynamic due to water erosion*

AUTOR: *María Gema Guzmán Díaz*

Campus de Rabanales
Ctra. Nacional IV, Km. 396 A
14071 Córdoba

www.uco.es/publicaciones
publicaciones@uco.es

UNIVERSIDAD DE CÓRDOBA

DEPARTAMENTO DE AGRONOMÍA

Programa de Doctorado

Dinámica de flujos biogeoquímicos y su aplicación

TESIS DOCTORAL

Development of sediment tracers to study soil redistribution and sediment dynamic due to water erosion

Desarrollo de trazadores de suelo para el estudio del arrastre y redistribución de sedimentos debidos a la erosión hídrica

Tesis doctoral presentada por María Gema Guzmán Díaz, en satisfacción de los requisitos necesarios para optar al grado de Doctor Ingeniero Agrónomo con mención europea, dirigida por los Drs. D. Juan Vicente Giráldez Cervera, de la Universidad de Córdoba y D. José Alfonso Gómez Calero, del Instituto de Agricultura Sostenible-CSIC.

Los Directores: El Doctorando

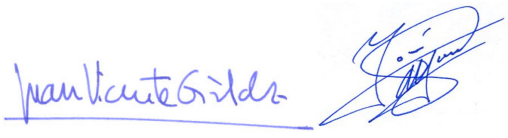

J. V Giráldez Cervera J.A. Gómez Calero Mª Gema Guzmán Díaz

Córdoba, Noviembre 2011

TÍTULO DE LA TESIS: Desarrollo de trazadores de suelo para el estudio del arrastre y redistribución de sedimentos debidos a la erosión hídrica

DOCTORANDO/A: María Gema Guzmán Díaz

INFORME RAZONADO DEL/DE LOS DIRECTOR/ES DE LA TESIS

Juan Vicente Giráldez Cervera y José Alfonso Gómez Calero, codirectores de la tesis informan que la doctoranda ha desarrollado los objetivos previstos compartiendo su formación con la investigación, completándola con estancias en cuatro centros, la Universidad de Lancaster, Inglaterra, (de Octubre a Diciembre de 2008),el Centro del ARS de Tucson, Estados Unidos de América, (de Septiembre a Noviembre de 2009), el CIEMAT (de Marzo a Junio 2010), y el BAW-IKT, Austria (de Septiembre a Diciembre de 2010). La tesis se presenta separada en capítulos, los cuales se encuentran en fase de envío o ya publicados.

Por todo ello, se autoriza la presentación de la tesis doctoral.

Córdoba, 21 de Noviembre de 2011

Firma de los directores

Fdo.: Juan Vicente Giráldez Cervera

Fdo.: José Alfonso Gómez Calero

Table of contents

List of figures

List of tables

Resumen

La erosión hídrica es motivo de preocupación para la sostenibilidad de los sistemas agrícolas en el mundo y especialmente en la cuenca del Mediterráneo. Las limitaciones de los métodos tradicionales de medida de la erosión, han impulsado el uso de trazadores ambientales para proporcionar información adicional y así implementar estrategias de conservación a diferentes escalas. Hay diferentes enfoques para la selección del trazador con respecto a sus propiedades, métodos de aplicación y su detección.

Debido a la dificultad para encontrar trazadores que reúnan todos los requisitos definidos por Zhang *et al*. (2001) y que proporcionen una evaluación fiable de la dinámica de la erosión y los sedimentos, nuevos trazadores aparecen cada año. El objetivo principal de esta tesis es el desarrollo de un trazador simple y barato para su uso en ensayos de erosión hídrica a escala de laboratorio y campo. En una primera etapa, se consideraron dos tipos de trazadores, óxidos de tierras raras (La_2O_3, Pr_6O_{11}, Nd_2O_3 and Sm_2O_3) y óxidos de hierro (magnetita Fe_3O_4, hematites α-Fe_2O_3 y goethita FeOOH). En una etapa posterior de los óxidos de tierras raras se descartaron debido a la complejidad e incertidumbres que intervienen en su determinación analítica, además del alto coste de su adquisición y análisis

En el Capítulo 1 se examinan los métodos de trazado existentes, adoptados en experimentos de erosión, distinguiendo entre ellos los radionúclidos, tierras raras, 'fingerprinting', y los óxidos magnéticos. Además, se describen y comparan los diferentes métodos, discutiendo las ventajas y desventajas de cada uno de ellos.

El Capítulo 2 describe los ensayos de laboratorio y las simulaciones de lluvia diseñados para comprender el comportamiento y el potencial de magnetita como un trazador de sedimento en cuatro suelos mediterráneos de distinta clase textural.

Los dos capítulos siguientes están dedicados a la exploración de los óxidos de hierro como trazadores erosión bajo lluvia simulada y natural para entender el movimiento del suelo debido a la erosión hídrica.

El Capítulo 3, analiza la dinámica de la erosión en un sistema de surcos-lomos cultivado con algodón, en simulaciones de lluvia a pequeña escala utilizando magnetita y a escala de ladera combinando magnetita, hematita y goethita durante una prueba de riego por aspersión. Se utilizó también un modelo de erosión para entender y extrapolar la dinámica de la erosión hídrica en los sistemas agrícolas bajo diferentes escenarios. En el Capítulo 4 el procedimiento del marcado del suelo con óxido de hierro magnético, fue puesto a punto en unas parcelas de olivar, combinando medidas de susceptibilidad magnética en laboratorio y campo. La variación del contenido de magnetita se utilizó para estimar la contribución, de cada zona dentro de las parcelas, a las pérdidas totales de suelo causadas por las precipitaciones naturales y la redistribución del suelo después del labrado.

Finalmente, el Capítulo 5 es un debate general sobre el trabajo, incluyendo en él las conclusiones más relevantes. Aunque el uso de óxido de hierro magnético implica algunas limitaciones, tales como la dificultad de conseguir un marcado uniforme del perfil del suelo, es posible cuantificar la contribución de las diferentes fuentes o áreas de deposición de sedimentos bajo diferentes manejos de suelo y cultivos. Por lo tanto, los trazadores basados en óxidos de hierro constituyen una herramienta útil y complementaria a las medidas tradicionales de pérdidas de suelo en los procesos de erosión.

Referencias

Zhang, X.C., Friedrich, J.M., Nearing, M.A., Norton, L.D. 2001. Potential use of rare earth oxides as tracers for soil erosion and aggregation studies. Sci. Soc. Am. J. 65: 1508–1515.

Summary

Water erosion is a matter of concern for the sustainability of agricultural systems in the world, and especially in the Mediterranean basin. The limitations of the traditional erosion measurement methods have prompted the use of environmental tracers to provide additional information for implementing conservation strategies at different scales. There are different approaches to the tracer selection with respect to their properties, methods of application and their detection.

Given the difficulties found in the use of tracers to fulfil all the requirements for a reliable assessment of the erosion and sediment dynamics defined by Zhang *et al*. (2001), new tracers are appearing every year. The main objective of this dissertation is the development of a simple and cheap tracer for its use in field and laboratory water erosion experiments. In a preliminary stage, two sets of tracers were considered; rare earth oxides (La_2O_3, Pr_6O_{11}, Nd_2O_3 and Sm_2O_3) and iron oxides (magnetite Fe_3O_4, hematite α-Fe_2O_3 and goethite FeOOH). In a subsequent stage, the rare earth oxides were discarded due to the complexity and uncertainties involved in their analytical determination, in addition to their high acquisition and analysis costs.

Chapter 1 reviews the existing tracer methods adopted in erosion experiments, distinguishing between them radionuclides, rare earths, fingerprinting, and magnetic oxides. The methods are also described and compared and their advantages and disadvantages are discussed.

Chapter 2 describes the laboratory tests designed and rainfall simulation experiments to understand the behaviour and potential of magnetite as a sediment tracer in four Mediterranean soils of a varied textural class.

The next two Chapters are devoted to the exploration of iron oxides as erosion tracers. They were used at hillslope scale under simulated and natural rainfall to understand soil movement by water erosion.

Chapter 3, analyses the erosion dynamics in a cotton crop plot planted in a furrow-bed system under rainfall simulations at a small scale using magnetite, and at a hillslope scale by the combination of magnetite, hematite and goethite during a sprinkler irrigation test. An erosion model was also used to understand and extrapolate the dynamics of water erosion in agricultural systems under different scenarios. In Chapter 4 the sediment tracking procedure using magnetic iron oxide was set up in olive orchard plots combining laboratory and field magnetic susceptibility measurements. The variation in magnetite content was used to estimate the contribution of each area within the plots to total soil losses caused by natural rainfall events and the soil redistribution after tillage.

Finally, Chapter 5 is a general discussion on the work including the most relevant conclusions in it. Although the use of magnetic iron oxides implies some limitations such as, the difficulty of obtaining a uniform tagging of soil profile, it is possible to quantify the contribution of the different sources or deposition areas of sediment under different soil managements and crops. Therefore, the tracers based on iron oxides constitute a useful tool, which is complementary to traditional soil loss measurements of erosion processes.

References

Zhang, X.C., Friedrich, J.M., Nearing, M.A., Norton, L.D. 2001. Potential use of rare earth oxides as tracers for soil erosion and aggregation studies. Sci. Soc. Am. J. 65: 1508–1515.

General introduction

Water erosion is a major environmental concern of agricultural systems in Spain, especially in the southern and south-eastern regions, due to a combination of crops on steep slopes, the Mediterranean climate and an inadequate soil management. In this context, the study of erosion processes is fundamental to the sustainability of agriculture, but sometimes it is limited by its cost and the problems inherent in each of the traditional techniques employed. This situation is general to erosion studies elsewhere in the world and there is an increasing interest in the development of new sediment tracers to identify and quantify, eroded/deposit areas and sediment movement in order to replace or supplement the information obtained using traditional techniques.

An alternative to these traditional methods is the use of sediment tracers to replace or supplement the information obtained with these techniques. Sediment tracers are substances or soil properties man-incorporated or present in the soil naturally, without interfering with soil movement, and thus allowing its monitoring to identify and/or quantify soil redistribution along an eroded area. The diversity of approaches to the design of sediment erosion studies is a sign that none of them have fulfilled all the requirements for being an ideal sediment tracer (defined by Zhang *et al*. 2001). This suggests the need for further study of this type of tracer substances.

There are few studies that evaluate the use of magnetic susceptibility in water erosion studies. At a laboratory scale, Armstrong *et al*. (2010, 2011) studied the effect of improving the natural magnetic susceptibility of a soil by heating control. At a larger scale, there are few studies that have demonstrated the potential use of magnetic susceptibility inherent to different soil materials in studies of erosion in large basins (Hatfield and Maher, 2008) but it requires differentiation between soil types and its use presents limitations at small-scale basins or slopes. However, there is the possibility of using substances with a high magnetic susceptibility that tag soil aggregates and allow the monitoring of soil movement.

At a laboratory scale, Hu *et al*. (2011) evaluated five different combinations of fine soil, magnetic powder and fly ash with cement or bentonite in rainfall simulation tests. At a plot scale, Parsons *et al*. (1993) applied crushed magnetite to study inter-rill sediment transport, while Ventura *et al*. (2001, 2002) developed magnetic plastic beads that presented serious problems of selectivity in the transport.

There is, in summary, a promising approach based on magnetic tracers for estimating soil losses due to rainfall events, and evaluating them in Mediterranean areas at different scales and soil managements. Therefore, the main objectives of this Thesis were:

Objectives

There is, in summary, a promising approach based on magnetic tracers for estimating soil losses due to rainfall events, and evaluating them in Mediterranean areas at different scales and soil managements. Therefore, the main objectives of this Thesis were:

(i) *To characterize different iron oxides, develop the tagging technique and evaluate their distribution in the tagged soil.*

(ii) *To study the behavior of iron oxides in water erosion studies at laboratory scale.*

(iii) *To develop a methodology for the analysis and quantification of the different iron oxides depending on their properties and the conditions of the study.*

(iv) *To address the potential of the iron oxides in two experiments of water erosion in agricultural areas under different soil managements at a hillslope scale: annual crop sown on a beds-furrow system and an olive tree orchard.*

References

Alves, T., Gómez-Macpherson, H., Gómez, J.A. 2008. A portable integrated rainfall and overland flow simulator. Soil Use Manage. 24: 163–170.

Armstrong, A., Quinton, J., Maher, B. 2011. Tracing sediment by enhancing soil magnetic properties. Geophysical Research Abstracts Vol. 13, EGU2011-9135.

Armstrong, A., Maher, B., Quinton, J. 2010. Enhancing the magnetism of soil: the answer to soil tracing? Geophysical Research Abstracts Vol. 12, EGU2010–2805, EGU General Assembly 2010.

Hatfield, R.G., Maher, B. 2008. Suspended sediment characterization and tracing using a magnetic fingerprinting technique: Bassenthwaite Lake, Cumbria, UK. Holocene. 18: 105–115.

Hu, G.Q., Dong, Y.J., Wang, H., Qiu, X.K., Wang, Y.H. 2011. Laboratory testing of magnetic tracers for soil erosion measurement. Pedosphere 21: 328–338.

Parsons, A.J., Wainwright, J., Abrahams, A.D. 1993. Tracing sediment movement in interrill overland flow on a semi-arid grassland hillslope using magnetic susceptibility. Earth Surf. Process. Landforms 18: 721–732.

Ventura, E., Nearing, M.A., Amore, E., Norton, L.D. 2002. The study of detachment and deposition on a hillslope using a magnetic tracer. Catena 48: 149–161.

Ventura, E., Nearing, M.A., Norton, L.D. 2001. Developing a magnetic tracer to study soil erosion. Catena 43: .277–291.

Zhang, X.C., Friedrich, J.M., Nearing, M.A., Norton, L.D. 2001. Potential use of rare earth oxides as tracers for soil erosion and aggregation studies. Sci. Soc. Am. J. 65: 1508–1515.

Chapter 1. Sediment tracers in water erosion studies

Abstract

Interest in the use of sediment tracers as a complementary tool to traditional water erosion or deposition measurements or assessment has increased due to the additional information they may provide such as sediment source identification and tracking of sediment movement over the landscape at various time scales. The potentials of sediment tracing techniques utilizing a wide range of materials, substances and soil properties have been evaluated through numerous investigations but it is difficult to find studies comparing them in a general way. This Chapter compares the origins, applicability and uses of recently developed tracing approaches. Five different groups of sediment tracers are distinguished (Radionuclides, Rare earths, Fingerprinting, Magnetism and Others). This Chapter presents a description of the commonalities and differences between the tracing techniques, an identification of their strengths and weaknesses and an examination of their potential for assessing soil erosion and soil redistribution. Research gaps and future trends are discussed.

Keywords: erosion, tracers, sediment, rare earth, radionuclides, fingerprinting, magnetic

In preparation as: Guzmán, G., Gómez, J.A., Quinton, J.N., Nearing, M.A., Mabit, L. Sediment tracers in water erosion studies: Current approaches and challenges.

1.1 Introduction

The transfer mobilization and transfer of sediment is a key area or research as scientists try to understand the mobilization of carbon and macronutrients in catchments and the sources of sediment reaching river systems. (Smith *et al*. 2001; Walling, 2005). Scientists have employed a range of methods to study these processes ranging from the collection of sediment on hillslopes, the mapping of soil erosion features and the sampling of river sediments. However, these techniques find it hard to link sediment sources to sinks.

Sediment tracing and fingerprinting are techniques which offer a potential solution to this problem They can both be considered as *substances or set of properties*, used: *(i) to determine sediment sources at a given point in the landscape, (ii) to track sediment movement along the landscape,* and/or *(iii) to determine rates of sediment movement*. Tracer approaches have been utilized in an extremely diverse set of studies across many disciplines of earth science. In studying littoral transport Duane and James (1980) used a sand tracer on the coast of California. In a hydrologic study Mahler *et al*. (1998) used clay tagged with a lanthanide tracer to determine sediment transport in karst formations. In geomorphology Martz and de Jong (1991) developed a sediment budget for a Canadian catchment using ^{137}Cs. In the study of sediment movement within a semiarid catchment in Arizona, Polyakov *et al*. (2009) used soil tagged with rare earth oxide. In a soil science study, Walling *et al*. (1999) looked at short and medium erosion rates in an agricultural land in Devon, UK by combining ^{7}Be and ^{137}Cs measurements Schoonover *et al*. (2007) used soil iron properties and forms to determine sediment sources in sixteen US catchments during a two year period In limnology Dearing *et al*. (2001) reconstructed sediment-sources linkages for the last 6000 years at Petit Lac d'Annecy in France using mineral magnetic data. In an agro-environmental investigation Arnscheidt *et al*. (2007) determined phosphorus diffuse pollution in three complex Irish catchments using a combination of physical, chemical and biological properties.

There have been a large number of sediment tracer studies using different tracers applied in a broad variety of conditions with different objectives. One of the reasons for the number of tracing techniques is that no single tracer fulfils all the requirements of an ideal tracer for erosion and sediment dynamics.

According to Zhang *et al*. (2001) the ideal tracer would have the following characteristics: *1- strong binding to soil particles or ready incorporation into soil aggregates; 2- high analytical sensitivity; 3- easy and inexpensive to quantify; 4- low background soil concentration; 5- no interference with sediment transport; 6- low plant uptake, 7- environmentally benign; 8- available in variants with similar, but distinguishable, physicochemical properties for multiple tracking*.

These demands have lead to increased specialization in the use of different tracer techniques and no comprehensive literature study has been published comparing data demonstrating the advantages and disadvantages of different tracer technologies in the same experiment. To date most studies have compared the estimations of erosion and sedimentation rates obtained from tracer analysis with model predictions (e.g. Busacca *et al*. 1993) or conventional measurements (e.g. Mabit *et al*. 2009). As a consequence the advantages and disadvantages of different tracing approaches are difficult to evaluate based on published results. There has also been a degree of compartmentalization in tracing research, with little exchange between scientists working with different tracing techniques.

The aim of this Chapter is to address some of these shortcomings by presenting a concise review of the different sediment tracers used in water erosion studies, with these three specific objectives: *(i) describe the current trends in tracer use in water erosion studies, with an indication of the scales used and the relative significance of the different approaches; (ii) describe the main steps in the development and application of the most utilized tracer techniques;* and *(iii) discuss the key advantages of the different approaches to suggest improvement in their use in the future.*

1.2. Use of the different tracing techniques

The bubble graph in Figure 1.1 presents the results of a search of the Web of Science database (*http://wokinfo.com/webtools/searchbox/*)using the following search terms in the title or as keywords: “erosion AND tracer” OR “sediment AND tracer” OR “sediment AND tracking”.

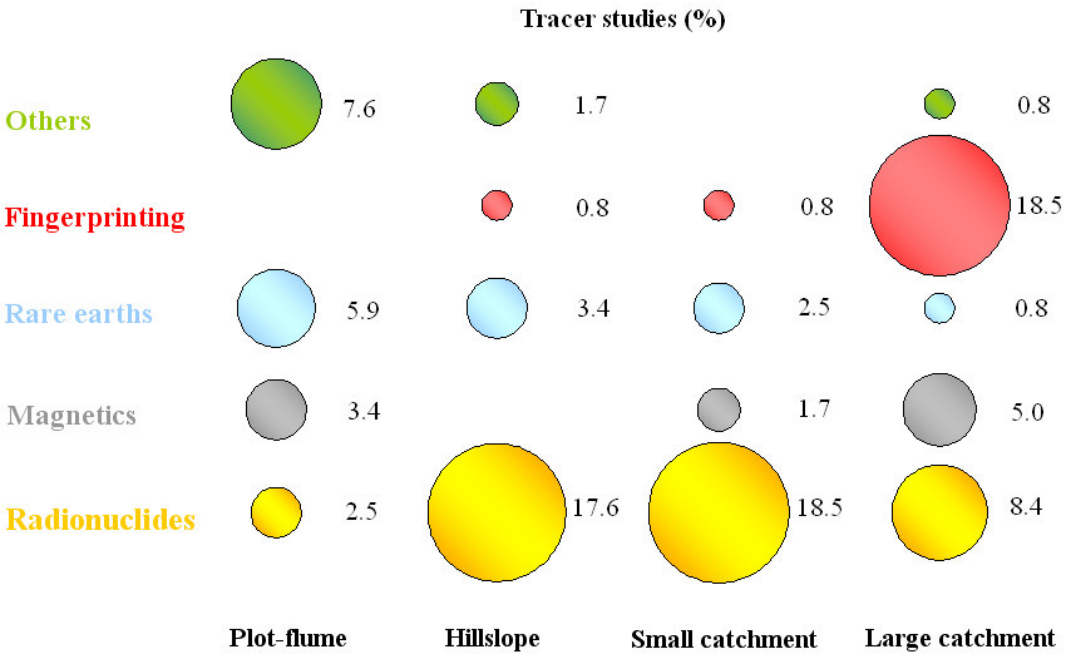

Figure 1.1. Bubble plot indicating the distribution of erosion studies with tracers found in the review by scale and kind of tracer.

The search was refined by manually checking that the articles corresponded to experiments involving sediment studies using tracers as defined in this review. To the Web of Science list a relevant articles or conferences papers were included. A total of 119 studies were found on June 2011 and classified by tracer type and scale investigated. Only studies that used tracers to make a determination of erosion or sedimentation rates were included in Figure 1.1. Review papers where not included in the analysis. The threshold between small catchment and large basin was set at 100 ha. Table 1.1 includes all the references consulted to establish Figure 1.1.

Tracer type	References
Radionuclides	* Dai *et al*. (2011), Porto *et al*. (2011), Li *et al*. (2010), Zhang and Walling (2005), Walling *et al*. (2000), Benninger *et al*. (1998), Kronvang *et al*. (1997), Olley *et al*. (1993), de Roo (1991), Martz and de Jong (1987) † Estrany *et al*. (2010), Mabit *et al*. (2009), Chiu *et al*. (2008), Mizugaki *et al*. (2008), Wilson *et al*. (2008), Yin and Li (2008), Ming-Yi *et al*. (2006), Bacchi *et al*. (2000), Lu and Higgitt (2000), di Stefano *et al*. (1999), Walling and He (1999b), Walling *et al*. (1999), Montgomery *et al*. (1997), Busacca *et al*. (1993), Martz and de Jong (1991), Loughran *et al*. (1988), Lance *et al*. (1986), Spomer *et al*. (1985), Brown *et al*. (1981) √ Belyaev *et al*. (2010), Fifield *et al*. (2010), Li *et al*. (2009), Walling *et al*. (2009), Mabit *et al*. (2008b), Olson *et al*. (2008), Hassouni and Bouhlassa (2006), Wallbrink *et al*. (2002), Higgitt *et al*. (2000), Schuller *et al*. (2000), Quine *et al*. (1999a), Wallbrink *et al*. (1999), Walling *et al*. (1999), Bajracharya *et al*. (1998), Zhang *et al*. (1998), Cuesta and Delgado (1997), Sutherland (1992), Xingbao *et al*. (1990), Kachanoski (1988), Kachanoski and de Jong (1984) ♣ Quine *et al*. (1999b), Syversen *et al*. (2001), Wallbrink and Murray (1993), Bernard *et al*. (1992), Woolridge (1965)
Rare earths	* Mahler *et al*. (1998) † Polyakov *et al*. (2009), Kimoto *et al*. (2006a), Polyakov *et al*. (2004) √ Deasy and Quinton (2010), Stevens and Quinton (2008), Wude *et al*. (2008), Yang *et al*. (2008), Matisoff *et al*. (2001) ♣ Michaelides *et al*. (2010), Kimoto *et al*. (2006b), Li *et al*. (2006), Polyakov and Nearing (2004), Pu-Ling *et al*. (2004), Xue *et al*. (2004), Wei *et al*. (2003), Zhang *et al*. (2003)
Fingerprinting	* Kouhpeima *et al*. (2011), Nosrati *et al*. (2011), Devereux *et al*. (2010), de Junet *et al*. (2009), Juracek and Ziegler (2009), Poulenard *et al*. (2009), Fox and Papanicolau (2008a,b), Minella *et al*. (2008), Rhoton *et al*. (2008), Rustomji *et al*. (2008), Schoonover *et al*. (2007), Walling *et al*. (2007), Cunha *et al*. (2006), Miller *et al*. (2005), Motha *et al*. (2003), Collins and Walling (2002), Russel *et al*. (2001), Rowan *et al*. (2000), Collins *et al*. (1998), Barcellos *et al*. (1997), Martinotti *et al*. (1997), Sawhney and Frink (1978) † Fox and Papanicolau (2007) √ Bellangera *et al*. (2004) ♣
Magnetism	* Maher *et al*. (2009), Dearing *et al*. (2001), Slattery *et al*. (2000), Yu and Oldfield (1993), Caitcheon (1993), Walling *et al*. (1979) † Royall (2001), Hardy *et al*. (2000) √ ♣ Armstrong *et al*. (2010), Guzmán *et al*. (2010), Ventura *et al*. (2002, 2001), Parsons *et al*. (1993)
Others	* Martinez -Carreras *et al*. (2010) † √ Schwertmann and Schmidt (1978) ♣ Spencer *et al*. (2011), Yu *et al*. (2011), Bennett *et al*. (2010), Mentler *et al*. (2009), Sharma *et al*. (2009), Olmez and Pink (1994), Plante *et al*. (1999), Wheatcroft *et al*. (1994), Young and Holt (1968), Riebe (1995)

Table 1.1. References of the erosion studies with tracers summarized in Figure 1.1 by scale and kind of tracer. *Indicates studies made at large catchments (>100ha), †indicates studies made at small catchments (<100ha), √indicates studies made at hillslope scale and ♣means studies made at small plot or laboratory scale.

Nuclear techniques, and especially radionuclides, were the most frequently employed tracers representing approximately 47 % of all the studies included in Table 1.1 and Figure 1.1. The majority of these studies used the concentration of ^{137}Cs in soil as a tracer. This tracer is an anthropogenic radioisotope dispersed into the atmosphere as a result of thermonuclear bomb testing. Since the 1950s ^{137}Cs global fallout has been used to determine erosion and sedimentation rates for medium timescales (tens of years), across a broad range of scales from hillslope (e.g. Wallbrink and Murray, 1993), small catchment (e.g. Higgitt *et al.* 2000) to large basins (e.g. de Roo, 1991). By combining field measurements with model analysis ^{137}Cs has also been used to determine rates of both water and tillage erosion (e.g. Quine *et al.* 1999a). Two other radionuclides have been tested and validated to quantify erosion and sedimentation rates at short and long timescales: *(i) ^{7}Be, a natural cosmogenic radionuclide used to estimate short term erosion rates (e.g. Walling et al. 1999)* and *(ii) ^{210}Pb, a natural geogenic radionuclide utilised to provide longer term estimations (approx. 100 years) of erosion and sedimentation rates (e.g. Walling and He, 1999b).* In addition to these three main radionuclides already present into the soil, other radioactive tracers such as ^{134}Cs (see Syversen *et al.* 2001) and ^{59}Fe (see Woolridge, 1965) have also been used for small scale and local investigation. These were incorporated into the soil prior to the experiment to provide short-term estimations of the magnitude of soil redistribution.

The second largest group of tracer studies in Figure 1.1 is grouped under the generic name Fingerprinting. They do not use a single tracer, but rather the differences in a variable number of soil properties (physical, chemical or biological) in the sediment originating from different areas of the landscape to determine the source origin of this sediment. The study of Rhoton *et al.* (2008) discriminated sediment sources of a 150 km^2 into six different sub-catchments using nine physical properties, fifteen chemical properties, stable carbon isotope (δ^{13}C) and radionuclides (^{137}Cs, ^{40}K, ^{226}Ra) measured in soil samples and sediment. The relative contribution of each sub-catchment was calculated using a multivariate mixing model and linear optimization procedures. Most of these studies have been developed at the large basin scale where differences in soil properties are easier to establish. Few are the studies that use this approach at smaller scales such as, hillslope (30 m^2) (Fox and Papanicolau, 2007) or small catchment (0.71 km^2) (Bellangera *et al.* 2004), who both used the ratio of δ^{13}C and δ^{15}N isotopes as discriminating properties.

Rare earth elements represent approximately 13 % of tracer studies found (Figure 1.1). This technique relies on rare earth elements being incorporated into the soil prior to the experiment, and the determination of the concentration in the soil and sediment after a period from weeks (e.g. Zhang *et al.* 2003) to up to four years (Kimoto *et al.* 2006a). There are several experiments at laboratory scale using earth elements as tracers at laboratory flume scale to study rill erosion (e.g. Lei *et al.* (2006)) or at plot scale (Tian *et al.* (1994)), to study soil erosion and its trend depending on different topographical positions under simulated rainfall. It is also possible to find some studies at hillslope scale (Deasy and Quinton, 2010) or small catchment scale (Polyakov *et al.* 2009). Only Mahler *et al.* (1998) reports using rare earth element at large scales in a study of sediment transport in a karst area in which a lanthanide-labelled clay was deployed.

Magnetic tracer studies also feature in Figure 1.1. They refer to approaches using magnetic properties in a different way. One discriminates sediment sources through the existing magnetic properties of soil constituents (e.g. Dearing *et al.* 2001). In many cases, this approach is similar to the fingerprinting studies mentioned above and also uses un-mixing models (e.g. Maher *et al.* 2009). A different approach is the use of magnetic tracing substances incorporated into the soils, whose concentration and distribution in soil and sediment can be measured before and after the experiment. Examples at small plot or laboratory scale include Ventura *et al.* (2002) who used magnetic beads and Guzmán *et al.* (2010) who deployed magnetic iron oxides.

A final set of erosion tracer studies in Figure 1.1 are those identified as “Others”. These tracers are mostly preliminary studies using alternative approaches to those previously mentioned or techniques found only in a few instances in the review, such as from Cu in soils (Schwertmann and Schmidt, 1978) and DNA microspheres (Sharma *et al.* 2009). These approaches are in their infancy and therefore have been employed mostly at hillslope or small scale.

1.3. Radionuclides

The most extensively soil redistribution tracers used worldwide are fallout radionuclides (FRN), such as ^{210}Pb ($t_{1/2}$=22.26 years), ^{7}Be ($t_{1/2}$=53.12 days), and ^{137}Cs ($t_{1/2}$=30.17 years) (Walling, 2003). All these radionuclides have a strong affinity to finer soil fractions and are mostly mobilized and transported by physical processes such as water, tillage and wind erosion. ^{137}Cs was produced during the atmospheric testing of thermonuclear weapons from the mid 1950s to the 1960s. It was released into the stratosphere and globally distributed. Global fallout of ^{137}Cs began in 1954, peaked into the 1960s after moratoriums on testing and the Test Ban Treaty signed in 1963, and decreased to almost zero by the 1980s. Locally, additional ^{137}Cs was released by the Chernobyl nuclear power plant accident in 1986 adding a second spike. ^{7}Be is a naturally occurring cosmogenic radionuclide produced in the stratosphere and troposphere as a result of nitrogen and oxygen spallation and is subsequently deposited as fallout.^{210}Pb is a naturally occurring product of the ^{238}U decay series that is derived from the decay of gaseous ^{222}Rn, the daughter of ^{226}Ra. ^{226}Ra exists naturally in soils and rocks; there is ^{210}Pb in soils generated in situ by the decay of ^{226}Ra. This is called supported ^{210}Pb and is in equilibrium with the amount of ^{226}Ra in soils. The ^{210}Pb used as soil erosion tracer is called unsupported ^{210}Pb ($^{210}Pb_{ex}$), which reaches the soil as fallout as a result of diffusion of small amounts of ^{222}Rn to the atmosphere.

The use of these three environmental radionuclides is based on their inventory in the soil. This inventory is periodically replenished in the case of ^{7}Be and $^{210}Pb_{ex}$ and in the case of the ^{137}Cs fallout decreasing according to its radioactive decay.

Other radionuclides that have been used as erosion tracers include ^{59}Fe ($t_{1/2}$=44.51 days) (e.g. Woolridge, 1965) and ^{134}Cs ($t_{1/2}$=2.06 years), (e.g. Syversen *et al.* 2001). These two radionuclides were incorporated into small controlled experimental areas (points and lines of 1.5 m in a bare area and a tilled plot of 225 m^2 respectively) as a liquid solution, providing a usable method for tracing surface soil movement.

Typically the quantification of the amount of a specific radionuclide in a given soil is expressed in mass activity ($Bq \cdot kg^{-1}$) or areal activity ($Bq \cdot m^{-2}$) measured in the laboratory using a gamma spectrometry facility. There are also some examples of direct field measurements through in-situ gamma detector or field gamma spectrometer (see Perrin *et al*. 2006).

The determination of sediment or erosion rates in the landscape is based *(i) on the determination of the reference inventory of the radionuclide in stable and undisturbed locations–sites such as flat permanent pastures or forests reflecting the original fallout input, without erosion or deposition processes* and *(ii) the comparison of the tracer inventory and its vertical distribution to the investigated disturbed soil profile*. Figure 1.2, adapted from Mabit *et al*. (2008a), illustrates the typical distribution of the areal activity of the various fallout radionuclides in reference sites (undisturbed soil) and cultivated sites exhibiting deposition or erosion. In undisturbed areas ^{137}Cs and ^{210}Pb are distributed mostly in the first 3 cm of the soil, albeit with the highest concentration close to the surface.

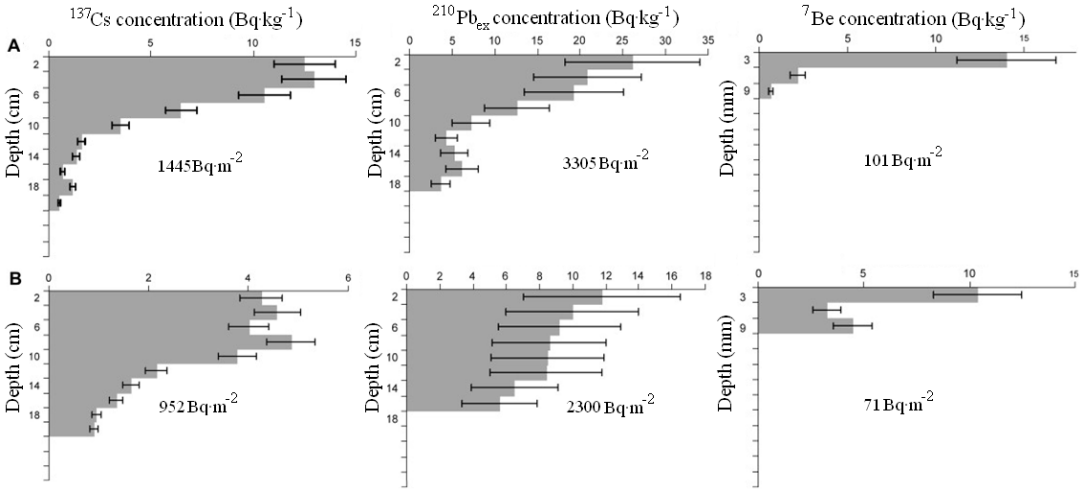

Figure 1.2. Typical depth distributions of Fallout radionuclides (from left to right: ^{137}Cs, $^{210}Pb_{ex}$ and ^{7}Be) in an undisturbed (A) and a cultivated (B) eroded soil in Morocco. NB: The uncertainty of the measured mass activity of each radioisotope is expressed at 2σ (adapted from Mabit *et al*. 2008a).

This reflects the existence of downward migration due to processes such as bioturbation or preferential water flow. Given its short half life, ^{7}Be is found in the first centimetres of the top soil. When applied to the soil surface as a solution in short-term experiments, the radionuclides are mostly concentrated in the top 2-4 cm of the soil (e.g. Syversen *et al.* 2001).

The first step in using FRN approach is to select a representative reference site as close as possible to the study area and to determine a sufficient number of samples to include the uncertainty linked to the spatial variability of the initial fallout. Because of the mechanisms regulating fallout distribution, the concentration of these tracers in reference areas is subjected to spatial variability at global, regional, field and plot scales. Sutherland, (1991, 1996) suggested that approximately eleven sampling points will usually be necessary to provide an accurate estimate of central tendency for many reference locations, assuming that independent random samples are selected. In investigated cultivated areas, the number of samples taken to determine inventory values varied widely from a few cores per hillslope transect (e.g. Cuesta and Delgado, 1997) or up to 60 on homogeneous agricultural fields (Owens and Walling, 1996), and between 68 and 80 in small catchments (Ritchie *et al*. 2009 and Wallbrink *et al*. 2002 respectively). Soil samples are usually collected to a deep enough depth (usually 50-60 cm) to measure the total content of radionuclides present into the profile and are often subdivided into regular depth increments (usually 5 to 10 cm in cultivated area; 2.5 or 5 cm in the case of the reference site) to obtain the radionuclide's vertical distribution.

The next step is to translate soil radiotracer activities into erosion or sedimentation rates, using appropriate conversion models. There are several existing validated models for each FRN (^{137}Cs, $^{210}Pb_{ex}$ and ^{7}Be) associated with user-friendly software for model implementation (Walling *et al*. 2002). As an example, the ^{137}Cs conversion models are summarized in Table 1.2 adapted from the review by Walling and He (1999a). The model used and the assumptions made in its calibration, have a direct impact on the soil redistribution magnitude obtained. Figure 1.3, adapted from Walling and He (1999a) illustrates the impact of model selection model and model assumptions on erosion rates.

Model	Approach
Empirical relationship †, √	Empirical measurements from plots measurements.
Proportional model †	Assume complete mixing of ^{137}Cs in the plow layer. Soil loss is proportional to ^{137}Cs loss since the beginning of accumulation.
Mass balance model †	It models the change of ^{137}Cs in soil profile due to time changes in ^{137}Cs inputs, losses due to erosion and incorporation of soils without ^{137}Cs from below the plow layer.
Profile distribution model √	Assuming a given shape of the ^{137}Cs profile distribution with depth in undisturbed soil.
Refined mass balance model †	Including also the removal of freshly deposited ^{137}Cs before cultivation and grain size selectivity associated with sediment mobilization and transport.
Mass balance including tillage †	It is a mass balance model including soil redistribution caused by tillage.
Diffusion and migration model √	It includes the redistribution of ^{137}Cs into the soil trough diffusion and migration processes.

Table 1.2. Review of models for estimating erosion rates from ^{137}Cs measurements from less (upper part of the Table) to more (lower part of the Table) complicated models. † means applicable to cultivated soils and √ indicates applicable to undisturbed soils.

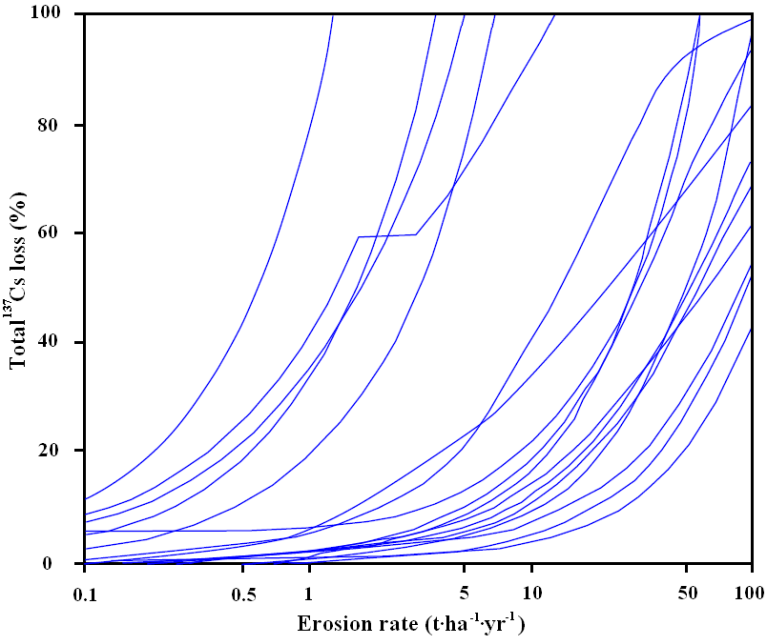

Figure 1.3. Relationship between percentage of ^{137}Cs inventory loss and erosion rates for different calibration models (adapted from Walling and He, 1999a).

Among the most widely used model is the mass balance model (Table 1.2),

$$\frac{d\,A(t)}{dt} = I(t) - \left(\lambda + \frac{R}{d}\right) A(t) \qquad (1.1)$$

Where t is time since start of ^{137}Cs accumulation, $A(t)$ cumulative activity per unit area, R is erosion rate, d is cumulative mass representing average plough depth, λ is a decay constant for ^{137}Cs, and $I(t)$ an annual flux at time t.

Using one of the conversion models in Table 1.3 it is possible to obtain point values of erosion or sedimentation rates from punctual ^{137}Cs activity level, interpolate the data and create a soil redistribution map (e.g. see Figure 1.4, adapted from Ritchie *et al*. 2009) and/or average the values in homogeneous areas and establish a full sediment budget (e.g. Figure 1.5, adapted from Wallbrink *et al*. 2002).

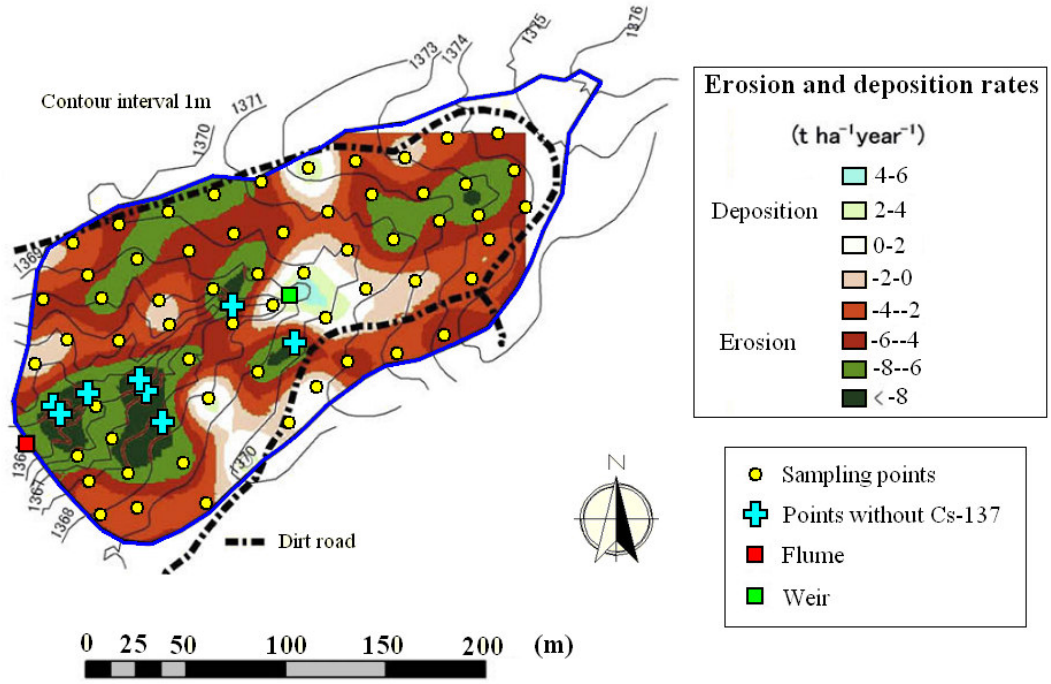

Figure 1.4. Soil redistribution patterns in the Lucky Hills sub-catchment of the Walnut Gulch Experimental catchment (adapted from Ritchie *et al*. 2009).

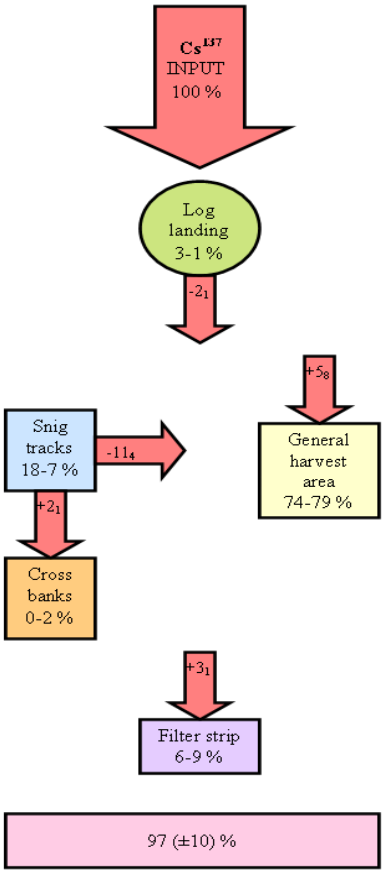

Figure 1.5. Sediment budget in a logged forest (adapted from Wallbrink *et al*. 2002).

Recently Parsons and Foster (2011) have described and challenged the fundamental assumptions considered in the ^{137}Cs erosion studies and the errors when inventories are determined. They concluded suspicious of the reliability of the results presented in these studies and therefore of the use of this radionuclide as an estimator of rates of erosion.

1.4. Rare Earth based tracers

Rare earth based tracers can provide a good example of the issues arising when developing the use of a specific tracer in water erosion studies for different soils and scales. The Lanthanides, or Rare Earth Elements (REE), are elements of atomic numbers from 57 to 71, and present similar chemical characteristics: La, Ce, Pr, Nd, Sm, Eu, Gd, Tb, Dy, Ho, Er, Tm, Yb and Lu. They offer a number of advantages as a tracer.

They can be detected at very low concentrations (up to parts per billions) using neutron activation analysis (INAA, e.g. Orvini *et al*. 2000) or by inductively coupled plasma-mass spectrometry (ICP-MS) after acid extraction (Zhang *et al*. 2001). The majority of the rare earth studies indicated in Table 1.1 and Figure 1.1 use ICP-MS with a similar acid extraction procedure, most of them following the method of Zhang *et al*. (2001), although use a slightly modified procedure (Deasy and Quinton, 2010). Because of the possibility of being detected at very low concentration they provide a promising tool to track sediment movement through the landscape.

Several studies have explored the incorporation methods of these tracers into the soil and the selectivity of their binding to different aggregate sizes, all of them using REE in their oxide forms. Zhang *et al*. (2001) found that the best way to incorporate these tracers into the soil was by serial dilutions with dried soil sieved to 6 mm and pre-wetted with deionised water to approximately 15% water content. When applied at larger field experiments the application methods varied. Sometimes incubated tagged soil has been spread on the surface followed by a light tillage, as done by Polyakov *et al*. (2004) in a small agricultural catchment in the USA Midwest; spread followed by water spray to improve binding to soil aggregates, as done by Polyakov *et al*. (2009), excavating and refilling with tagged soil in selected areas of a hillslope, as done by Yang *et al*. (2008), or spraying as water solution in wheel track areas along a hillslope, as done by Deasy and Quinton (2010) or by mixing of REO with sand before spreading (Stevens and Quinton, 2008).In all cases the interpretation and analysis of the experimental measurements were conditioned by the initial distribution of the tracer along the soil profile, which was restricted to the upper few millimetres in the case of surface applications of Polyakov *et al*. (2009) and Deasy and Quinton (2010).

The second question to be addressed by some of the preliminary studies is the selectivity in the aggregate binding to soil aggregates of different sizes. Zhang *et al*. (2001) determined the concentration of five REE (La, Pr, Nd, Sm, Gd) in tagged soil aggregates separated by wet sieving. The soil used was well structured silt-loam soil and the results in Figure 1.6 (adapted from Zhang *et al*. 2001) suggest a more or less homogeneous distribution along different aggregate sizes.

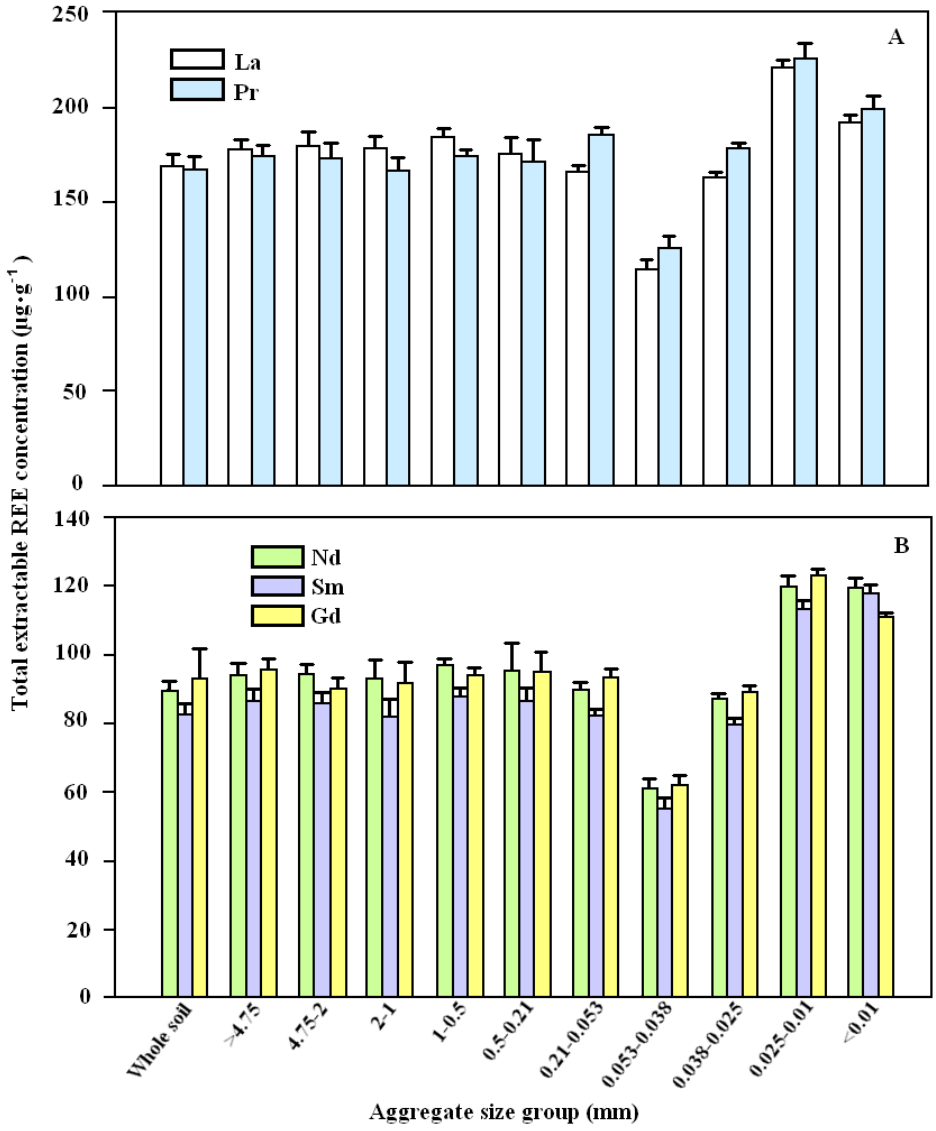

Figure 1.6. Total extractable rare earth element (REE) concentrations of the tagged REE-tagged soil (whole) and individual aggregate size groups after sieving (adapted from Zhang *et al*. 2001).

These results support the assumption of non-selective binding among the soil aggregates used in the calculations of tracer erosion rated made in experiments using REE on these kinds of soils (e.g. Zhang *et al*. 2003, Polyakov and Nearing, 2004). However, this assumption of non-selective binding to different soil aggregates is not always achieved. Kimoto *et al*. (2006b) made a similar analysis using the same five REE in a coarse-textured soil in a semi-arid area from the Walnut Gulch experimental catchment located in south eastern Arizona, USA.

Table 1.3 adapted from Kimoto *et al*. (2006b) shows the trend towards an increased concentration in the finer aggregate sizes. They explained this trend as a function of the higher clay content of the finer aggregate sizes, which provide the chemically active clay surfaces to which the REE bind. They suggest that in situations where selective binding takes place, the REE analysis should be made by separating samples into sub-samples of aggregate sizes that present homogeneous binding of REE (four separate particle size groups in their study) and including those differences in the calculations of trace erosion rates. They noted the increased complication and costs of this approach compared to situations of uniform binding.

Particle size group	Particle size (mm)	Ratio									
		Kendall area					Lucky Hills area				
		La	Pr	Nd	Sm	Gd	La	Pr	Nd	Sm	Gd
Group D	4.7-8.0	2.5	1.9	7.1	2.1	5.8	2.1	1.4	4.3	3.1	5.5
	2.0-4.7	4.2	4.0	8.6	5.0	11.9	4.0	2.8	7.6	6.6	10.3
Group C	.7-2.0	5.8	6.7	11.5	8.6	23.1	4.4	3.0	9.7	9.0	14.2
	.3-.7	7.4	9.2	15.3	12.4	31.5	4.4	3.3	10.0	10.6	16.4
Group B	.18-.3	5.7	7.2	11.7	10.1	23.3	7.0	5.2	15.4	17.0	24.9
	.09-.18	6.7	9.0	14.0	12.4	31.3	8.5	7.2	15.3	19.7	30.2
	.04-.09	33.0	51.6	43.9	47.5	126.3	19.3	18.1	27.7	34.8	60.9
Group A	.02-.04	96.9	110.3	77.3	103.2	234.4	55.1	55.8	53.1	50.6	131.5
	.01-.02	95.7	103.1	76.0	77.9	215.8	49.3	104.9	50.4	39.3	173.2
	<.01	41.0	47.3	35.3	24.1	66.5	50.3	54.0	40.8	26.3	96.5

Table 1.3. Total extractable rare earth element (REE) concentrations of the REE-tagged soil and individual aggregate size groups after sieving (adapted from Kimoto *et al*. 2006b).

The studies of Zhang *et al*. (2001) and Kimoto *et al*. (2006b) also demonstrated that, as expected due to their strong binding to soil particles, REE was not leached in soil column experiments.

Polyakov and Nearing (2004) confirm the validity of the formulas used in determining erosion and deposition rates of REE through an indoor-flume experiment using simulated rainfall. The authors tagged five different sections of a uniform slope, 4m long and 4m wide, with different REE (Gd, Sm, Pr, La, Nd). By sampling the soil surface and the sediment measured at the outlet of the flume and determining the REE concentration before and after each rainfall simulation, they were able to determine erosion and sedimentation rates along the flume slope as well as sediment source during the simulations. Once samples have been collected the REE concentration directly measured by ICP-MS needs to be corrected for soil background (B_i) and extraction efficiency (E_i) of the element in question. The corrected concentration of sediment from segment (or tracer) i in time-step j (CC_i^j) can be computed from the direct measurement (C_i^j) as:

$$CC_i^j = \left(C_i^j - B_i^j\right) / E_i \tag{1.2}$$

Where *i,* is the tracer index and *j* is the time-step index.

The amount of sediment delivered from segment *i* to the flume outlet in the time-step *j* (L_i^j) can be computed as:

$$L_i^j = T^j \, x \, CC_i^j / O_i \tag{1.3}$$

Where T^j is the total mass of the sediment delivered at the flume outlet during time−step *j* and O_i is the original average concentration of the tracer for segment *i*.

Equation (1.3) can be rearranged to determine a ratio of sediment discharged to that originated from segment *i* during time *j* for each segment (R_i^j), equation (1.4):

$$R_i^j = CC_i^j / O_i = L_i^j / T^j \tag{1.4}$$

The sum of the sediment ratio for each segment should give the sediment ratio, defined as the ratio between the amount of sediment delivered to the outlet and the amount of sediment generated on hillslopes, for the whole flume at each time step, equation (1.5):

$$R^j = \sum R_i^j \tag{1.5}$$

This should be equal to 1 if the tracer determination if tracer is completely recovered. Weighting each R_i^j for the sediment mass delivered at each time step j (w^j), it is possible to determine the sediment ratio for the whole rainfall simulation,

$$R = \sum w^j R^j \tag{1.6}$$

Zhang *et al*. (2003) obtained independent measurements of net sediment detachment by comparing high resolution scanning of soil surface before and after each six rainfall simulations performed at plot scale (4×4 m), using five REE. The close agreement between the approaches (Figure 1.7, adapted from Zhang *et al*. 2003) and *R* values close to 1, demonstrates the applicability of the REE method to small scale experiments. In addition, by analysing sediment collected from the end of flume during the simulations for REE, it is possible to provide information on sediment sources during the simulations. Zhang *et al*. (2003) also determined erosion and sedimentation rates $(D_{i,k}^n)$ at a given flume position *k* comparing REE concentrations *i* in surface soil samples before and after a given rain *n* using equation (1.7) based on mass balance considerations.

$$D_{i,k}^n = CC_{i,ki}^n \; x \; M_k \; / \; O_i \tag{1.7}$$

Where $CC_{i,k}^n$ is the tracer concentration for a determined position and rain event and M_k is the mass sample from position *k*. $D_{i,k}{}^n > 1$ can be interpreted as sediment deposition of tagged soil with tracer *i* while $D_{i,k}{}^n < 1$ means net erosion of tagged soil with that tracer. Through integrating all the sampling points and tracers, it is possible to obtain delivery ratios for the whole flume Figure 1.8, adapted from Zhang *et al*. 2003).

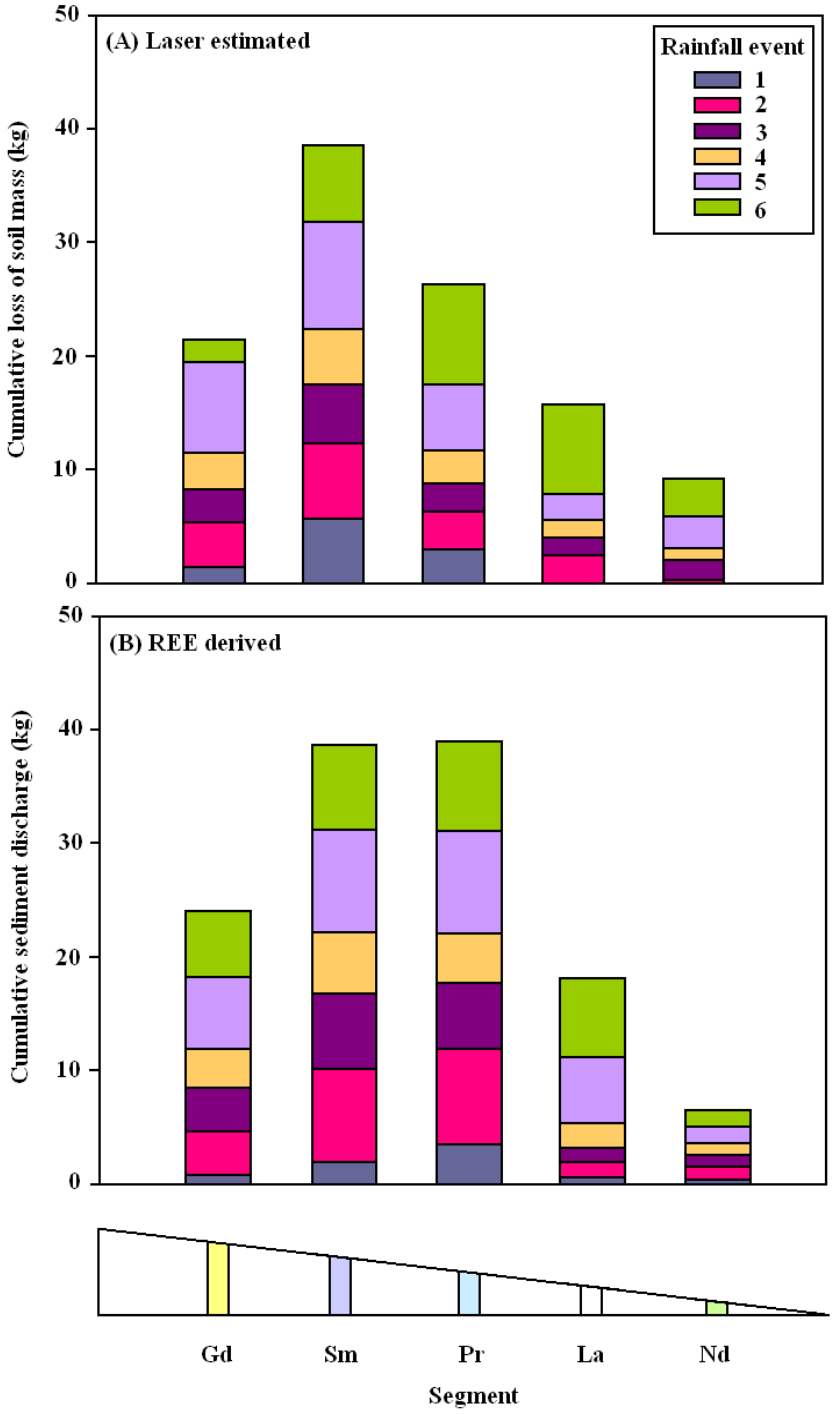

Figure 1.7. (A) Laser measured and (B) REE cumulative sediment discharge from each traced-segment for six consecutive rainfall events (adapted from Zhang *et al*. 2003).

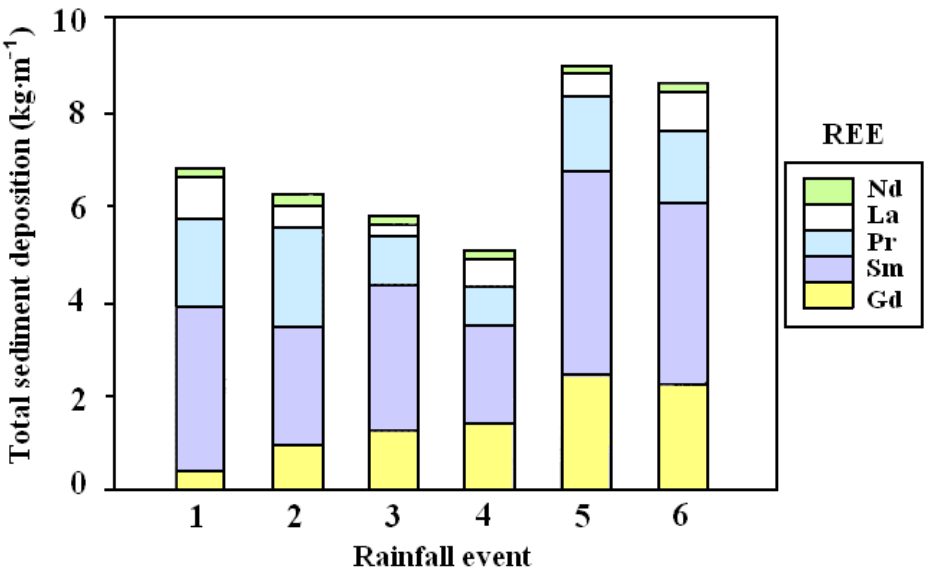

Figure 1.8. Total sediment deposition (D^n) per unit plot width from each segment and for each rainfall event (adapted from Zhang *et al.* 2003).

Michaelides *et al*. (2010) studied the detachment and deposition processes in a laboratory experiment by tagging selected areas of a soil-filled flume (2.5 m wide by 6 m length) with a break in the slope. The use of REE tracers helped to identify areas of sediment redistribution. Some of the potential limitations of the techniques, among them the preferential binding to the finer soil fraction of the soil, were highlighted. Yang *et al*. (2008) used a similar approach but in outdoor areas under natural rainfall. They determined erosion rates by tagging selected points in hillslopes under different cover vegetation and determining the differences in tracer concentration in the soil profile before and after the rainfall period, and using mass balance equations to calculate rates.

REE can also be used at larger spatial erosion scales by tagging of larger areas in fields and catchments conditions to determine sediment redistribution under natural rainfall. To date the area of these experiments has ranged from 0.015 to 0.6 ha. Polyakov *et al.* (2004) divided the North Appalachian Experimental catchment in Ohio (0.68 ha) into geomorphological homogeneous areas and tagged each one using a different REE (Figure 1.9, adapted from Polyakov *et al*. 2004).

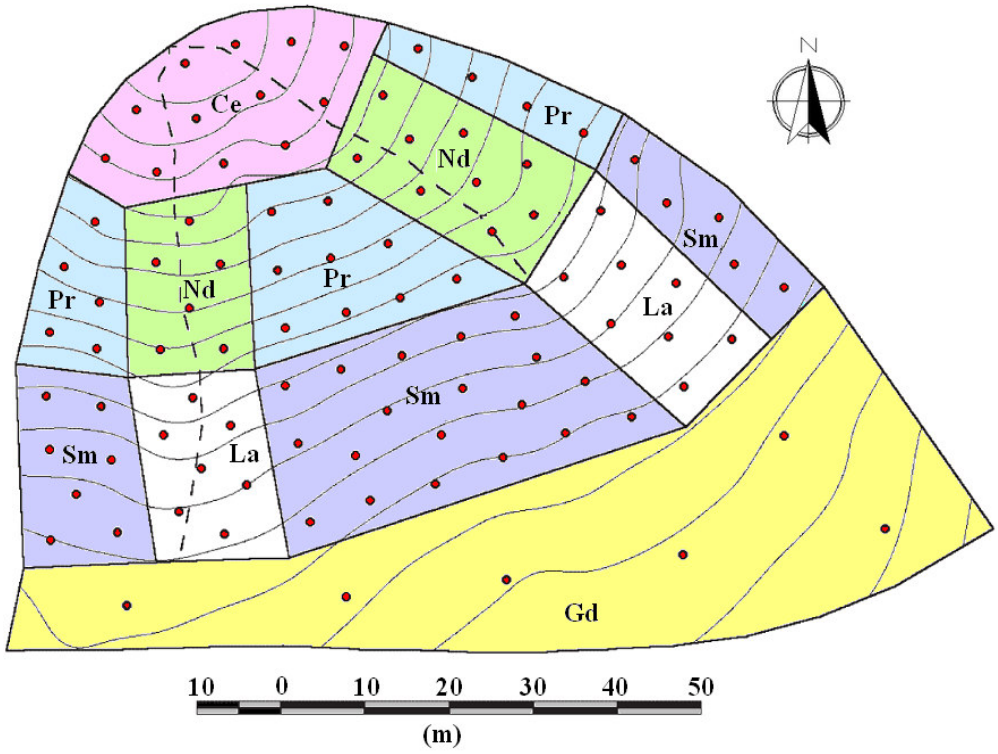

Figure 1.9. Topography, location of channels, and location of surface sampling points on the experimental catchment. The elementary morphological units are delineated by polygons and labeled with the corresponding rare earth element name: toe-slope (Ce), lower (Pr) and upper (Sm) backslopes, lower (Nd) and upper (La) channels, and shoulder (Gd). Contour intervals are 0.5 m (adapted from Polyakov *et al*. 2004).

Using sediment samples from different rainfall events and soil samples taken from the upper 30 mm of soil, the authors studied sediment redistribution and sediment budgets within the catchment for a period of approximately five months. It is worth noting the large sampling density used in this study: 94 sampling points each of which comprised of 30 sub-samples taken in a 2 m radius around the sample point.

The assumptions of non-selective binding to soil, and equations based on mass balance and enrichment ratios calibrated for this soil in laboratory experiments were used to obtain results as those depicted in Figure 1.10 (adapted from Polyakov *et al*. 2004).

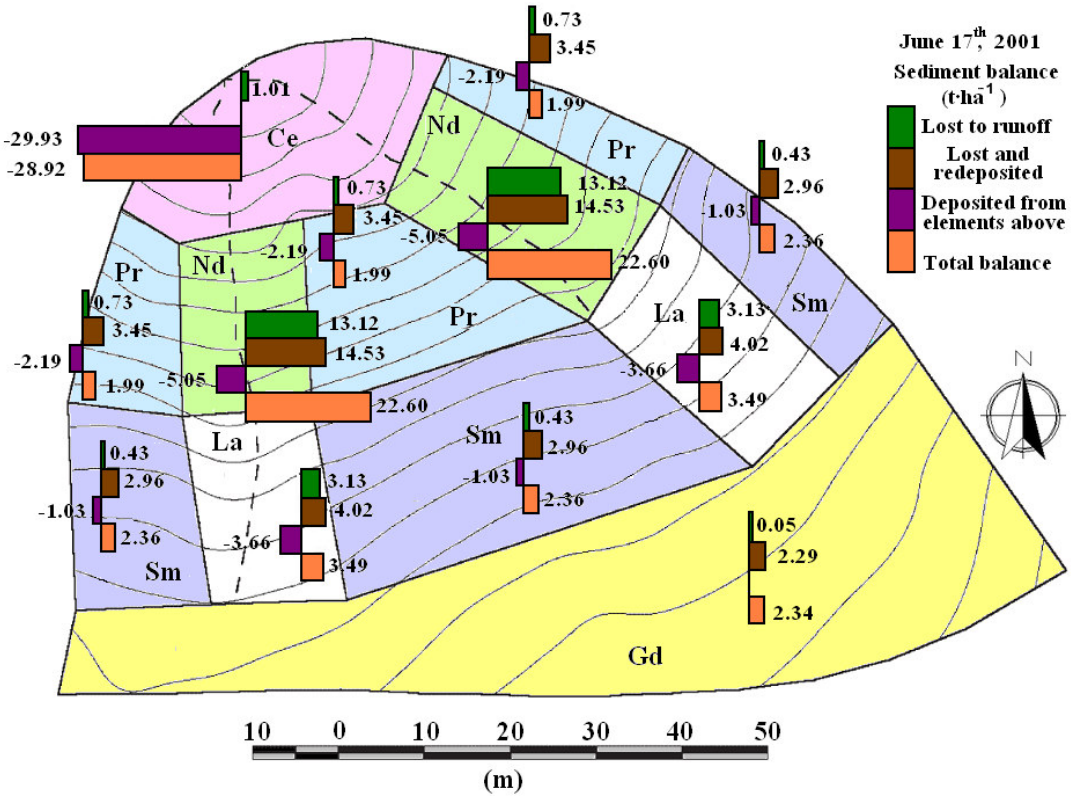

Figure 1.10. Sediment balance on the catchment by June 17th, 2001 (adapted from Polyakov *et al*. 2004).

Kimoto *et al*. (2006a) followed a similar approach in the same semiarid catchment in Ohio described above. They used surface application of the tracer, so only the upper mm of the soil was tagged. They obtained sediment redistribution and sediment budgets for the different geomorphological units of the catchment. However, they point out that that the tagging of the upper mm of the soil makes it suitable only for short-term studies as the tagged soil layer may be rapidly eroded.

A similar approach was followed by Deasy and Quinton (2010) who tagged only the upper millimetres of undisturbed soil in short-term experiments. They used three REE (Gd, Pr, Sm) upper, to tag mid and downslope hillslope areas with a length varying from 66 to 99m. Within these slopes a 4th tracer (Nd) was used to tag the soil in the tractor wheel marks. During three rainfall events they used the concentration of the different tracers in the sediment collected at the slope bottom to show that the upslope area was the most eroding area of the hillslope while the wheel tracks acted mainly as conduits for sediment transport.

1.5. Fingerprinting

The approach and objective of tracers used in fingerprinting, also called sediment source studies, is different to that outlined in the previous sections. This approach is based on comparing the composition, for a given set of soil properties, of the sediment collected at the end of a catchment with the properties of soils from different areas within the catchment. Using this approach it is possible to attribute what fraction of the lost sediment at the catchment outlet or deposition reservoir, comes from each area of the catchment. A large number of different properties have been used in these kinds of studies. Table 1.4 summarizes the properties used in the fingerprinting studies indicated in Table 1.1.

Class	Soil or sediment property
Chemical † (Concentration)	Organic C, Inorganic C, Total C, C/N, pH, Extractable Ca, Extractable Mg, Extractable K, Extractable Na, Al_p, Al_o, Al_d, Fe_p, Fe_o, Fe_d, Mn_p, Mn_o, Mn_d, $\delta^{13}C$, $\delta^{15}N$, Total Si, Al, Ag, Bi, Cd, Cr, Hg, Fe, Ca, Mg, Mn, Na, K, Ti, P, Zn, Sr, Pb, Ni, Cu, As, Mo, Sn, U, Pb, Sb, Sn, Inorganic P, Organic P, Total P, ^{204}Pb, ^{206}Pb, ^{207}Pb, ^{208}Pb
Physical	Sand, clay and silt fraction, Water dispersible clay, Aggregation index, Frequency dependent magnetic susceptibility (0.47 y 4.7 KHz), ^{137}Cs, ^{40}K, ^{226}Ra, Unsupported ^{210}Pb, Anhysteretic remanent magnetization (ARM), Isothermal remanent magnetization (SIRM and IRM at -0.1 T), Infrared spectroscopy
Biological	Sterol rations, *E. coli*, *enterococci* bacterial signatures

Table 1.4. Summary of soil properties measured in some of the fingerprinting studies mentioned in Table 1.1. †Subscripts *p*, *o* and *d* denote pyrophosphate-, oxalate-, and dithionate- extractable, respectively.

The number and type of properties used in specific studies varies, depending on the catchment characteristics, objectives of the study, and availability of analytical capabilities. Some studies have used a small number of properties, for example Fox and Papanicolau (2007) used $\delta^{15}N$, $\delta^{13}C$ and C/N to distinguish between sediment coming from upland rill/interrill erosion and floodplain headcut erosion in a small agricultural catchment (0.71 km^2). Others have used a larger number of determinants, as in the study of Russell *et al*. (2001) which ranged from 8 to 12 depending on the catchment and objective.

One of the challenges in these kinds of studies is how to account for the selectivity in the sediment transport process and its impact on the concentration of the measured soil property in the sediment. A common strategy is to analyze the selected properties in the fine fraction of the soil and sediment, using the <53 μm to <63 μm, (Fox and Papanicolau, 2007 and Rowan *et al*. 2000) fraction. Sometimes the screening is limited to a coarser fraction, as in the case of Rhoton *et al*. (2008) in which the fraction <2 mm was used. An additional step to correct for the selectivity in the sediment transport and the bias introduced into the comparison of soil and sediment tracer concentrations is correcting by the ratio of the specific surface area of the suspended sediment and that of the potential source material (e.g. Collins *et al.* 1998). However, some authors have noted that the relationship between geochemical and radionuclide concentrations and specific surface area is non-linear for specific surface areas $>1 m^2 g^{-1}$, proposing instead that empirical non-linear relationships experimentally determined from fractionation of the source material should be used (e.g. Russell *et al*. 2001).

In some studies, such as Fox and Papanicolau (2007), the properties used to discriminate the sediment source are decided *a priori*, and subsequently reduced following a statistical analysis. This process is well described in Collins and Walling (2002) and Walling (2005), and has been used with minor modifications by several researches such as, Minella *et al*. (2008).

In the first stage the null hypothesis that the source material samples are drawn from the same population is tested. To maximize the discrimination between the sources, while minimizing the size of the properties subset, a second stage of statistical analysis, based on a stepwise multivariate discriminating function, is used to select the optimum set of fingerprint properties from those identified in the first stage. From this analysis it is also possible to establish the associated uncertainties with the fingerprint property values used to characterize each source. The final step is to estimate the relative contribution of each source to the sediment samples collected at the catchment outlet. This is done usually using a multivariate mixing model, equation (1.8).

$$y_i = \sum a_{is} P_s \tag{1.8}$$

Where y_i is the concentration of the element i in the suspended sediment sample, a_{is} is the concentration of the element i in source s and P_s is the relative contribution of source s. This model assumes that the suspended sediment retains the characteristics of its source and that the suspended sediment comprises material only from the identified sources, so $\Sigma P_i = 1$, and $0 < P_s < 1$.

Examples of applying such mixing models are described by Yu and Oldfield (1989) and Walling and Collins (2000). The model in equation (1.8) is over determined and it must be fitted iteratively by minimizing an objective function. These approaches have been applied to different both intra-event and multi event samples. Solution of equation (1.8) is not unique and its equifinality has been explored to provide an estimation of the uncertainty of sediment source predictions. For instance Rowan *et al.* (2000) provided an analysis using the GLUE procedure to explore all the possible solutions of the multivariate mixing models and give the different contribution of each sediment source in probabilistic terms (Figure 1.11).

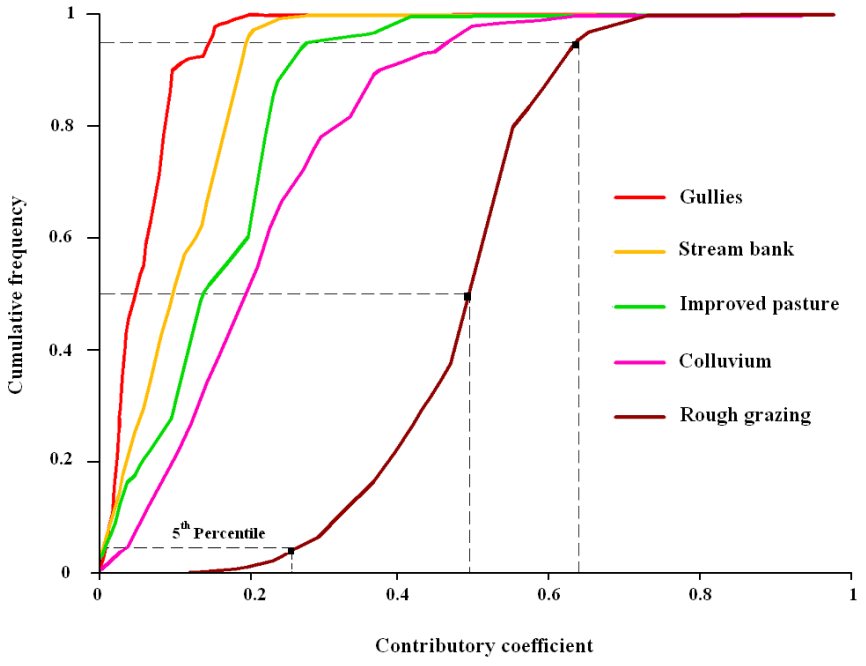

Figure 1.11. Cumulative frequency distribution of the contributory coefficient for the different source areas in the Wyresdale Park Lake (adapted from Rowan *et al.* 2000).

Biomarkers have also been used as sediment fingerprints. For example, compound-specific isotope (CSI) $\delta^{13}C$ values of selected organic biomarkers extracted from catchment source soils and sediment mixtures have been to supplement conventional bulk $\delta^{13}C$ values of those soils and sediments in a fingerprinting approach i.e. IsoSource (see Phillips and Gregg, 2001, 2003). Recently Nosrati *et al*. (2011) has proposed enzyme activity as potential sediment tracers. This suggests that as the understanding of soil biological activities increases in the future, the ability to discriminate sediment source can be improved using new or complementary soil properties.

1.6. Magnetic properties

Given their importance in sediment tracer studies (Figure 1.1), magnetic properties are discussed independently. Magnetic properties of soil mineral constituents, especially iron oxides (magnetite, maghemite, hematite, goethite and pyrrohite) allow the discrimination of different types of soil. There are two uses of magnetic properties in sediment tracer studies. One uses magnetic properties naturally present in soils materials as sediment fingerprint (see Section 1.5). The second use is the application to the soil of tracing tracer whose concentration can be determined from measurements of its magnetic properties. Table 1.5 summarizes some of these properties measured in both kinds of studies, which are based on measuring the magnetization of the sample under different magnetic fields.

It is beyond the scope of this review to provide a thorough discussion of the magnetic properties of minerals, but a good introduction can be found in several texts, for example Maher (2007). The second kind of study includes those in which a magnetic tracer is added to the soil and its movement is measured using magnetic susceptibility. Tracer have included crushed magnetite Parsons *et al*. (1993), magnetic beads of 3.2 mm size (Ventura *et al*. 2002) or tagged soil with magnetic silt size iron oxide (Guzmán *et al*. 2010). Hu *et al*. (2011) have developed five types of magnetic tracers using combinations of fine soil, magnetic powder and fly ash with cement or bentonite.

Property	Brief description
Low frequency magnetic susceptibility χ_{LF}	Magnetic susceptibility is the ratio between the magnetization of the material and the magnetic field strength under which is measured. In this case at low frequency (0.47 kHz)
High frequency magnetic susceptibility χ_{LF}	Magnetic susceptibility at high frequency (4.7 kHz).
Isothermal remanent magnetization *IRM*	Isothermal remanent magnetization is the remanence left in the sample after a steady field (1-1000 mT) has been applied for a short time (e.g. 100 sec) and then switched off at a constant (isothermal) temperature, often room temperature. It is classified depending on the strength of the field, e.g. soft (0-20 mT), mid (20-300 mT), hard (300-1000 mT)
Saturated isothermal remanent magnetization *SIRM*	It is the maximum IRM
Anhysteretic remanent magnetization *ARM*	Magnetization acquired by the combined effects of a large alternating field and a small DC field

Table 1.5. Summary of magnetic soil properties measured in erosion tracers in soils.

The soil and sediment processing for magnetic fingerprinting studies is similar to the one described in the previous Section. Bias introduced by selective transport is a major concern and has been addressed by processing the samples and analyzing only the material most likely to be transported. For example, Slattery *et al*. (2000) analyzed material screened to <63 μm, because in their 6.2 km^2 English study catchment there was no evidence of suspended sediment of a larger size. Maher *et al*. (2009) analyzed the medium sand fraction between 250 to 355 μm, because this was the best suited for the transport process in their study of tropical sediment provenance in NE Australia. On other occasions, the sample has been divided into sand, clay and silt fraction, as in Yu and Oldfield's (1993) sediment source study for a reservoir in Spain. It is also possible to correct the bias by specific surface or empirical functions as in the case of the fingerprinting studies previously described (Section 1.5). The interpretation of magnetic fingerprinting has relied on a variety of statistical approaches, from full un-mixing models, as in Slattery *et al*. (2000) and Yu and Oldfield (1993), to alternative techniques such as cluster analysis (Maher *et al*. 2009).

In the case of incorporated magnetic tracers all these studies have been made at small scale (from 1 to 522 m^2). Parsons *et al.* (1993) applied crushed magnetite in selected transects perpendicular to the longitudinal slope on a 18×29 m long plot during rainfall simulations to study inter-rill sediment transport. Ventura *et al.* (2002), applied magnetic beads all over the surface to study detachment and deposition on a 4 m^2 plot under simulated rainfall. In both cases they obtained information about soil distribution and detachment, although both noted potential problems due to the higher density of the magnetic tracer compared to soil aggregates. Guzmán *et al.* (2010) used silt-size magnetite incubated with blank soils that was incorporated into 1 m^2 plots used in rainfall simulations. This approach identified the need to correct by selective transport of the finer soil fraction that tends to be enriched in tracer concentrations. An alternative already in development is the *in situ* magnetization of soil materials through intense and localized heating (Armstrong *et al.* 2010), although it remains at a preliminary stage.

1.7. Other tracers found in literature

There are some other materials that have been, or are being, developed as potential soil tracers. Young and Holt (1968) used fluorescent glass particles. Their bulk density (2.6 g cm^{-3}), and size (44-125 μm) was similar to that of the soil mineral particles. They were observed with UV light after rainfall simulation experiments at plot scale (4×10 m). Plante *et al.* (1999) developed laboratory scale ceramic tracer spheres with a 13% Dysprosium concentration that could be quantified using instrumental neutron activation analysis. Schwertmann and Schmidt (1978) describe the use of copper applied into the soil as fungicide as a tracer to determine long term soil erosion in a fashion that resembles some of the early applications of ^{137}Cs. Another alternative has been the use of sediment material segregated by grain size and labelled with gold and silver after immersion in a solution with these elements and their concentration measured using instrumental neutron activation analysis (Olmez and Pink, 1994). Wheatcroft *et al.* (1994) used this approach in a preliminary study of sediment movement in Massachusetts Bay.

Sharma *et al*. (2009) presented preliminary results of a polymer microsphere tracer. Each microsphere was coded with a unique DNA sequence, of which there are essentially limitless combinations, and can be measured using real-time polymerase chain reactions. These polymers are also relatively short lived, which can be an advantage in some experimental conditions. At laboratory scale, Mentler *et al*. (2009) presented first results of the potential use of organophilic clays as sediment tracers in erosion studies, obtaining extraction efficiencies of about 85%, and Spencer *et al*. (2011) presented the results of a field experiment to use holmium labelled montmorillonite to track fine sediment in urban water management systems.

1.8. Summary

A comprehensive literature review on soil tracers was carried out to illustrate the main approaches, challenges, and progress, with a scale issue emphasis. Most studies considered here suggest that there are different approaches already established with a significant number of research works supporting their development and application. Among them, radioactive tracers, especially ^{137}Cs, are the most widespread. There are studies covering a broad range of scales and models to achieve the best interpretation of analytical results, including effects such as selective transport of finer particles or diffusive processes into the soil profile and along the landscape due to tillage and wind erosion. The use of environmental radionuclides provides information about soil erosion rates, spatial patterns of soil redistribution and erosion/deposition areas medium-term, depending on the half life of the radionuclide studied. They do not present limitations of spatial scales and the information they provide is useful for other tracer approaches such as, fingerprinting studies Among the numerous advantages offered by radionuclides , the use of these tracers possess important limitations that must be considered based on the information that they provide. Some of these limitations are the cost of the analysis and the specialization of the staff, the assumptions and uncertainties of the technique and the impossibility of detecting short-term changes in erosion rates due to different land management practices (Zapata, 2003).

Rare earth tracers have attained significant use in small and medium scale erosion studies in the last two decades providing spatial and temporal soil erosion distribution. Some of the publications generated during its inception present a very useful blueprint for the development of new tracers. REE has many of the desirable characteristics for being ideal sediment tracers such as, the possibility of multiple tracers, the strong-binding ability and their easy detection at low concentrations in soil but their use entails some notable limitations such as, the preferential bound to soil finer aggregates or the incorporation to soil profile without disturbing it. Apart from the cost, the analytical technique (e.g. ICP-MS after acid extraction) presents complexity and uncertainties when REE concentrations are over soil background values.

Fingerprinting studies combine soil properties and un-mixing models, allow the identification and quantification of sediment sources depending on differences in soil properties, identification and quantification of sediment sources depending on differences in soil properties, especially at large scales, where these differences are easier to prove. This approach has already been well established with sophisticated techniques to evaluate the uncertainty of the predictions. To obtain consistent results it is important to employ a variety of sediment properties. Some limitations of this approach could be enrichment of finer particle sizes for some soil properties or possible changes on sediment properties compared to the original ones from the source areas.

Several research works using magnetic properties as a tracer have common issues with fingerprinting studies but with the advantage of using physical technology for the determination of properties allowing relatively inexpensive processing of a large number of samples. Despite the relative simplicity of using and measuring magnetic properties compared to other tracer measurements, some of the incorporated magnetic tracers used, show a higher density compared to soil minerals, thus interfering with soil movement. This seems to be solved by incorporating silt-sized magnetite but shares some limitations with REE such as, the mixing and the incorporation into the soil profile or the preferential bound for finer soil particles.

Depending on the magnetic property measured or magnetic tracer employed, this approach would be useful in a broad range of spatial and temporal scales under different soil managements. At the moment, most of these studies have been carried out at a large scale in the case of soil mineral magnetic properties or at a laboratory/plot scale for incorporated magnetic tracers.

A significant number of new tracers have been developed or are in progress at small scale. Their potential as sediment tracers have been evaluated under controlled conditions and most of them are in a preliminary stage for concrete objectives. They also have limitations inherent to the nature of each substance but common to previous groups of tracers already described. This reflects the fact that none of the existing tracers suits the needs of a given team for a specific problematic.

It is interesting to synthesize a number of issues that are common to all the review tracing techniques revised, although some of them have been studied in more detail for particular studies and techniques. One of them is the incorporation of a tracer in situations of undisturbed soils, where there is no possibility of tagging soil in the laboratory for its later application to the soil surface or soil profile. Another is the need for using mathematical models to convert changes in concentration into changes in erosion or deposition rates, to take into account effects such as downward migration, selectivity in the transport, soil disturbance, etc. Finally, the development of "ephemeral" tracers that disappear in months or years, as in the case of DNA microsphere spheres, is important to maintaining the ability of using experimental areas for further experiments without the problems caused by the contamination of tracers used in previous experiments.

Radionuclides and fingerprinting studies seem to be well ahead of the other tracing technologies, indicating a significant uncertainty on the final erosion and deposition rates, or sediment source attribution if these issues are not properly addressed.

Future research should focus, among other issues, on reducing the uncertainty of the impact on the conversion of concentrations into rates or sediment source, from which a good understanding of the tracer distribution along the tagged soil profile and its affinity to particular soil aggregate sizes will be the key. For new tracers in development, studies already published in fingerprinting and radionuclides might provide significant help. The ability to develop tracers which requires inexpensive analysis techniques, able to process quickly a large number of samples would be a key line of research in the future, given the need to understand the behaviour of the tracer under many different conditions and the important role that spatial variability might play in understanding soil dynamic due to water erosion. For these new tracers, the possibility of properly incorporating the tracer into undisturbed soils also seems a purposeful objective, since that ability is very limited with current tracers.

1.9. Acknowledgements

Thanks to the support provided by the Spanish Ministry of Science and Innovation (Projects AGL2006–10927–C03–01, AGL2009-12936-C03-01) and FEDER funds.

1.10. References

Armstrong, A., Maher, B., Quinton, J. 2010. Enhancing the magnetism of soil: the answer to soil tracing? Geophysical Research Abstracts Vol. 12, EGU2010–2805, EGU General Assembly 2010.

Arnscheidt, J., Jordan, P., Li, S., McCormick, S., McFaul, R., McGrogan, H.J., Neal, M., Sims, J.T. 2007. Defining the sources of low-flow phosphorus transfers in complex catchments. Science of the Total Environment 382: 1–13.

Bacchi, O.O.S., Reichard, K., Sparovek, G., Ranieri, S.B.L. 2000. Soil erosion evaluation in a small watershed in Brazil trough ^{137}Cs fallout redistribution analysis and conventional models. Acta Geologica Hispanica 35: 251–259.

Bajracharya, R.M., Lal, R., Kimble, J.M. 1998. Use of radioactive fallout cesium-137 to estimate soil erosion on three farms in west central Ohio. Soil Science 163: 133–142.

Barcellos, C., de Lacerda, L.D., Ceradini, S. 1997. Sediment origin and budget in Sepetiba Bay (Brazil) - an approach based on multielemental analysis. Environmental Geology 32: 203–209.

Bellangera, B., Huona, S., Velasquez,F., Vallesc, V.,Girardina, C., Mariotti, A. 2004. Monitoring soil organic carbon erosion with δ13C and δ15N on experimental field plots in the Venezuelan Andes. Catena 58: 125–150.

Belyaev, V.R., Golosov, V.N., Kuznetsova, J.S., Markelov, M.V. 2010. Quantitative assessment of effectiveness of soil conservation measures using a combination of (137)Cs radioactive tracer and conventional techniques. Catena 79: 214–227.

Bennett, P., He, .F., Zhao, D., Aiken, B., Feldman, L. 2010. In situ testing of metallic iron nanoparticle mobility and reactivity in a shallow granular aquifer. J Contam. Hydrol. 116: 35–46.

Benninger, L.K., Suayah, I.B., Stanley, D.J. 1998. Manzala lagoon, Nile delta, Egypt: modern sediment accumulation based on radioactive tracers. Environmental Geology 34: 183–193.

Bernard, C., Laverdière, M.R., Pesant, A.R. 1992. Variabilité de la relation entre les pertes de césium et de sol par érosion hydrique. Geoderma 52: 265–277.

Brown, R.B., Kling, G.F., Cutshall, N.H. 1981. Agricultural erosion indicated by ^{137}Cs redistribution: II. Estimates of erosion rates. Sci. Soc. Am. J. 45: 1191–1197.

Busacca, A.J., Cook, C.A., Mulla, D.J. 1993. Comparing landscape-scale estimation of soil erosion in the Palouse using Cs-137 and RUSLE. Journal of Soil and Water Conservation 48: 361–367.

Caitcheon, G.G. 1993. Sediment source tracing using environmental magnetism. Anew approach with examples from Australia. Hydrol. Process. 7: 349–358.

Chiu, Y.J., Borghuis, A.M., Lee, H.Y., Chang, K.T., Chao, J.H. 2008. Estimation of soil erosion in a reservoir watershed using Cs-137 fallout radionuclide. International Journal of Sediment Research 22: 304–317.

Collins, A.L., Walling, D.E. 2002. Selecting fingerprint properties for discriminating potential suspended sediment sources in river basins. Journal of Hydrology 261: 218–244.

Collins, A.L., Walling, D.E., Leeks, G.J.L. 1998. Use of composite fingerprint to determine the provenance of the contemporary suspended sediment load transported by rivers. Earth Surf. Process. Landforms 23: 31–52.

Cuesta, M.J., Delgado, A. 1997. Técnicas isotópicas para la cuantificación de la erosión. Agricultura 776: 230–236.

Cunha, M.E.T., Yabe, M.J.S., Lobo, I., Aravena, R.D.E. 2006. Isotopic composition as a tool for assessment of origin and dynamic of organic matter in tropical freshwater. Environmental Monitoring and Assessment 121: 461–478.

Dai, Z., Du, J., Chu, A., Zhang, X. 2011. Sediment characteristics in the North Branch of the Yangtze Estuary based on radioisotope tracers. Environmental Earth Sciences 62: 1629–1634.

de Junet, A., Abril, G., Guerin, F., Billy, I., de Wit, R. 2009. A multi-tracers analysis of sources and transfers of particulate organic matter in a tropical reservoir (Petit Saut, French Guiana). River Research and Applications 25: 253–271.

de Roo, A.J.J. 1991. The Use of ^{137}Cs as a tracer in an erosion study in south Limburg (The Netherlands) and the influence of Chernobyl fallout. Hydrol. Proc. 5: 215–227.

Dearing, J.A., Yuquan, H., Doody, P., James, P.A., Brauer, A. 2001. Preliminary reconstruction of sediment-sources linkages for the past 6000 yrs at the Petit Lac d'Annency, France, based on mineral data. Journal of Paleolimnology 25: 245–258.

Deasy, C., Quinton, J.N. 2010. Use rare earth oxides as tracers to identify sediment sources areas for agricultural slopes. Solid Earth Discussions 2: 195–212.

Devereux, O.H., Prestegaard, K.L., Needelman, B.A., Gellis, A.C. 2010. Suspended-sediment sources in an urban watershed, Northeast Branch Anacostia River, Maryland. Hydrol. Process. 24: 1391–1403.

di Stefano, C., Ferro, V., Porto, P. 1999. Linking sediment yield and caesium-137 spatial distribution at basin scale. Journal of Agricultural Engineering Research 74: 41–62.

Duane, D.B., James, W.R. 1980. Littoral transport in the surf zone elucidated by an Eulerian sediment tracer experiment. Journal of Sedimentary Research 50: 929–942.

Estrany, J., Garcia, C., Walling, D.E. 2010. An investigation of soil erosion and redistribution in a Mediterranean lowland agricultural catchment using caesium-137. International Journal of Sediment Research 25: 1–16.

Fifield, L.K.,Wasson, R.J.,Pillans, B., Stone, J.O.H. 2010. The longevity of hillslope soil in SE and NW Australia. Catena 81: 32–42.

Fox, J.F., Papanicolaou, A.N. 2008a. Application of the spatial distribution of nitrogen stable isotopes for sediment tracing at the watershed scale. Journal of Hydrology 358: 46–55.

Fox, J.F., Papanicolaou, A.N. 2008b. An un-mixing model to study watershed erosion processes. Advances in Water Resources 31: 96–108.

Fox, J.F., Papanicolaou, A.N. 2007. The use of carbon and nitrogen isotopes to study watershed erosion processes. Journal of the American Water Resources Association 43: 1047–1064.

Guzmán, G., Barrón, V., Gómez, J.A. 2010. Evaluation of magnetic iron oxides as sediment tracers in water erosion experiments. Catena 82: 126–133.

Hardy, I.A.J., Carter, A.D., Leeds-Harrison, P.B., Foster, I.D.L., Sanders, R.M. 2000. The origin of sediment in field drainage water. In Foster, I.D.L. (Ed). Tracers in Geomorphology. John Wiley & Sons. Chichester.

Hassouni, K., Bouhlassa, S. 2006. Estimate of soil erosion on cultivated soils using ^{137}Cs measurements and calibration models: A case study from Morocco. Can. J. Soil Sci. 86: 77–87.

Higgitt, D.L., Lu, X.X., Pu, L.J. 2000. Soil erosion assessment using ^{137}Cs examples from contrasting environments in Southern China. In Foster, I.D.L. (Ed). Tracers in Geomorphology. John Wiley & Sons. Chichester.

Hu, G.Q., Dong, Y.J., Wang, H., Qiu, X.K., Wang, Y.H. 2011. Laboratory testing of magnetic tracers for soil erosion measurement. Pedosphere 21: 328–338.

Juracek, K.E., Ziegler, A.C. 2009. Estimation of sediment sources using selected chemical tracers in the Perry lake basin, Kansas, USA. International Journal of Sediment Research 24: 108–125.

Kachanoski, R.G. 1988. Comparison of measured soil 137-Cesium losses and erosion rates. Can. J. Soil Sci. 67: 199–203.

Kachanoski, R.G., de Jong, E. 1984. Predicting the temporal relationship between soil cesium 137 and erosion rate. J. Environ. Qual. 13: 301–304.

Kimoto, A., Nearing, M.A., Shipitalo, M.J., Polyakov, V.O. 2006a. Multi-year tracking of sediment source in a small agricultural watershed using rare earth elements. Earth Surf. Process. Landforms 31: 1763–1774.

Kimoto, A., Nearing, M.A., Zhang, X.C., Powell, D.M. 2006b. Applicability of Rare Earth Element Oxides as Sediment Tracers for Coarse-textured Soils. Catena 65: 214-221.

Kouhpeima, A., Feiznia, S., Ahmadi, H. 2011. Tracing fine sediment sources in small mountain catchment. Water Science and Technology 63: 2324–2330.

Kronvang, B., Grant, R., Laubel, A.L. 1997 Sediment and phosphorus export from a lowland catchment: Quantification of sources. Water, Air and Soil Pollution 99: 465–476.

Lance, J.C., McIntyre, S.C., Naney, J.W., Rousseva, S.S. 1986. Measuring sediment movement at low erosion rates using Cesium-137. Sci. Soc. Am. J. 50: 1303–1309.

Lei, T.W., Zhang, Q.W., Zhao, J., Nearing, M.A. 2006. Tracing sediment dynamics and sources in eroding rills with rare earth elements. European J. of Soil Sci. 57: 287–294.

Li, H., Zhang, X., Wang, K., Wen, A. 2010. Assessment of sediment deposition rates in a karst depression of a small catchment in Huanjiang, Guangxi, southwest China, using the cesium-137 technique. Journal of Soil and Water Conservation 65: 223–232.

Li, Y.S., Wang, G.X., Ding, Y.J., Zhao, L., Wang, Y.B. 2009. Application of the ^{137}Cs tracer technique to study soil erosion of alpine meadows in the headwater region of the Yellow River. Environmental Geology. 58: 1021–1028.

Li M., Li Z.B., Ding W.F., Liu P.L., Yao, W.Y. 2006. Using rare earth element tracers and neutron activation analyses to study rill erosion process. Applied radiation and isotopes: including data, instrumentation and methods for use in agriculture, industry and medicine 64: 402–408.

Loughran, R.J., Elliott, G.L., Campbell, B.L., Shelly, D.J. 1988. Estimation of soil erosion from caesium-137 measurements in a small, cultivated catchment in Australia. International Journal of Radiation Applications and Instrumentation. Part A. Applied Radiation and Isotopes 39: 1153–1157.

Lu, X.X., Higgitt, D.L. 2000. Estimating erosion rates on sloping agricultural land in the Yangtze Three Gorges, China, from caesium-137 measurements. Catena 39: 33–51.

Mabit, L., Klik, A., Benmansour, M., Toloza, A., Geisler, A., Gertsmann, U.C. 2009. Assessment of erosion and deposition rates within an Austrian agricultural watershed by combining ^{137}Cs, $^{210}Pb_{ex}$ and conventional measurements. Geoderma 150: 231–239.

Mabit, L., Benmansour, M., Walling D.E. 2008a. Comparative advantages and limitations of Fallout radionuclides (^{137}Cs, ^{210}Pb and ^{7}Be) to assess soil erosion and sedimentation. Journal of Environmental Radioactivity 99: 1799–1807.

Mabit, L., Bernard, C., Makhlouf, M., Laverdière, M.R. 2008b. Spatial variability of erosion and soil organic matter estimated from ^{137}Cs measurements and geostatistics. Geoderma 145: 245–251.

Maher, B.A. 2007. Environmental magnetism and climate change. Contemporary Physics 48, no 5: 247–274.

Maher, B.A., Watkins, S.J., Brunskill, G., Alexander, J., Fielding, C.R. 2009. Sediment provenance in a tropical fluvial and marine context by magnetic 'fingerprinting' of transportable sand fractions. Sedimentology, v. 56, no. 3 pp. 841–861.

Mahler, B.J., Bennett, P.C., Zimmerman, M. 1998. Lanthanide-labeled clay: a new method for tracing sediment transport in karst. Ground Water 36: 835–843.

Martinez-Carreras, N., Udelhoven, T., Krein, A., Gallart, F., Iffly, J.F., Ziebel, J., Hoffmann, L., Pfister, L., Walling, D. E. 2010. The use of sediment colour measured by diffuse reflectance spectrometry to determine sediment sources: Application to the Attert River catchment (Luxembourg). Journal of Hydrology 382: 49–63.

Martinotti, W., Camusso, M., Guzzi, L., Patrolecco, L., Pettine, M. 1997. C, N and their stable isotopes in suspended and sedimented matter from the Po estuary (Italy). Water, Air and Soil Pollution 99: 325–332.

Martz, L.W., de Jong, E. 1991. Using Cs-137 and landform classification to develop a net soil erosion budget for a small Canadian prairie watershed. Catena 18: 298–308.

Martz, L.W., de Jong, E. 1987. Using Cs-137 to assess the variability of net erosion and its association with topography in a Canadian Prairie landscape. Catena 14: 439–451.

Matisoff, G., Ketterer, M.E., Wilson, C.G., Layman, R., Whitin, P.J. 2001. Transport of rare earth element-tagged soil particle in response to thunderstorm runoff. Environ. Sci. Technol. 35: 3356-3362.

Mentler, A., Strauss, P., Schomakers, J., Hann, S., Köllensberger, G., Ottner, F. 2009. Organophilic clays as a tracer to determine erosion processes. Geophysical Research Abstracts,Vol. 11, EGU2009–13192. EGU General Assembly 2009.

Michaelides, K., Ibraim, I., Nord, G., Esteves, M. 2010. Tracing sediment redistribution across a break in slope using rare earth elements. Earth Surf. Process. Landforms 35: 575–587.

Miller, J.R., Lord, M., Yurkovich, S., Mackin, G., Kolenbrander, L. 2005. Historical trends in sedimentation rates and sediment provenance, Fairfield Lake, western North Carolina. Journal of the American Water Resources Association 41: 1053–1075.

Minella, J.P.G., Walling, D.E., Merten, G.H. 2008. Combining sediment source tracing techniques with traditional monitoring to assess the impact of improved land management on catchment sediment yields. Journal of Hydrology 348: 546–563.

Ming-Yi, Y., Jun-Liang T., Pu-Ling, L. 2006. Investigating the spatial distribution of soil erosion and deposition in a small catchment on the Loess Plateau of China, using 137Cs. Soil Till. Res. 87: 186–193.

Mizugaki, S., Onda, Y., Fukuyama, T., Koga, S., Asai, H., Hiramatsu, S. 2008. Estimation of suspended sediment sources using ^{137}Cs and $^{210}Pb_{ex}$ in unmanaged Japanese cypress plantation watersheds in southern Japan. Hydrol. Process. 22: 4519–4531.

Montgomery, J.A., Busacca, A.J., Frazier B.E., McCool, D.K. 1997. Evaluating soil movement using Cesium-137 and the revised universal soil loss equation. Sci. Soc. Am. J. 61: 571–579.

Motha, J.A., Wallbrink, P.J., Hairsine, P.B., Grayson, R.B. 2003. Determining the sources of suspended sediment inforested catchment in southeastern Australia. Water Resources Research 39, 1056, 14 PP, doi: 10.1029/2001WR000794.

Nosrati, K., Govers, G., Ahmadi, H., Sharifi, F., Amoozegar, M. A., Merckx, R., Vanmaercke, M. 2011 An exploratory study on the use of enzyme activities as sediment tracers: biochemical fingerprints? International Journal of Sediment Research 26: 136–151.

Olley, J.M., Murray, A.S., Mackenzie, D.H., Edwards, K. 1993. Identifying natural and anthropogenic radioactivity. Water Resources Research 29: 1037–1043.

Olmez, I., Pink, F.X. 1994. New particle-labeling technique for use in biological and physical sediment transport studies. Eviron. Sci. Technol. 28: 1487–1490.

Olson, K.R., Gennadiyev, A.N., Golosov, V.N. 2008. Comparison of fly ash and radio-cesium tracer methods to assess soil erosion and deposition in Illiniois landscapes (USA).

Orvini, E., Speziali, M., Salvini, A., Herborg, C. 2000. Rare Earth Elements determination in environmental matrices by INAA. Microchemical Journal 67, 97–104.

Owens, P.N., Walling, D.E. 1996. Spatial variability of caesium-137 inventories at reference sites: an example from two contrasting sites in England and Zimbabwe. Applied Radiation and Isotopes 47: 699–707.

Parsons, A.J., Foster, I.D.L. 2011. What can we learn about soil erosion from the use of ^{137}Cs? Earth-Science Reviews 108: 101–113.

Parsons, A.J., Wainwright, J., Abrahams, A.D. 1993. Tracing sediment movement in interrill overland flow on a semi-arid grassland hillslope using magnetic susceptibility. Earth Surf. Process. Landforms 18: 721–732.

Perrin, J., Carriera, F., Guillot, L. 2006. Determination of the vertical distribution of radioelements (K, U, Th, Cs) in soils from portable HP-Ge spectrometer measurements: A tool for soil erosion studies. Applied Radiation and Isotopes 64: 830–843.

Phillips, D.L., Gregg, J.W. 2003. Source partitioning using stable isotopes: coping with too many sources. Oecologia 136: 261–269.

Phillips, D.L., Gregg, J.W. 2001. Uncertainty in source partitioning using stable isotopes. Oecologia 127: 171–179.

Plante, A.F., Duke, M.J.M., McGill, W.B. 1999. A tracer sphere detectable by neutron activation for soil aggregation and translocation studies. Sci. Soc. Am. J. 63: 1284–1290.

Polyakov, V.O, Nearing, M.A. 2004. Rare earth element oxides for tracing sediment movement. Catena 55: 255–276.

Polyakov, V.O., Kimoto, A., Nearing, M.A., Nichols, M.H. 2009. Tracing sediment movement on a semiarid watershed using rare earth elements. Sci. Soc. Am. J. 73: 1559–1565.

Polyakov, V.O., Nearing, M.A., Shipitalo, M.J. 2004. Tracking sediment redistribution in a small watershed: implications for agro-landscape evolution. Earth Surf. Process. Landforms 29: 1275–1291.

Porto, P., Walling, D.E., Callegari, G. 2011. Using (137)Cs measurements to establish catchment sediment budgets and explore scale effects. Hydrol. Process. 25: 886–900.

Poulenard, J., Perrette, Y., Fanget, B., Quetin, P., Trevisan, D., Dorioz, J.M. 2009. Infrared spectroscopy tracing of sediment sources in a small rural watershed. Science of the Total Environment 407: 2808–2819.

Pu-Ling L. Jun-Liang T., Pei-Hua, Z., Ming-Yi Y., Hui S. 2004. Stable rare earth element tracers to evaluate soil erosion. Soil and Tillage Research 76: 147–155.

Quine, T.A., Walling, D.E., Chakela, Q.K., Mandiringana, O.T., Zhang, X. 1999a. Rates and patterns of tillage and water erosion on terraces and contour strips: evidence from caesium-137 measurements. Catena 36: 115–142.

Quine, T.A., Govers, G., Poesen, J., Walling, D., van Wesemael, B., Martinez-Fernandez, J. 1999b. Fine-earth traslocation by tillage in stony soils in the Gudalentin, south-east Spain: an investigation using caesium-134. Soil and Tillage Research 51: 279–301.

Rhoton, F.E., Emmerich, W.E., DiCarlo, D.A., McChesney, D.S., Nearing, M.A., Ritchie, J.C. 2008. Identification of suspended sediment sources using soil characteristics in a semiarid watershed. Sci. Soc. Am. J. 72: 1102–1112.

Riebe, B. 1995. Monitoring the translocation of soil particles using a neutron activated tracer. In: K.H., Hartge and B.A. Stewart (Ed.) Soil structure: its development and function. CRC Press. Boca Raton, FL.

Ritchie, J.C., Nearing, M.A., Rhoton, F.E. 2009. Sediment budgets and source determinations using fallout Caesium-137 in a semiarid rangeland watershed, Arizona, USA. Journal of Environmental Radioactivity 100: 637–643.

Rowan, J.S., Goodwill, P., Franks, S.W. 2000. Uncertainty estimation in fingerprinting suspended sediment sources. In Foster, I.D.L. (Ed). Tracers in Geomorphology. John Wiley & Sons. Chichester.

Royall, D. 2001. Use of mineral magnetic measurements to investigate soil erosion and sediment delivery in a small agricultural catchment in limestone terrain. Catena 46: 15–34.

Russell, M.A., Walling, D.E., Hodgkinson, R.A. 2001. Suspended sediment sources in two small lowland agricultural catchments in the UK. Journal of Hydrology 252: 1–24.

Rustomji, P., Caitcheon, G., Hairsine, P. 2008. Combining a spatial model with geochemical tracers and river station data to construct a catchment sediment budget. Water Resources Research 44, W01422, 16 PP, doi:10.1029/2007WR006112.

Sawhney, B.L., Frink, C.R. 1978. Clay minerals as indicators of sediment source in tidal estuaries of Long Island Sound. Clays and Clay Minerals 26: 227–230.

Schoonover, J.E., Lockaby, B.G., Shaw, J.N. 2007. Channel morphology and sediment origin in streams draining the Georgia Piedmont. Journal of Hydrology 342: 110–123.

Schuller, P., Sepúlveda, A., Trumper, R.E., Castillo, A. 2000. Application of the ^{137}Cs technique to quantify soil redistribution rates in palehumults from Central-South Chile. Acta Geologica Hispanica 35: 285–290.

Schwertmann, U., Schmidt, F. 1978. Estimation of long term soil loss using copper as a tracer. Workshop on Assessment of Erosion in USA and Europe, Ghent.

Sharma, D., Meyer, D., Luo, D., Regan, D., Walter, D. 2009. Using Nanobiotechnology to circumvent the "Nonpoint" problem in nonpoint source pollution: Possibilities, challenges, and progress to date. Geophysical Research Abstracts, Vol. 11, EGU2009–12657. EGU General Assembly 2009.

Slattery, M.C., Walden, J., Burt, T.P. 2000. Use of mineral magnetic measurements to fingerprinting suspended sediment sources: results from a linear mixing model. In Foster, I.D.L. (Ed). Tracers in Geomorphology. John Wiley & Sons. Chichester.

Smith, S.V., Renwick, W. H., Buddemeier, R.W., Crossland, C. J. 2001. Budgets of soil erosion and deposition for sediments and sedimentary organic carbon across the conterminous United States. Global Biogeochemical Cycles 15: 697–707.

Spencer, K. L., Droppo, I. G., He, C., Grapentine, L., Exall, K. 2011. A novel tracer technique for the assessment of fine sediment dynamics in urban water management systems. Water Research 45: 2595–2606.

Spomer, R.G., McHenry, J.R., Piest, R.F. 1988. Sediment movement and deposition using Cesium-137 tracer. Trans. ASAE 28: 767–772.

Stevens, C.J., Quinton, J.N. 2008. Investigating source areas of eroded sediments transported in concentrated overland flow using rare earth element tracers. Catena 74: 31–36.

Sutherland, R.A. 1996. Caesium-137 soil sampling and inventory variability in reference samples; literature survey. Hydrol. Process. 10: 34–54.

Sutherland, R.A. 1992. Cesium-137 estimates of erosion in agricultural areas. Hydrol. Process. 6: 215- 225.

Sutherland, R.A. 1991. Examination of caesium-137 areal activities in control (uneroded) locations. Soil Technology 4: 33–50.

Syversen, N., Øygarden,L., Salbu, B. 2001. Cesium-134 as a Tracer to Study Particle Transport Processes within a Small Catchment with a Buffer Zone. J. Environ. Qual. 30: 1771–1783.

Tian, J.L., Zhou, P.H., Liu, P.L. 1994. REE tracer method for studies on soil erosion. International Journal of Sediment Research 9: 39–46.

Ventura, E., Nearing, M.A., Amore, E., Norton, L.D. 2002. The study of detachment and deposition on a hillslope using a magnetic tracer. Catena 48: 149–161.

Ventura, E., Nearing, M.A., Norton, L.D. 2001. Developing a magnetic tracer to study soil erosion. Catena 43: .277–291.

Wallbrink, P.J., Murray, A.S. 1993. Use of fallout radionuclides as indicators of erosion processes. Hydrol. Process. 7: 297–304.

Wallbrink, P.J., Roddy, B.P., Olley, J.M. 2002. A tracer budget quantifying soil redistribution on hillslopes after forest harvesting. Catena 47: 179–201.

Wallbrink, P.J., Murray, A.S., Olley, J.M. 1999. Relating suspended sediment to its original soil depth using fallout radionuclides. Sci. Soc. Am. J. 63: 369–378.

Walling, D.E. 2005. Tracing suspend sediment sources in catchments and river systems. Science of the Total Environment 344: 159–184.

Walling, D.E. 2003. Using environmenral radionuclides as tracers in sediment budgets investigations. In: J. Boge, T. Fergus and D.E. Walling. (Eds). Erosion and sediment transport: Measurement in rivers. IAHS Publication 283. Wallingford.

Walling, D.E., Collins, A.L. 2000. Integrated Assessment of Catchment Sediment Budgets: A Technical Manual. University of Exeter.

Walling, D.E., He, Q. 1999a. Improved models for estimating soil erosion rates from Cesium-137 measurements. J. Environ. Qual. 28: 611–622.

Walling, D.E., He, Q. 1999b. Using fallout lead-210 measurements to estimate soil erosion on cultivated land. Sci. Soc. Am. J. 63: 1404–1412.

Walling, D.E., Schuller, P. Zhang, Y., Iroume, A. 2009. Extending the timescale for using beryllium 7 measurements to document soil redistribution by erosion. Water Resources Research 45, W02418, 13 PP, doi:10.1029/2008WR007143.

Walling, D.E., Collins, A.L., Stroud, R.W. 2007. Tracing suspended sediment and particulate phosphorus sources in catchments. Journal of Hydrology 350: 274–289.

Walling, D.E., He, Q., Appleby, P.G. 2002. Conversion models for use in soil-erosion, soil-redistribution and sedimentation investigations. In: Zapata F. (Ed), Handbook for the assessment of soil erosion and sedimentation using environmental radionuclides, Chapter 7. Kluwer Dordrecht, the Netherlands, pp. 111–164.

Walling, D.E., Golosov, V.N., Panin, A.V., He, Q. 2000. Use of radiocaesium to investigate erosion and sedimentation in areas with high levels of Chernobyl fallout. In Foster, I.D.L. (Ed). Tracers in Geomorphology. John Wiley & Sons. Chichester.

Walling, D.E., He, Q., Blake, W. 1999. Use of ^{7}Be and ^{137}Cs measurements to document short- and medium-term rates of water-induced erosion on agricultural land. Water Resources Research 35: 3865–3874.

Walling, D.E., Peart, M.R., Oldfield, F., Thompson, R. 1979. Suspended sources identified by magnetic measurements. Nature 281: 110–113.

Wei, S. Puling, L., Mingyi, Y., Yazhou, X. 2003. Using REE tracers to measure sheet erosion changing to rill erosion. Journal of Rare Earths 21:587–590.

Wheatcroft, R.A., Olmez, I., Pink, F.X. 1994. Particle bioturbation in Massachusetts Bay: Preliminary results using a new deliberate tracer technique. Journal of Marine Research 52: 1129–1150.

Wilson, C.G., Kuhnle, R.A., Bosch, D.D., Steiner, J.L., Starks, P.J., Tomer, M.D., Wilson, G.V. 2008. Quantifying relative contributions from sediment sources in Conservation Effects Assessment Project Watersheds. Journal of Soil and Water Conservation 63: 523–532.

Woolridge, D.D. 1965. Tracing soil particle movement with Fe-59. Soil Science Society of America Proceedings 29: 469–472.

Wude, Y., Zhaoqian, W., Guoping, S., Guangwei, D. 2008. Quantitative determination of red-soil erosion by an Eu tracer method. Soil and Tillage Research 101: 52–56.

Xingbao, Z., Higgitt, D.L., Walling, D.E. 1990. A preliminary assessment of the potential for using caesium-137 to estimate rates of soil erosion in the Loess Plateau of China. Hydrological Sciences Journal 35: 243–252.

Xue,Y.Z., Liu, P.L., Yang, M.Y., Ju, T.J. 2004. Study of spatial and temporal processes of soil erosion on sloping land using rare earth elements as tracers. Journal of Rare Earths 22: 707–713.

Yang, W., Song, X., Sui, G., Ding, G. 2008. A Europium tracer method for investigating vertical distribution of Loess slope land soil erosion. Communications in soil science and plant analysis, v. 39: 824–842.

Yin, C.Q., Li, L.Q. 2008. An investigation on suspended solids sources in urban stormwater runoff using Be-7 and Pb-210 as tracers. Water Science and Technology 57: 1945–1950.

Young, R.A., Holt, R.F. 1968. Tracing soil movement with fluorescent glass particles. Soil Science Society of America Proceedings 32: 600–602.

Yu, L., Oldfield, F. 1993. Quantitative sediment source ascription using magnetic measurements in a reservoir-catchment system near Nijar, S.E. Spain. Earth Surface Processes and. Landforms 18: 441–454.

Yu, L., Oldfield, F. 1989. A multivariate mixing model for identifying sediment source from magnetic measurements. Quaternary Research 32: 168–181.

Yu, C., Gao, B., Munoz-Carpena, R., Tian, Y., Wu, L., Perez-Ovilla, O. 2011 A laboratory study of colloid and solute transport in surface runoff on saturated soil. Journal of Hydrology 402: 159–164.

Zapata, F. 2003. The use of environmental radionuclides as tracers in soil erosion and sedimentation investigations: recent advances and future developments. Soil and Tillage Research Volume 69, Issues 1-2, pp. 3-13.

Zhang, X., Walling, D.E. 2005. Characterizing Land Surface Erosion from Cesium-137 Profiles in Lake and Reservoir Sediments. J. Environ. Qual. 34: 514–523.

Zhang, X., Quine, T.A., Walling, D.E. 1998. Soil erosion rates on sloping land on the Loess Plateau near Ansai, Shaanxi Province, China: an investigation using ^{137}Cs and rill measurements. Hydrol. Process. 12: 171–189.

Zhang, X.C., Nearing, M.A, Polyakov, V.O., Friedrich, J.M. 2003. Using rare-earth oxide tracers for studying soil erosion dynamics. Sci. Soc. Am. J. 67: 279–288.

Zhang, X.C., Friedrich, J.M., Nearing, M.A., Norton, L.D. 2001. Potential use of rare earth oxides as tracers for soil erosion and aggregation studies. Sci. Soc. Am. J. 65: 1508–1515.

Chapter 2. Evaluation of magnetic iron oxides as sediment tracers in water erosion experiments

Abstract

Water erosion is one of the major concerns with regard to sustainability of agricultural systems in Mediterranean countries (e.g. olive farming areas in Southern Spain). The limitations of the technologies traditionally used in erosion measurement has created increased interest in the use of innovative erosion tracers useful for monitoring erosion and determining deposition rates in the field. In this work, we evaluated the potential of magnetic iron oxide (Fe_3O_4) as a soil tracer. Particle size distribution of the magnetic iron oxide, mobility under drainage conditions and the effect of the aggregate size distribution in blank and tagged soils were studied. The use of magnetic iron oxide to estimate soil losses at small-scale was also examined using a portable rainfall simulator and measuring magnetic susceptibility before and after each simulated rainfall. The properties of the magnetic iron oxide, including a particle size distribution similar to that of soil aggregates, strong binding to soil particles, little mobility in soil, very high magnetic susceptibility relative to the typically low background values of the studied soils, innocuous to environment and low cost, make it an effective soil tracer for estimating soil losses at a small-scale.

Keywords: erosion, tracers, magnetic, iron oxides

Published as: Guzmán, G., Barrón, V., Gómez, J.A. 2010. Evaluation of magnetic iron oxides as sediment tracers in water erosion experiments. Catena 82: 126–133.

2.1. Introduction

Soil erosion and deposition is a process involving various types of mechanisms (e.g. splash vs. rill erosion) that play different roles depending on the scale of measurement and the characteristics of the terrain. The traditional technology for measuring water erosion, such as runoff tanks or water flow meters at hillslope- and watershed-scale respectively, provides an average value for net sediment losses (the balance between total erosion minus deposition) and is relatively expensive to maintain (Lal, 1994). Researchers have pursued the development of erosion tracers capable of tracking sediment within the landscape, or for the determination of average soil losses without the need to maintain relatively expensive infrastructures.

According to Zhang *et al*. (2001), an ideal tracer for studying soil erosion and sediment sources should be able to bind strongly with soil particles or easily incorporated into soil aggregates; possess a high analytical sensitivity; afford easy, inexpensive measurements; have low background concentrations in soil; not interfere with sediment transport; have a low biological uptake; be environmentally benign; and have availability of multiple tracer signals. Researchers have not yet found an optimum tracer (that is, one fulfilling all these requirements) despite the endeavors in this direction over the years.

A great deal of attention has been devoted to the use of radionuclides, used for studying soil erosion in a medium–long term. Some are anthropogenic, such as ^{59}Fe (Wooldridge, 1965) or ^{137}Cs (Walling and He, 1999) coming as a fallout after a nuclear explosion, and some are of cosmogenic origin, such as ^{210}Pb or ^{7}Be (Wallbrink and Murray, 1993). In most cases, the studies measure radionuclides that have been incorporated into the soil by natural processes, such as atmospheric deposition of nuclear test material. In some studies, however, researchers have deliberately incorporated them into the soil (e.g. Syrvesen *et al*. 2001); only a few test of this type have been conducted because of the radiological hazards involved.

One of the greatest problems in using radionuclides is the difficulty of obtaining an appropriate reference for their concentration in the soil profile in the absence of erosion. Another difficulty is understand the process governing radionuclide loss and mobilization in the soil profile (e.g. by effect of mixing by tillage or selective transport of finer soil particle by runoff) in order to select and calibrate an appropriate model (Walling and He, 1999). Exotic materials have been used as water erosion tracers, such as glass beads and fluorescent dyed particles (Young and Holt, 1968), magnetic plastic beads (Ventura *et al*. 2002) or tillage erosion tracers, such as steel nuts (Lindstrom *et al*. 1992). However, these pose the problem that they are selectively transported because they have different density, size and shape from soil aggregates, and they failing to bind to the soil (Ventura *et al*. 2002). Also, they must be employed in large amounts which restrict their use to small areas.

Other researchers have labeled soils using noble metals (e.g. Ag, Au, Wheatcroft *et al*. 1994), organophilic clay quats (Mentler *et al*. 2009) and rare earth oxides (Polyakov and Nearing, 2004; Polyakov *et al*. 2004; Stevens and Quinton, 2008). One of the most developed among these approaches is that using rare earth oxides mixed as a dry powder with soil and incorporated by excavation or surface tillage of the soil. Zhang *et al.* (2001, 2003) and Kimoto *et al*. (2006) have demonstrated its use for sediment tracing in small basins under temperate and semiarid conditions, respectively. Kimoto *et al*. (2006) observed a differential binding of these tracers in soil containing large sand and rock fractions, which complicates the interpretation of the experimental results and increases the number of analyses and their cost. The binding affinity for the smaller, more chemically active, soil clay particles is a common feature not only of rare earth oxides, but also of other tracers such as ^{137}Cs and magnetic minerals (Crockford and Willet, 2001).

Magnetic soil properties such as magnetic susceptibility have been extensively used, both in isolation and in combination with other soil properties, for sediment fingerprinting in catchments (e.g. Royall, 2001; Owens *et al*. 2000) by exploiting the difference in magnetic properties of minerals developing in soils of different origin (or evolution) within the study area and using mixing models to interpret the results.

Southern Spain experiences severe erosion problems (Kirkby *et al*. 2004) because of the combination of steep slopes, Mediterranean type of climate and inappropriate soil management. There is also a shortage of erosion data at the hillslope- and watershed-scale (e.g. Gómez *et al*. 2008), which has hindered a better understanding of erosion process and with a view to accurately assessing soil conservation techniques for implementation in the region.

Few erosion tracers have been tested in southern Spain, and most were based on ^{134}Cs (Quine *et al*. 1999) and ^{137}Cs radionuclides (Schoorl *et al*. 2004a,b). One of the reasons for the scarcity of these studies is their high cost, especially in systems such as perennial crops that exhibit large spatial variability, such as orchards because of tree effects above and below ground (e.g. Gómez *et al*. 1999). Having an erosion tracer which could be used without much complexity and at moderate cost in erosion studies would afford a better method of studying erosion processes and experimentally evaluating soil conservation techniques.

This Chapter reports the results on the use of magnetic iron oxide as an erosion tracer. Magnetic iron oxide is a black powder normally used as a concrete pigment for construction. It is commercially available in large amounts at moderate price (2.5 €·kg^{-1}). It binds to the different soil aggregates and its background concentration within soils allows its easy, non-destructive and relatively inexpensive determination via magnetic properties, such as magnetic susceptibility. These characteristics make magnetic iron oxide a useful tool to study detachment and deposition of soil after rainfall events.

The main objectives of this Chapter are as follows: *(i) to understand the short-term vertical mobility and distribution of the magnetic iron oxide used as a tracer of four typical soils of agricultural areas in southern Spain* and *(ii) to evaluate the performance of the magnetic iron oxide in small scale rainfall simulation experiments in order to explore its lateral mobility and possibilities at a larger scale.*

2.2. Materials and methods

2.2.1. Soil and magnetic tracer characteristics

Four soils representative of different cultivation areas in Andalusia and spanning a diversity of textural classes were collected from agricultural fields. The key properties of the four soils, hereafter designated Alameda, Benacazón, Conchuela and Pedrera, are described in Table 2.1.

Property	Soil			
	Alameda	Benacazón	Conchuela	Pedrera
Bulk density ($Mg \cdot m^{-3}$)	1.4 ± 0.0	1.4 ± 0.1	1.4 ± 0.0	1.6 ± 0.1
Clay (%)	11.5 ± 0.2	11.8 ± 0.8	48.6 ± 0.3	34.6 ± 1.2
Silt (%)	46.3 ± 0.7	8.5 ± 0.6	44.3 ± 0.5	33.8 ± 0.7
Sand (%)	42.2 ± 0.6	79.7 ± 0.8	7.1 ± 0.8	31.6 ± 1.5
Organic matter (%)	0.9 ± 0.1	1.6 ± 0.5	1.4 ± 0.3	1.6 ± 0.1
Soil taxonomy*	*Typic Xerofluvent*	*Petrocalcic Palexeralf*	*Typic Haploxerert*	*Calciorthidic Xerochrept*

Table 2.1. Basic properties of the studied soils. Average values ± standard deviations. *(USDA Soil Taxonomy, 1999).

The tracer used was a synthetic magnetic iron oxide (Fe_3O_4) commercially available as Bayferrox® 318 M and used mainly as a black powder pigment. Some of its properties are shown in Table 2.2.

Characteristics	
Fe_2O_3 content (%)	~92
SiO_2+Al_2O_3 content (%)	<3
Particle shape	Spherical
Predominant particle size (μm)	0.2
Density ($Mg\ m^{-3}$)	~4.6

Table 2.2. Characteristics of the used magnetic iron oxide. Source: Datasheet Bayferrox® 318M (available at *http://www.csc−jaekle.de/fileadmin/MeBl/380/MeBl_380405_EN.pdf*).

Its crystallochemical composition was determined by X-ray diffraction analysis on a Siemens D5000 instrument using CoKα radiation. Particle size and shape were examined with a JEOL JSM 6300 scanning electron microscope. Additionally particle size distribution in the magnetic iron oxide was determined with the pipette method according to Zhang *et al*. (2001), using variable times from 1 to 10.800 s, calculated for some predetermined sizes (53-0.5 μm). Measurements were conducted at room temperature (≈25 °C).

2.2.2. Soil-tracer mixture preparation

Samples of the four types of soil were taken from the field, air dried and passed through a 6 mm sieve. The sieved soil was then mixed by serial dilutions in dry soil with the magnetic iron oxide according to Zhang *et al*. (2001) in order to increase the background magnetic susceptibility (~10^{-7} $m^3 \cdot kg^{-1}$) by two orders of magnitude. The concentration of the magnetic iron oxide in the four soils was 2.4 % of the total dry weight of each mixture. The soil–tracer mixture was slightly wetted with tap water, air dried and mechanically disaggregated; the procedure was repeated three times to ensure binding of the magnetic iron oxide to the soil and uniform distribution in it.

2.2.3. Magnetic susceptibility measurement

Tagged and untagged air dried soil samples were subjected to mass specific susceptibility (χ) measurements at a low frequency (0.47 kHz), using a Bartington® meter and an MS2B® dual frequency sensor. Soil sample masses ranged from 2 to 20 g depending on the amount of sample obtained or taken in each test performed. All measurements were made in triplicate. Samples were mechanically disaggregated and sieved through a 2 mm screen opening sieve before measurement.

2.2.4. Measurement of aggregate size distribution

Aggregate size distribution of blank and tagged soil was determined by dry sieve analysis, using a Retsch AS 200 basic ® apparatus. Two hundred grams of air dried soil was sieved for 150 s at amplitude 2 mm, which provided 11 different sizes from 8000 μm to 10 μm (viz. 8000, 4000, 2000, 1000, 500, 250, 125, 63, 45, 25, 10 μm). All analyses were performed in triplicate.

2.2.5. Particle size analysis

Particles size analyses of different soil and sediment samples were determined following the standard hydrometer method preceded by soil dispersion of the sample (Gee and Bauder, 1986). Particle size was determined for each of the aggregate size smaller than 2 mm of the blank soil obtained by dry sieving, see Section 2.2.4. The particle size of the sediment collected during the rainfall simulations experiments, see Section 2.2.7 and from the soil surface (0-0.03 m) after the same rainfall simulation. All particle size analyses were performed in duplicate.

2.2.6. Percolation test

Plastic boxes (0.35 m wide, 0.45 m long and 0.35 m deep) with a drainage system at the bottom were prepared to study the mobility of the magnetic iron oxide under drainage in the tagged soils. The boxes were filled with blank unsieved soil that was placed in five layers 0.03 m deep each. Each layer was consolidated independently by slightly moistening its surface and pressing it by hand down to a preset reference level marked on the soil box walls. Tagged soil prepared as described above was placed in two layers of 0.03 m deep each on top of the unsieved soil. A layer of permeable weed barrier cloth was used to identify and maintain the delineation between blank and tagged soil. Also, a control box for each of soil type was used where the two top 3 cm soil layers were also untagged (sieved at 6 mm as the tagged soil).

Using the methodology described by Zhang *et al*. (2001), 2 L of deionized water was carefully poured every 4 days over a period of 40 days, and the resulting leachate was collected to measure magnetic susceptibility before the next addition. After the percolation test was completed, each soil layer of 0.03 m was removed separately using a graduate spatula and air dried to measure its magnetic susceptibility.

2.2.7. Rainfall simulations

A portable rainfall simulator (Alves *et al*. 2008) was used to assess the potential of the magnetic iron oxide for estimating soil losses by water erosion at a small-scale. Four wood boxes, one per soil type (0.7 m wide, 1.0 m long and 0.3 m deep) with drainage orifices at the bottom covered by a piece of geotextile were prepared and filled with soil in several steps. The arrangement of the soil layers were a compromise between the intention of reproducing a field situation, and the need to minimize the amount of soil sieved to prepare the boxes. The first two layers, 0.03 m thick each, were untagged, unsieved soil. These two layers were needed to make a larger soil depth and favor the drainage. On top of them, two layers 0.04 m thick each of untagged sieved soil (at 6 mm screen opening) were placed to make a good transition between tagged sieve soil and blank unsieved soil. Finally, a 0.04 m thick layer of tagged soil (prepared as explained in Section 2.2.2 above) was placed on top. Each layer was consolidated independently as described in the percolation test. The weight of soil in each layer was recorded in order to estimate bulk density.

The experiment involved three rainfall simulations at 60 mm/h rainfall intensity. Rainfall was simulated for one, two and three hours in the first, second and third simulation, respectively, with a drainage period of one day between the first and the second simulation, and two days between the second and third to ensure the complete drainage of soil. Each box had a slope of 12 %. The bottom side of the box acting as runoff outlet was leveled to the soil surface to prevent sediment deposition before each event.

Runoff and sediment samples collected during the rainfall simulations were used to determine total runoff and sediment loss, and the latter also to measure magnetic susceptibility and the particle sizes of the eroded sediment. To account for soil losses by splash not accounted in the soil losses by runoff calculated from the runoff samples taken during the experiment, each box was weighed on a 150 kg scale with 0.03 % accuracy before and after each rainfall event, and its soil moisture was measured by gravimetric sampling in order to calculate the dry weight of soil. This allowed an estimation of the combined soil losses due to splash and runoff by difference from the original soil weight.

Approximately 20 h after each simulation, samples of soil were collected at different points from the boxes in order to measure magnetic susceptibility and bulk density of the top layer (0-4 cm). To avoid repeated sampling at the same point, the soil surface was split into grids 0.12×0.1 m in size and each grid recorded. Following sampling after the first and second rainfall simulations the hole made during the sampling (2.5 cm diameter) was refilled with tagged soil up to surface level. In addition, surface soil layers were sampled at variable depths (0-0.5, 0.5-1, 1-3 cm) at the end of the final simulation in order to determine particle size.

To estimate soil losses we used a mass balance based on the magnetic susceptibility readings of the top 4 cm of the soil and lost sediment. First, all measurements of magnetic susceptibility were converted into net magnetic susceptibility calculated by subtracting the background magnetic susceptibility of the blank soil from that of the tagged soil.

Magnetic susceptibility changes in the sampled soil (0-0.04 m) occur due to two main processes: *(i) loss of the magnetically tagged topsoil due to splash and runoff erosion, which results in a decrease in magnetic susceptibility of the sampled soil*, and *(ii) incorporation of the underlying and untagged soil into the depth of sampling because of soil consolidation which also results in a decrease of magnetic susceptibility of the whole sample, even without soil loss*.

The net loss of magnetic susceptibility, $\Delta\chi$, is defined by equation (2.1) derived from the mass balance of the applied tracer at the sampling depth assuming that there is no uptake by vegetation or vertical movement of by percolation of the magnetic tracer:

$$\Delta\chi = \left[\left(\frac{\chi_o - \chi_f}{\chi_o}\right) - \left(\frac{\chi_o - \chi_o \cdot f_c}{\chi_o}\right)\right]\frac{1}{f_s} \tag{2.1}$$

Where χ_o is the net magnetic susceptibility of the soil at the beginning of the experiment; χ_f the net magnetic susceptibility of the soil after the rainfall simulation; f_c is a consolidation factor defined as the ratio of the bulk density at the beginning of the experiment divided by the bulk density at the time of sampling; f_s is a selectivity factor to account for possible increase in the magnetic susceptibility of the sediment compared to the topsoil due to preferential factor of smaller aggregates and is calculated as the ratio of the net magnetic susceptibility of the sediment divided by the net magnetic susceptibility of the tagged soil. In this model f_c has an upper limit of one, meaning that if the tagged top soil were subjected to a decrease in its density (for example, a vertic soil may expand) we would have not detected differences in the magnetic susceptibility readings. This is because these measurements are normalized by the weight of the sample, hence would take into consideration that decrease in density.

The $\Delta\chi$ was converted into soil loss using equation (2.2), based on the consideration that loss of net magnetic susceptibility due to loss of the tracer is proportional to the soil loss after the corrections introduced in equation (2.1):

$$S = \frac{w}{a} \cdot \Delta\chi \tag{2.2}$$

Where S (kg/m^2) is the estimated soil losses, w (kg) the weight of soil in the tagged layer at the beginning of the experiment, a (m^2) the area of tagged soil layer in the boxes, respectively.

2.3. Results and discussion

2.3.1. Characterization of the magnetic iron oxide

The magnetic iron oxide exhibited the typical diffraction X-ray lines for the mineral magnetite, Fe_3O_4 (File 19-629 Powder Diffraction File from the Joint Committee on Powder Diffraction Standards), in addition to three weak peaks that were assigned to impurities of goethite, α-FeOOH, and quartz, SiO_2 (Figure 2.1), as per the manufacturer´s specifications (content of $SiO_2 + Al_2O_3$ <3%; Table 2.2).

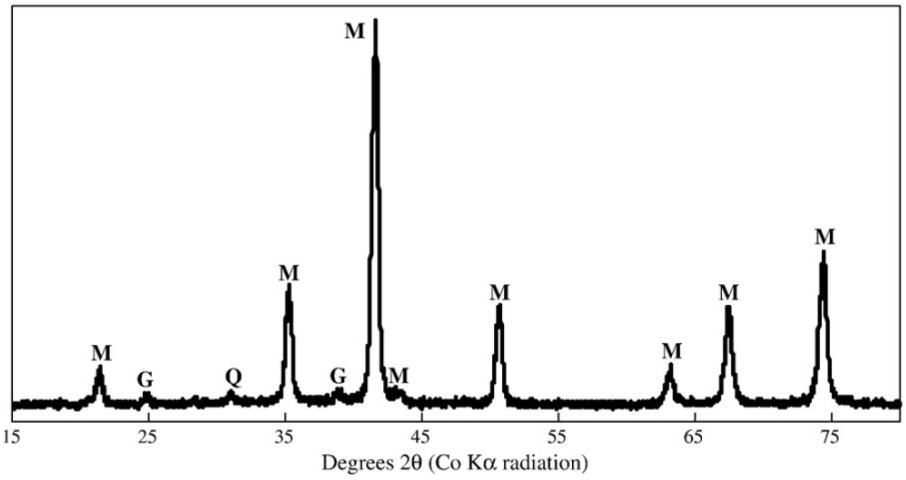

Figure 2.1. Powder X-ray diffraction pattern for the magnetic iron oxide. M-magnetite; G- goethite; Q- quartz.

Transmission electron microscopy images showed small individual particles (<0.4 μm) forming large clusters or aggregates in micrometric sizes (Figure 2.2). In fact, based on the particle size results provided by the pipette method, more than 95 % of the total weight of the magnetic iron oxide corresponded to the silt size range for soils (50-2 μm) (Figure 2.3). The seventeen couples of experimental points of particle size distribution were fitted to the following sigmoid equation 2.3 with r^2=0.99.

$$y = 98.7/\{1 + \exp[-(x - 6.3)/0.7]\} \qquad (2.3)$$

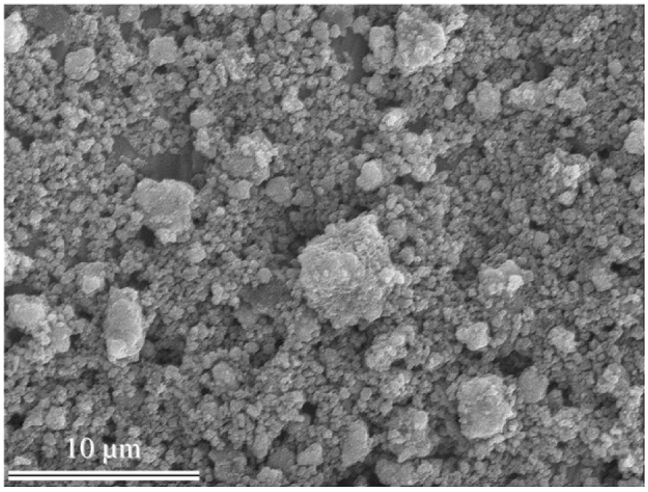

Figure 2.2. Scanning electron micrograph of the magnetic iron oxide.

From distribution in Figure 2.3, D_{50} for the magnetic iron oxide was calculated as 6.5 µm.

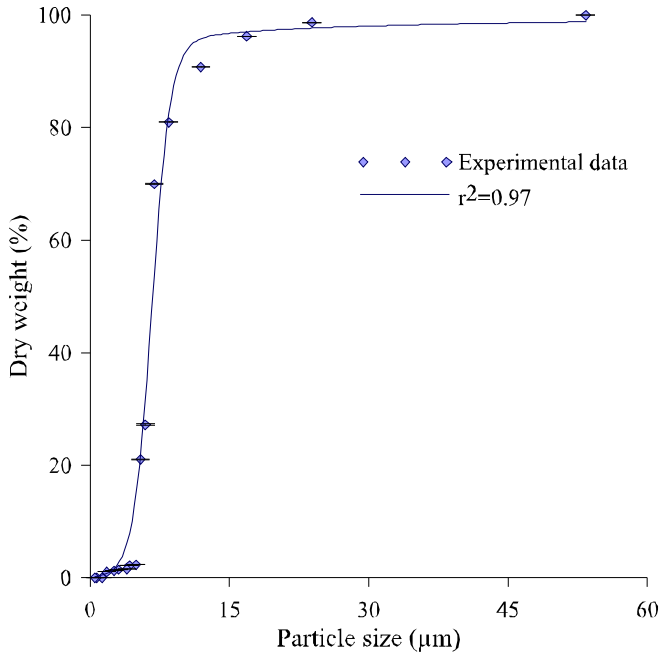

Figure 2.3. Particle size distribution of the magnetic iron oxide, average experimental data and standard deviation.

The magnetic susceptibility value obtained, χ, 485×10^{-6} $m^3 \cdot kg^{-1}$ falls within the typical range for magnetite (Peters and Dekkers, 2003) and is four orders of magnitude higher than those for the studied soils (see Section 2.3.3).

2.3.2. Effect of tagging with magnetic iron oxide on aggregation

Figure 2.4 shows the distribution of the dry weight of the soil into aggregate sizes upon dry sieving in tagged and untagged soil. The overall distribution changed relatively little by effect of tagging, over the short period examined, despite the increase in 2.7 % in the iron oxide content of the soils; some aggregate sizes, mostly in the larger ones (>1 mm), however, exhibited significant differences comparing tagged and untagged distributions (p values were lower than 0.05 and 0.01 in some cases). The differences in the larger aggregates can be ascribed to the short time available for the tagged soil to form them after the sieving and mixing involved in the tagging process. This was especially so in the Conchuela soil (a vertic soil). The results of Figure 2.4 suggest that the differences in aggregate size distribution from the original, untagged soil were relatively small. Depending on the type of experiment to be performed, such differences can be further reduced by tagging the soil months in advance in order to allow further aggregation of tagged soil, or, if the scale used allows processing of the untagged soil (in sieving–drying–wetting cycles) identically as the tagged soil.

2.3.3. Distribution of magnetic tracer according to aggregate size

Figure 2.5 depicts the magnetic susceptibility, χ, of the tagged and untagged soils. Since χ for tagged soil was basically due to magnetic iron oxides particles attached to soil aggregates (and two orders of magnitude higher than for untagged soil) it can be useful as a proxy for the concentration of magnetic tracer.

Magnetic susceptibility increased (indicating a higher concentration of magnetic iron oxide) with decreasing aggregate size, below 125 μm, in the four tagged soils, where b was approximately twice the lowest values measured in the largest aggregates. The magnetic tracer concentrated relatively uniformly between aggregate sizes over the range 8000 to 250 μm (Figure 2.5).

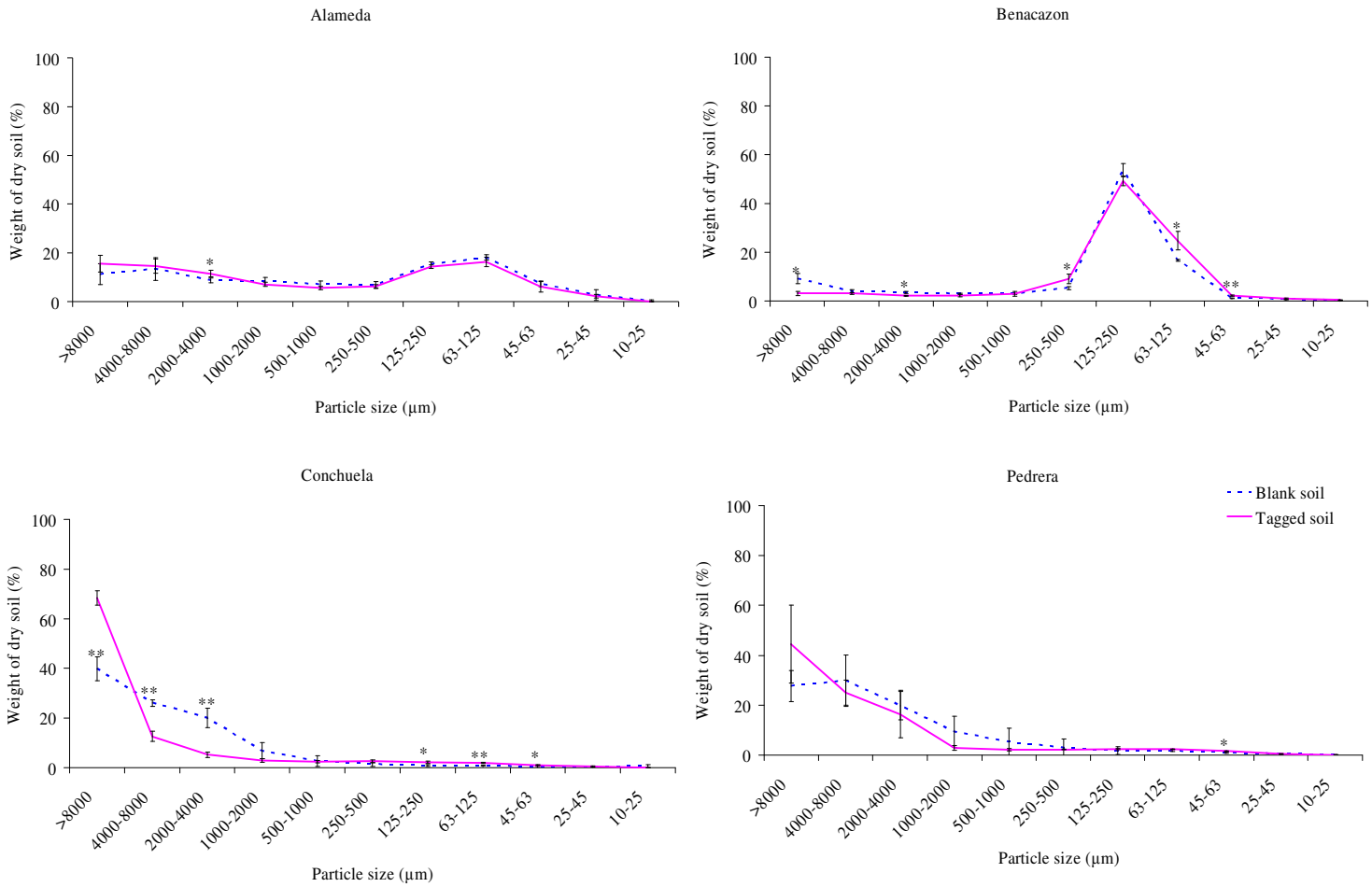

Figure 2.4. Aggregate size distribution of tagged and untagged soils. One star means significant differences at $p<0.05$, and two mean significant differences at $p<0.01$.

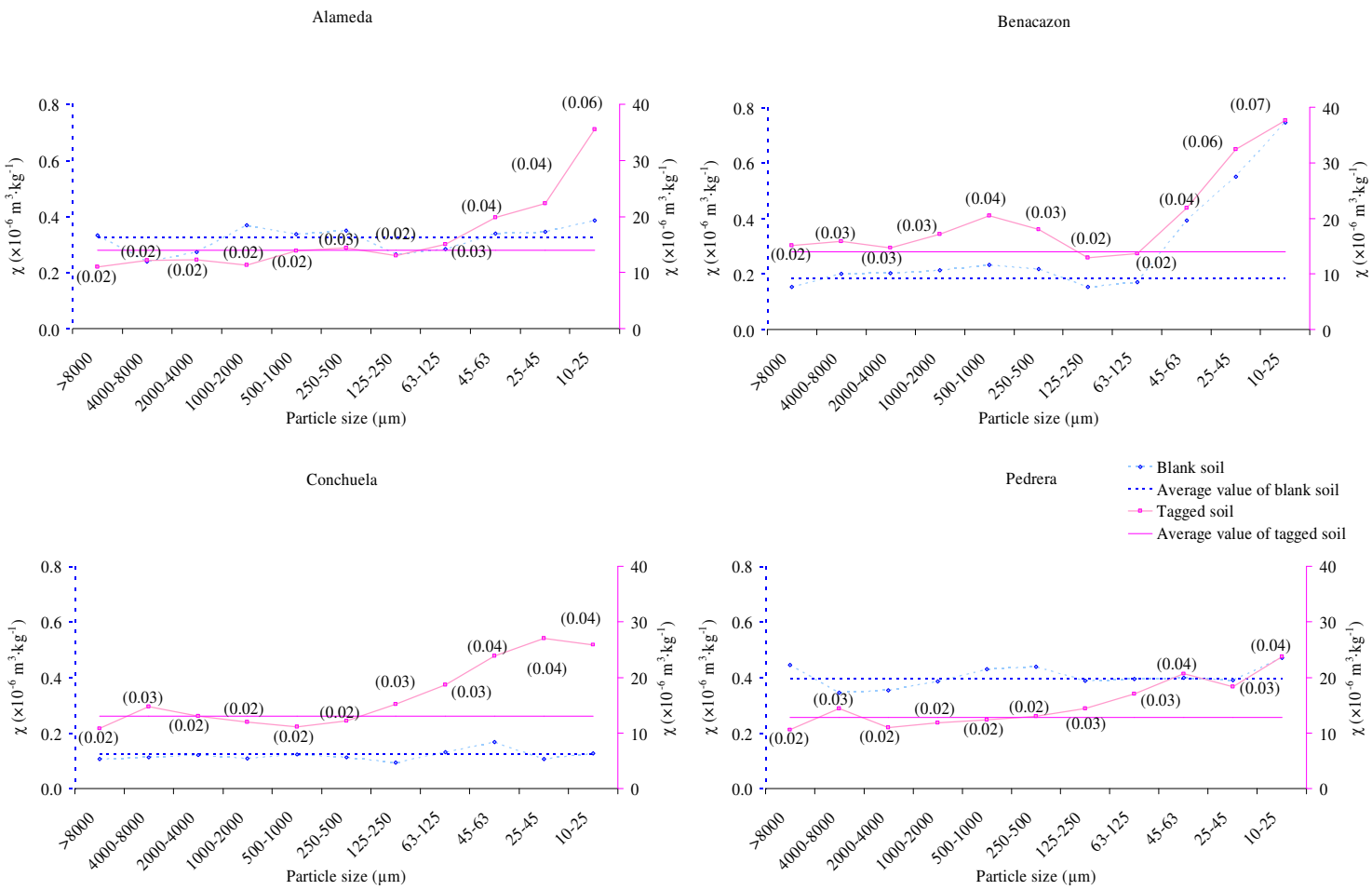

Figure 2.5. Magnetic susceptibility of the different aggregate sizes in the tagged and untagged soils. For tagged soil, the magnetic iron oxide fraction for each particle size is shown in brackets. Note that the primary y-axis shows χ for the untagged soil and the secondary y-axis χ for the tagged soil.

There was significant correlation between magnetic susceptibility and the clay content of each aggregate size in the four tagged soils (Table 2.3), the smaller aggregates having the higher clay contents and magnetic susceptibility.

Soil	χ /clay Blank soil R	χ /clay Blank soil R
Alameda	0.72	0.85
Benacazón	0.96	0.93
Conchuela	0.14	0.90
Pedrera	0.63	0.87

Table 2.3. Correlation between magnetic susceptibility and clay content of the different aggregate sizes in each soil type. Blank and tagged soils.

It should be noted that the smaller aggregate sizes that departed significantly from the average magnetic susceptibility for each soil accounted for only a small fraction of the total soil weight (Figures 2.4 and 2.5). The untagged soil, exhibiting the greatest differences in clay content between aggregate sizes (Benacazón) had a similar variation in magnetic susceptibility (due to magnetic iron oxides naturally present in it) with aggregate size; the other three soils exhibited a more uniform distribution of background χ among aggregate sizes (Figure 2.5).The variability in χ, and hence that in magnetic tracer distribution, among aggregate sizes fell within the ranges found by other authors in studies of rare earth oxides, which are slightly larger in size than the magnetic oxide used in these experiments, and were incorporated into the soil by following a similar procedure. Kimoto *et al*. (2006) found an average variation of around 3800 % in the concentration of the rare earth oxide tracers in very coarse soils in an arid environment depending on the aggregate size; the differences peaked in the aggregates smaller than 40 μm and were smallest in those larger than 2 mm. They ascribed this non-uniform binding pattern to the high tagging selectivity of clay minerals, which concentrated in the smaller aggregates in their soils. In order to correct the error derived from this non-uniform binding pattern in situations of selective transport of different aggregate sizes, these authors recommend analyzing the tracer concentration in terms of aggregate size in the sediment.

Previously, Zhang *et al.* (2001) had used the same rare earth oxides, mixed in a similar way, on a silt loam soil in the US Midwest and found a more uniform distribution of their tracers among aggregate sizes than that of Kimoto *et al.* (2006), and also slightly more uniform than that reflected in Figure 2.5; however, there were still significant differences in concentration (around 175 %) between the aggregate sizes with the highest and lowest concentrations. Zhang *et al.* (2001) assumed that they had achieved uniform incorporation of their tracers into the soil, and also that no separation by aggregate size was needed to correct for selective transport. This approach was later shown to be effective by Zhang *et al.* (2003) by operating at the flume-scale with the same silt loam soil.

The selectivity of tracers for a given particle or aggregate size, and selective transport by erosion, are two recurrent issues in sediment tracing studies, not only with rare earth oxide tracers, but also with the ^{137}Cs models used to determine sediment losses and transfer within the landscape. The most sophisticated ^{137}Cs models use a particle size correction factor to consider the effect of selective transport (Walling and He, 1999); however, it is not uncommon to assume non-selective transport (Zhang *et al.* 1998). In fingerprinting studies of sediment sources based on various soil properties (from ^{137}Cs to different element concentration), the correction factor is determined as the ratio of specific surface area between the bulk sediment sample and the sediment following sieving through a given screen mesh (usually 63 μm), the sieved sample being used for analysis (e.g. Owens *et al.* 2000).

Binding uniformity in the magnetic iron oxide following mixing according to Zhang *et al.* (2001), while not perfect, is not far from what these authors deem uniform. Given the small fraction of total soil weight contained in the small aggregates, we can assume that, except in those situations where selective transport of fine particles is substantial, it probably has little effect on the accuracy of measurements made with the magnetic tracer. However, the simplicity of the analytical techniques involved, separation by aggregate sizes, measurement of particle size analysis and magnetic susceptibility, might allows to measure and correct, if required, soil or sediment samples by aggregate sizes with uniform magnetic susceptibility or, as shown below by particle size composition in sediments.

2.3.4. Mobility of the magnetic iron oxide in soil

Tables 2.4 and 2.5 show the main results of the percolation tests as performed under controlled conditions in the soil boxes. Table 2.4 compares the magnetic susceptibility of the soils immediately after mixing and following standing in the boxes.

Soil	Magnetic susceptibility of tagged soil ($\times 10^{-6}$ m^3 kg^{-1})		Probability (p)
	Just mixed at the laboratory (n = 12)	Placed in boxes at the end of the experiment (n = 12)	
Alameda	14.0 ± 0.92	13.4 ± 0.74	NS 0.128
Benacazón	14.0 ± 0.62	13.6 ± 0.27	NS 0.079
Conchuela	13.1 ± 1.67	13.5 ± 0.74	NS 0.428
Pedrera	12.8 ± 1.38	13.6 ± 0.29	NS 0.070

Table 2.4. Average magnetic susceptibility, standard deviation and probability of significant differences for tagged soil before and after the percolation test. (NS = not significant, p>0.05).

Table 2.5 compares magnetic susceptibility at the end of the percolation tests in the untagged soil layers (6–21 cm) with that in untagged soil in the control box.

Soil	Magnetic susceptibility of untagged soil ($\times 10^{-6}$ m^3 kg^{-1})		Probability (p)
	Untagged soil layers in tagged soil boxes 6–21 cm (n = 18)	Untagged soil layers in untagged soil boxes 0–21 cm (n = 30)	
Alameda	0.33 ± 0.04	0.31 ± 0.02	NS 0.128
Benacazón	0.16 ± 0.01	0.17 ± 0.01	NS 0.099
Conchuela	0.14 ± 0.01	0.12 ± 0.01	NS 0.452
Pedrera	0.43 ± 0.02	0.41 ± 0.02	NS 0.063

Table 2.5. Average, standard deviation and probability of significant differences between magnetic susceptibility of the untagged soil layers in the control and tagged soil boxes at the end of the percolation experiment. (NS = not significant, p>0.05).

The lack of significant differences in this respect suggests that the procedure followed to prepare the soil boxes minimizes losses of the tracer, that the magnetic iron oxide binds strongly to soil particles and that leaching is minimal in the short-term. The magnetic susceptibility readings of percolated water (results not shown) coincided with those for deionized water, which indicates that no leaching of the magnetic iron oxide occurred. Therefore, the magnetic tracer seems to be immobile in the short-term under leaching conditions in the studies soils, which is consistent with the findings of Zhang *et al*. (2001) and Kimoto *et al*. (2006) in rare earth oxides. By comparison with other iron oxides one can expect the tracers to exhibit some mobility through the soil in the long-term by a process similar to clay illuviation or mechanical mobilization. With ^{137}Cs, one can also expect vertical migration of the tracer in the long-term by physical processes such as strong adsorption onto soil particles (Ritchie and McHenry, 1990). The simplicity and moderate cost of sampling and analysis of magnetic susceptibility will afford systematic monitoring of potential long-term migration of the tracer into the soil profile.

2.3.5. Evaluation of soil losses in rainfall simulation experiments

Figure 2.6 compares the cumulative soil losses measured after each rainfall simulation (on the 1×0.7 m boxes) with the estimated soil losses obtained from mass balance of the remaining tracer based on the decrease in magnetic susceptibility of the tagged soil layer sampled after each rainfall simulation (Table 2.6) as determined from equations (2.1) and (2.2).

As can be seen from Figure 2.6, measurements of magnetic susceptibility of the tagged soil depth captured the magnitude of the erosion rate without bias. In addition, Figure 2.6 provides an indication of the potential accuracy of the magnetic erosion tracers under the assumed optimal conditions. We understand for optimal conditions the possibility of taking a relatively large number of samples in relation to the surface explored (0.7 m^2) and the capability of controlling the different sources of error, such as consolidation of the soil surface, selective detachment of soil aggregates in the soil surface or uneven tagging of the soil surface.

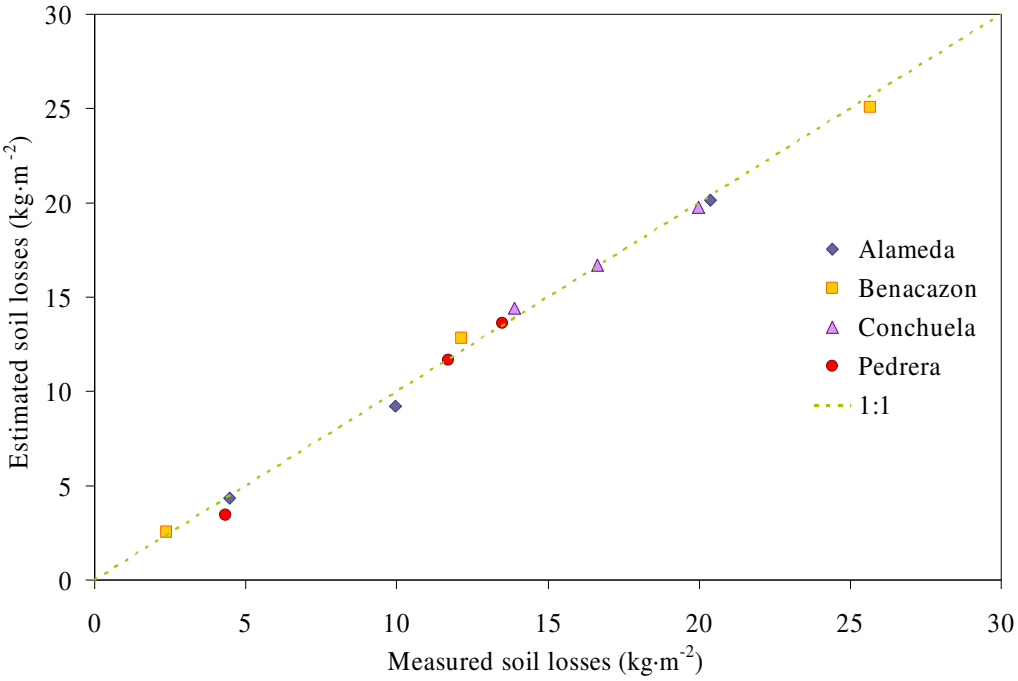

Figure 2.6. Measured and calculated (based on magnetic susceptibility measurements) soil losses after rainfall simulations in the four soils.

Magnetic susceptibility ($\times 10^{-6}$ m^3 kg^{-1})				
Soil	Alameda	Benacazón	Conchuela	Pedrera
Blank soil	0.32 ± 0.01	0.18 ± 0.01	0.13 ± 0.01	0.39 ± 0.03
Tagged soil	14.12 ± 0.64	13.89 ± 0.27	14.82 ± 0.35	15.89 ± 0.24
Soil samples (0–0.04 m)				
1st simulation	12.82 ± 1.01	13.14 ± 1.05	12.12 ± 2.17	15.10 ± 1.94
2nd simulation	11.94 ± 0.85	10.53 ± 2.32	11.70 ± 0.99	12.88 ± 1.56
3rd simulation	9.73 ± 1.15	8.09 ± 2.40	11.00 ± 1.37	12.77 ± 1.65
Sediment	13.50 ± 1.89	12.21 ± 1.50	13.11 ± 0.27	14.87 ± 0.21
Probability (p)	NS 0.238	NS 0.101	NS 0.074	NS 0.112

Table 2.6. Average and standard deviation of magnetic susceptibility for blank and tagged soils, soil samples (0-0.04m) after each rainfall simulation and sediments after the third rainfall event, for the four studied soils. Probability of significant differences between the magnetic susceptibility values for tagged soil and sediment. (NS = not significant, p>0.05).

Figure 2.7 shows the relative error in the erosion values and provides an estimate of the uncertainty in erosion predictions with this magnetic oxide as a tracer for determining erosion rates in this highly controlled experiment.

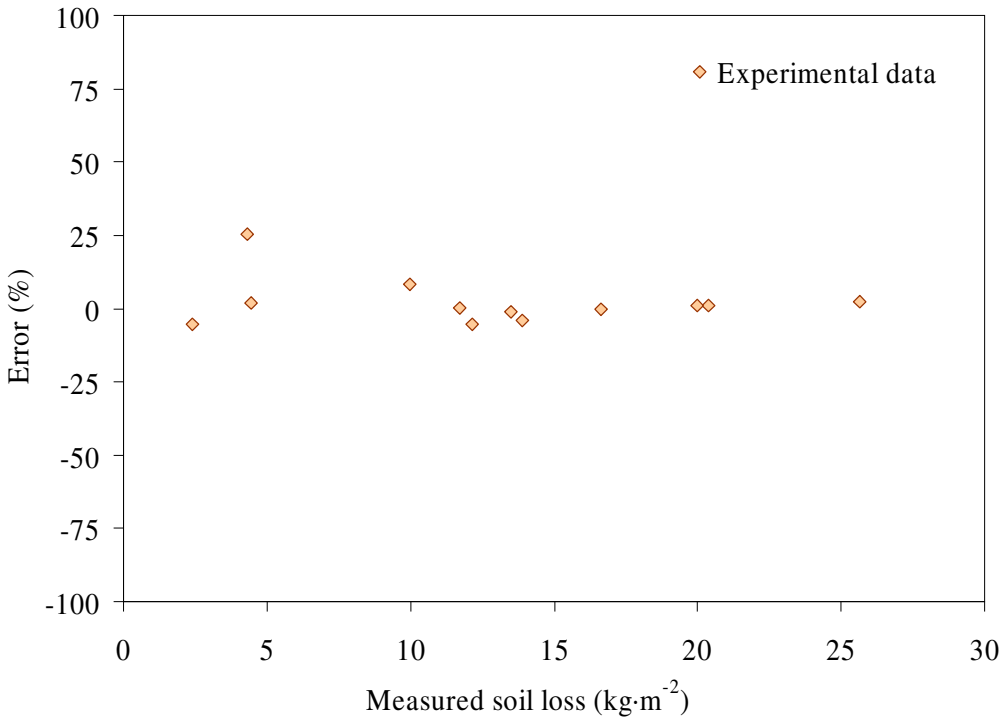

Figure 2.7. Empirical relationship between relative errors in estimated soil losses as a function of total soil losses derived from the results of the rainfall simulation experiment.

Ventura *et al*. (2002) found the tracer not to move in phase with soil aggregates at the small plot-scale. This behavior can be explained because of the size and density of the tracer compared to soil sediment, and simulated rainfall intensity. Rather, they found preferential erosion of tracer, and hence an increase in magnetic susceptibility in the eroded sediment. In this work, conducted at a smaller scale we observed no selective transport of smaller clay particles in the sediment (Table 2.7), thus, the clay, silt and sand contents of the sampled top 4 cm of soil exhibited no significant change, in this respect.

Soil	Alameda	Benacazón	Conchuela	Pedrera
Soil surface after simulation (0–0.005 m)				
Clay (%)	11.4 ± 0.7	9.8 ± 0.0	52.4 ± 2.4	25.6 ± 1.3
Silt (%)	45.2 ± 0.6	6.8 ± 0.9	39.4 ± 0.5	31.8 ± 2.0
Sand (%)	43.4 ± 0.1	83.4 ± 0.9	8.1 ± 1.9	42.7 ± 2.1
Blank soil (0.005–0.01 m)				
Clay (%)	13.5 ± 1.6	9.8 ± 0.0	53.8 ± 0.5	30.1 ± 1.0
Silt (%)	44.5 ± 1.6	6.2 ± 0.0	38.1 ± 0.5	34.5 ± 1.2
Sand (%)	42.0 ± 0.0	84.1 ± 0.0	8.1 ± 0.0	35.4 ± 0.7
Blank soil (0.01–0.03 m)				
Clay (%)	12.9 ± 0.7	7.8 ± 0.0	51.2 ± 1.0	29.4 ± 1.0
Silt (%)	41.8 ± 0.4	11.3 ± 0.9	42.3 ± 2.2	35.2 ± 1.2
Sand (%)	45.4 ± 1.1	80.9 ± 0.9	6.5 ± 3.2	35.4 ± 0.7
Tagged sediment				
Clay (%)	12.4 ± 0.2	9.8 ± 0.0	48.7 ± 0.6	34.6 ± 0.7
Silt (%)	46.0 ± 0.7	10.6 ± 1.9	45.9 ± 1.2	36.7 ± 0.7
Sand (%)	41.7 ± 0.9	79.6 ± 1.9	5.4 ± 1.8	28.7 ± 0.0

Table 2.7. Clay, silt and sand content (%) of the soil surface (0–0.005 m), blank soil (0.005–0.01, 0.01–0.03 m) and tagged sediment after the rainfall simulations.

This lack of selectivity resulted in no increase in magnetic susceptibility in the sediments transported by overland flow. A comparison of magnetic susceptibility between tagged soils and sediments revealed the absence of significant differences (Table 2.6).

Further studies at larger scale and considering a broader range of erosive events would allow expand the potential use of this tracer at hillslope-scale and advance in the interpretation of results in situations of selectivity in particle size of the transported sediment.

2.4. Conclusions

This Chapter presents results on the assessment of a sediment tracer based on a magnetic, silt size, iron oxide powder commercially available in large amounts at a moderate price, which affords quick, and relatively inexpensive, analyses with simple equipment. Applying a dry mix of the tracer to disturbed soil resulted in its nearly uniform binding to soil aggregates for the soils used in this work except in the smallest aggregates sizes where they were higher. This seems not to be a significant limitation since such aggregates constitute a minor fraction (by weight) in the studied soils.

However, the ability to make magnetic susceptibility readings at an affordable cost, would allow one to analyze soil or sediment samples by aggregate sizes in order to address the problems associated with preferential binding, as suggested by the results of Kimoto *et al*. (2006) with rare earth oxides. No alternative method for incorporating the tracer into the soil in a less disturbing manner (viz. a liquid solution affording tagging of the top few centimeters of the soil) is currently available. This is probably the greatest limitation to date of the use of the proposed magnetic tracer and it restricts the application of this technique only to situations where the soil can be disturbed by tillage to incorporate the tracer into the soil. This is a common limitation for various other erosion tracers (e.g. rare earth oxides, organophilic clays, ^{137}Cs, magnetized beads) and should remain as one of the key lines of research aimed at improving the use of these tracers in erosion studies.

The percolation results suggest that the magnetic tracer is not leached by infiltrating water; however, long-term experiments would be required to assess mobility in the soil profile by effect of pedogenic processes or bioturbation. The results of rainfall simulation experiments testify to the usefulness of the magnetic tracer for evaluating erosion rates. Given its accuracy (approximately 0.5 $kg \cdot m^{-2}$), the proposed technique would be especially suitable for evaluating relatively large soil losses (e.g. during short periods of intensive erosion or long periods of moderate erosion) or, in combination with soil loss measurements, for identifying the relative weight of different erosion losses by splash and overland flow.

At its present stage of development the evaluated erosion tracer might be a useful tool (a complement for other tracers or experimental approaches) in erosion studies. One of its main advantages is the simplicity of the magnetic susceptibility analysis. This allows a large number of measurements in a short time by the same team performing the experiments. The magnetic susceptibility meter supposes a moderate investment of approximately 5000 euros. This tracer also offers the possibility of non-destructive measurements of magnetic susceptibility of the soil surface with a view to mapping areas of detachment and deposition and their matching with absolute values obtained via the tracer mass balance. Further studies currently under way might allow one to expand its use on larger runoff plots and at the hillslope scale under natural and simulated rainfall.

2.5. Acknowledgements

This work was funded by the Spanish Ministry of Science and Innovation (Projects AGL2006–10927–C03–01, AGL2006–10927–C03–02) and FEDER funds.

2.6. References

Alves, T., Gómez-Macpherson, H., Gómez, J.A. 2008. A portable integrated rainfall and overland flow simulator. Soil Use and Management 24: 163–170.

Crockford, R.H., Willet, I.R. 2001. Application of mineral magnetism to describe profile development of toposequences of a sedimentary soil in south-eastern Australia. Australian Journal of Soil Research 3: 927–949.

Gee, G.W, Bauder, J.W. 1986. Particle-size analysis. In: Klute, A. (Ed.), Methods of soil analysis. Part 1: Physical and mineralogical methods. ASA & SSSA, Madison, WI, (Agronomy Monograph no. 9), pp. 383–411.

Gómez, J.A., Giráldez, J.V., Vanwalleghem, T. 2008. Comments on "Is soil erosion in olive groves as bad as often claimed?" by L. Fleskend and L. Stroosnijder. Geoderma 147: 93–95.

Gómez, J.A., Giráldez, J.V., Pastor, M., Fereres, E. 1999. Effects of tillage method on soil physical properties, infiltration and yield in an olive orchard. Soil Till. Res. 52: 167–175.

Kimoto, A., Nearing, M.A., Zhang, X.C., Powell, D.M. 2006. Applicability of rare earth element oxides as sediment tracers for coarse-textured soils. Catena 65: 214–221.

Kirkby, M.J., Jones, R.J.A., Irvine, B., Gobin, A., Govers, G., Cerdan, O., Van Rompaey, A.J.J., Le Bissonnais, Y., Daroussin, J., King, D., Montanarella, L., Grimm, M., Vieillefont, V., Puigdefabregas, J., Boer, M., Kosmas, C., Yassoglou, N., Tsara, M., Mantel, S., Van Lynden, G.J., Huting, J. 2004. Pan-European Soil Erosion Risk Assessment: The PESERA Map, Version 1, October 2003. Explanation of Special Publication Ispra 2004 No.73 (S.P.I.04.73). European Soil Bureau Research. Report No.16, EUR 21176, 18pp. and 1 map in ISO B1 format. Office for Official Publications of the European Communities, Luxembourg. Available at: http://eusoils.jrc.it/ESDB_Archive/pesera/docs/EROSIONA4.pdf.

Lal, R. 1994. Soil Erosion Research Methods. 2nd Edition. Soil and Water Conservation Society. Ankeny. IA.

Lindstrom, M.J., Nelson, W.W., Schumacher, T.E. 1992. Quantifying tillage erosion rates due to moldboard plowing. Soil Till. Res. 24: 243–255.

Mentler, A., Strauss, P., Schomakers, J., Hann, S., Köllensberger, G., Ottner, F. 2009. Organophilic clays as a tracer to determine erosion processes. Geophysical Research Abstracts,Vol. 11. EGU General Assembly.

Owens, P.N., Walling, D.E., Leeks, G.J.L. 2000. Tracing fluvial suspended sediment sources in the catchment of the river Tweed, Scotland, using composite fingerprints and numerical mixing models. In: Foster, I.D.L., (Ed.), Tracers in Geomorphology. John Wiley & Sons, Chichester.

Peters, C., Dekkers, M. J. 2003. Selected room temperature magnetic parameters as a function of mineralogy, concentration and grain size. Physics and Chemistry of the Earth 28: 659–667.

Polyakov, V.O., Nearing, M.A. 2004. Rare earth element oxides for tracing sediment movement. Catena 5: 255–276.

Polyakov, V.O., Nearing, M.A., Shipitalo, M.J. 2004. Tracking sediment redistribution in a small watershed: implications for agro-lanscape evolution. Earth Surf. Process. Land. 29: 1275–1291.

Quine, T. A., Govers, G., Poesen, J., Walling, D., van Wesemael, B., Martínez Fernández, J. 1999. Fine-earth translocation by tillage in stony soils in the Guadalentin, south-east Spain: an investigation using caesium-134. Soil & Tillage Research 51: 279–301.

Ritchie, J. C., McHenry, J. R. 1990. Application of radioactive fallout Cesium-137 for measuring soil erosion and sediment accumulation rates and patterns: A review. Journal of Environmental Quality 19: 215 –233.

Royall, D. 2001. Use of mineral magnetic measurements to investigate soil erosion and sediment delivery in a small agricultural catchment in limestone terrain. Catena 46: 15–34.

Schoorl, J.M., Boix Fayos, C., de Meijerc, J.R., van der Graaf, E. R., Veldkamp, A. 2004a. The 137Cs technique applied to steep Mediterranean slopes (Part I): the effects of lithology, slope morphology and land use. Catena 57: 15–34.

Schoorl, J.M., Boix Fayos, C., de Meijerc, J.R., van der Graaf, E. R., Veldkamp, A. 2004b. The 137Cs technique applied to steep Mediterranean slopes (Part II): landscape evolution and model calibration. Catena 57: 35–54.

Soil Taxonomy. A Basic System of Soil Classification for Making and Interpreting Soil Surveys. Second Edition. 1999. United States Department of Agriculture–Natural Resources Conservation Service.

Stevens, C.J., Quinton, N.J. 2008. Investigating source areas of eroded sediments transported in concentrated overland flow using rare earth element tracers. Catena 74: 31–36.

Syrvesen, N., Øygarden, L., Salbu, B. 2001. Cesium-134 as a tracer to study particle transport processes within a small catchment with a buffer zone. J. Environ. Qual. 30: 1771–1783.

Ventura, E., Nearing, M. A., Amore, E., Norton, L. D. 2002. The study of detachment and deposition on a hillslope using a magnetic tracer. Catena 48: 149–161.

Wallbrink, P.J., Murray, A.S. 1993. Use of fallout radionuclides as indicators of erosion processes. Hydrological Processes 7: 297–304.

Walling, D., He, Q. 1999. Improved models for estimating soil erosion rates from Cesium-137 measurements. Journal of Environmental Quality 28: 611–622.

Wheatcroft, R.A., Olmez, I., Pink, F.X. 1994. Particle bioturbation in Massachusetts Bay: Preliminary results using a new deliberate tracer technique. Journal of Marine Research 52: 1129–1150.

Wooldridge, D.D. 1965. Tracing soil particle movement with Fe-59. Soil Science Society of America Journal 50: 730–736.

Young, R.A., Holt R.F. 1968. Tracing soil movement with fluorescent glass particles. Soil Science Society of America Proceedings 32: 600–602.

Zhang, X., Quine, T.A., Walling, D.E. 1998. Soil erosion rates on sloping cultivated land on the Loess Plateau near Ansai, Shaanxi province, China: an investigation using 137Cs and rill measurements. Hydrological Processes, 12: 171–189.

Zhang, X.C., Friedrich, J.M., Nearing, M.A., Norton, L.D. 2001. Potential use of rare earth oxides as tracers for soil erosion and aggregation studies. Soil Science Society of America Journal 65: 1508–1515.

Zhang, X.C., Nearing, M.A., Polyakov, V.O., Friedrich, J.M. 2003. Using rare-earth oxide tracers for studying soil erosion dynamics. Soil Science Society of America Journal 67: 279–288.

Chapter 3. Sediment movement in an irrigated maize-cotton alternative under rainfall simulations, estimated by sediment tracers

Abstract

Water erosion poses a grave threat to the future of southern Spain agriculture. Nevertheless more precise information is required to establish rational soil and water conservation strategies. Soil erosion has been evaluated at the plot scale using three iron oxides (magnetite, hematite and goethite) as tracers in several experiments in a furrow-irrigated- cotton cropland. In most of the simulated rainfall events in the plot trial, the beds were the main source of sediment when they are bare (0.98). The sediment fraction decreases (0.31) as the furrows are partially covered with standing residues on the beds. At the hillslope scale, iron oxides measured were examined and their respective contributions were interpreted with a simple mixing model. A simple soil erosion model based on the kinematic wave approach to the Saint-Venant equations for water and sediment movement explains the results with appreciable precision.

Key words: furrows, water erosion, iron oxides, sediment tracer, mixing model, erosion model

In preparation as: Guzmán, G., Cañasveras, J.C., Boulal, H., Gómez-Macpherson, H., Barrón, V., Laguna, A., Giráldez, J.V., Gómez, J.A. Study of sediment movement in an irrigated maize-cotton system using rainfall simulations, sediment tracers and a simulation model.

3.1. Introduction

In southern Spain, irrigated cropping land on mild slopes faces frequent degradation problems caused by water erosion (Fernández-Gómez *et al*. 2004). The combination of sparse intense rains, inadequate management methods that maintain the soil bare and unprotected during the year increases the erosion risk.

The traditional agricultural system in the region includes the rotation of maize–cotton in conventionally tilled beds under sprinkler irrigation. The system gradually evolves to permanent beds leaving crop residues on the soil surface. Permanent beds is a conservation agriculture practice where crops are planted on the top of the beds and soil labour is restricted to reshaping the bottom of the furrow reducing soil compaction to the fixed wheel tracks in specific furrows (Liebig *et al*. 1993, Tullberg *et al*. 2007). This soil management system was recently evaluated in a sprinkler irrigated farm in southern Spain with good results such as increasing water infiltration and reducing soil erosion losses with respect to a conventional management system (Boulal *et al*. 2007, Boulal and Gómez-Macpherson, 2010).

Soil erosion constitutes a serious threat for the future of agriculture in southern Spain with important environmental consequences. Nevertheless, there is no precise information on the soil loss rates in different systems and agronomic conditions. The use of erosion tracers can provide information to assess the adequacy of management systems for conservation agriculture in the area. An erosion or sediment tracer is any substance that, after its incorporation into the soil, can be tracked, detecting its source area and the successive steps of its path along the landscape. Many substances have been used as sediment tracers, such as radionuclides (*e.g.* Walling *et al*. 1999), rare earth oxides (Xue *et al*. 2004) or organophilic clays (Mentler *et al*. 2009). In Chapter 1, tracing techniques including fingerprinting, have been reviewed.

The main objective of fingerprinting studies is to detect the source of sediment, from the observed differences among soil properties in different areas induced through selective tagging by sediment tracers. An alternative approach based on the analysis of the concentration of sediment tracers in soil was adopted by Polyakov *et al*. (2004) for tracking sediment redistribution in a small watershed or by Deasy and Quinton (2010) to evaluate erosion in wheel tracks within erosion plots.

Guzmán *et al*. (2010a) have evaluated the potential of magnetic iron oxide as a sediment tracer with promising results, obtaining a good correlation between weighted and estimated soil losses based on magnetic susceptibility measurements at laboratory scale. Based on the latter results Guzmán *et al*. (2011) recommended the use of different iron oxides (magnetite, hematite and goethite) as sediment tracers detecting them with a combination of magnetic susceptibility and diffuse reflectance spectroscopy (DRS) measurements. DRS have been widely adopted in pedogenetic studies, and have gained relevance in the acquisition of remote sensing data at the laboratory and field scales. In addition, DRS measurements do not require the use of chemicals which could have an environmental impact. Cañasveras *et al*. (2009) suggested that DRS is useful for *(i) the characterization of soil zones according to their surface sealing and water erosion susceptibility,* and *(ii) for their screening without any further laboratory analysis required. DRS can be used for determining iron oxides mineralogy in weathered soils* (Sellitto *et al*. 2009).

The purpose of this Chapter is *the application of three different tracers to the exploration of the sources and the yield of sediment in a bed-furrow area under several environmental and agronomic conditions.*

3.2. Materials and Methods

3.2.1. Study area

The experimental field was located at the experimental farm of Alameda del Obispo in Córdoba (latitude 35º 50’ 40”N, longitude 4º 51’ 02”W).

The climate is Mediterranean with an average annual rainfall of 595 mm and an average annual ET_o of 737 mm. The plot was divided into three equivalent blocks of the same length as the original, (144×18 m), delimited by the irrigation laterals. Each block consisted of several sub-plots with two different soil managements: conventionally tilled bed planting (CB) and permanent bed planting system (PB). Each sub-plot was conformed by ten 0.85 m spaced furrow-bed sets, where the furrows were 0.59 m wide and 0.25 m deep. Wheel tracks were simulated in some of the subplots as an additional treatment. The wheel tracks were located alternately in the plot, with a separation of 1.7 m between the mean vertical planes of the tractor wheels.

A cotton (*Gossypium hirstium L.*)–maize (*Zea mays L.*) rotation was established in the experimental field under sprinkler irrigation. The first cotton crop was sown in 2007 keeping a clean fallow period between successive crops. In late February 2009, the maize stubble was chopped and left on the soil surface in PB while, in CB, it was incorporated into the soil before forming beds, in March 2009. Later, in May 2009, the cotton crop was sown. The cotton was hand-picked in September 2009. Soil management, crop characteristics and experimental field properties are fully described in Boulal *et al*. (2010a,b).

The rainfall simulation tests were performed during the 2009/2010 period when cotton was established in the experimental field. Initially, the rain was simulated only in the subplots under a conventional bed planting system, in order to incorporate sediment tracers to the furrows surface in a homogeneous way. The first set of rainfall simulations started in March 2009 when the bed plantings were just formed. A second set of simulations was performed during March 2010, with residues standing between the emergent plants. The third rainfall simulation test was carried out during the night, to minimize wind effects, in July 2009 when the cotton crop covered about 50% of the ground.

3.2.2. Sediment tracers

Three different synthetic iron oxides were used as sediment tracers: magnetite (Fe_3O_4), hematite (α-Fe_2O_3) and goethite (FeOOH), commercially available as Bayferrox® 318M, 110 and 920, respectively. Their characteristics allowed a relatively easy detection by measuring the magnetic susceptibility, in the case of magnetite, and spectral properties by diffuse reflectance spectroscopy for hematite and goethite.

Magnetic susceptibility was measured using a Bartington® meter and a MS2B® dual frequency sensor for laboratory measurements. For the case of hematite and goethite measurements, the total iron (Fe_d) was determined in the laboratory by the method of Mehra and Jackson (1960), modified by one extraction at 25ºC for 16 h. Diffuse reflectance spectra were recorded from 300 to 2500 nm in 0.5 nm steps using a Cary 5000 UV–Vis–IR spectrophotometer (Varian Inc., Palo Alto, CA) equipped with an integrating sphere. These spectra were transformed into the Kubelka-Munk (K-M) function, with the reflectance *R*:

$$f(R) = \left[\frac{(1-R)^2}{2R} \right] \tag{3.1}$$

The second derivative of the K-M function was used to estimate the amplitudes of goethite and hematite characteristic bands, (Kosmas *et al*. 1984). The amplitudes of goethite and hematite were computed as: *(i) for goethite, the difference between the minimum at ~420 nm and the maximum at ~445 nm, (AG_t)*; and *(ii) for hematite, the difference between the minimum at ~535 nm and the maximum at ~580 nm, (AH_m).*

The ratio between the concentration of iron oxides $H_m/(G_t+H_m)$, and their amplitudes $AH_m/(AG_t+AH_m)$ are compared in Figure 3.1. Using this ratio, and the total content of iron oxide of magnetite, hematite and goethite, absolute hematite and goethite content was determined.

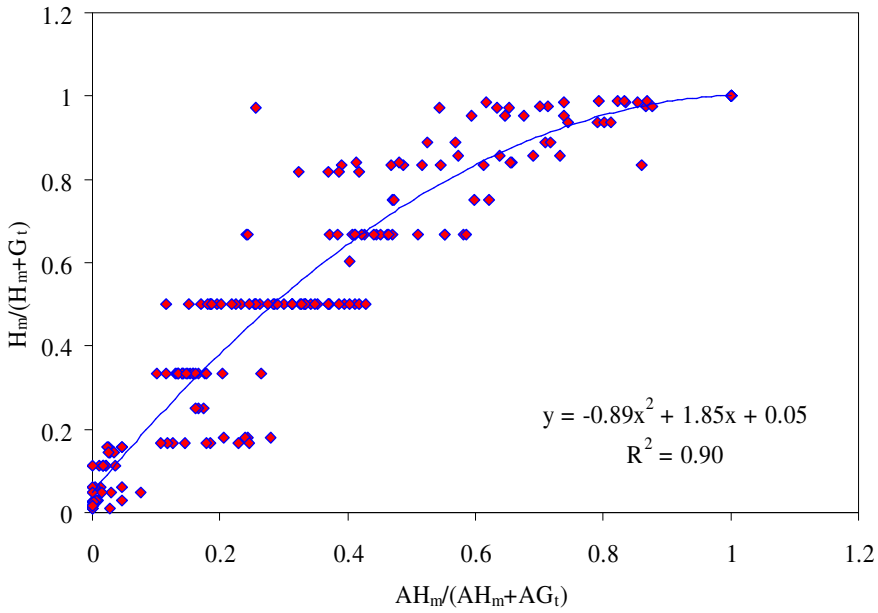

Figure 3.1. Comparison of the the ratios between amplitudes, $AH_m/(AH_m+AG_t)$, and concentrations of hematite and goethite, $H_m/(H_m+G_t)$, with the parabolic regression line.

A total of 192 different combinations of soil and iron oxides at different concentrations of magnetite (3, 1.5, 0.1 and 0 %), hematite and goethite (4, 3, 2, 1.5, 1, 0.75, 0.5, 0.25, 0.1, 0.05 and 0.02 %) were prepared to validate the quadratic relationship deduced in Figure 3.1. Computed and measured concentrations of hematite and goethite were compared, separately, and assembled in different magnetite intervals (3, 1.5, 0.1 and 0 %). The slopes of the linear regression lines were lower than 1 for all the cases, and were the lowest when magnetite concentration was the highest, Table 3.1.

Magnetite (%)	Hematite		Goethite	
(M)	slope	r^2	slope	r^2
3.0	0.55	0.92	0.70	0.90
1.5	0.65	0.92	0.88	0.93
0.1	0.81	0.95	0.95	0.94
0.0	0.80	0.94	0.93	0.96

Table 3.1. Slopes and regression coefficients obtained representing weighted concentrations against measured concentrations of hematite and goethite depending on magnetite concentration.

Representing magnetite concentrations against their corresponding slope values two linear trend lines were obtained, one for hematite $f_{(h)}$ and one for goethite $f_{(g)}$. Dividing the measured concentrations of hematite and goethite by these functions, the corrected slopes were closer to 1,

$$H_{cor} = \frac{H_{mea}}{f_{(h)}} = \frac{H_{mea}}{-0.09M + 0.80} \qquad r^2 = 0.98 \qquad (3.2)$$

$$G_{cor} = \frac{G_{mea}}{f_{(g)}} = \frac{G_{mea}}{-0.08M + 0.95} \qquad r^2 = 0.94 \qquad (3.3)$$

Where H_{cor} and G_{cor} are the corrected hematite and goethite concentrations (%), H_{mea} and G_{mea} are the measured hematite and goethite concentrations (%), f_h and f_g are correction factors obtained in terms of magnetite concentration M (%).

Figure 3.2 shows the validation curves, regression coefficients (R^2) and the RSME (% in weight) obtained representing (a) magnetite (M) concentrations and corrected (b) hematite (H) and (c) goethite (G) concentrations against theoretical concentrations. It also shows the standard deviation of the average value of each concentration.

Prior to the field experiment the binding capacity to soil particles of hematite was evaluated through a percolation test, to characterize its potential use as sediment tracers in three soils with different textural classes: sandy loam, silty clay and loam. The last textural class corresponds to Alameda, the soil of the study site. Blank soil particles with a diameter smaller than 6 mm were mixed with the three iron oxides to increase by 1.5 % the background soil concentration according to the method proposed by Guzmán *et al*. (2010a). The bottom of each of three pots in the percolation test was covered with a piece of geotextile and a 0.20 m of blank soil layer over it. Another piece of geotextile was placed to separate the untagged from the tagged soil. 40 mL of deionised water was added every 2 days during a 20 day period, collecting the leachate before the next water pulse to analyse the iron content.

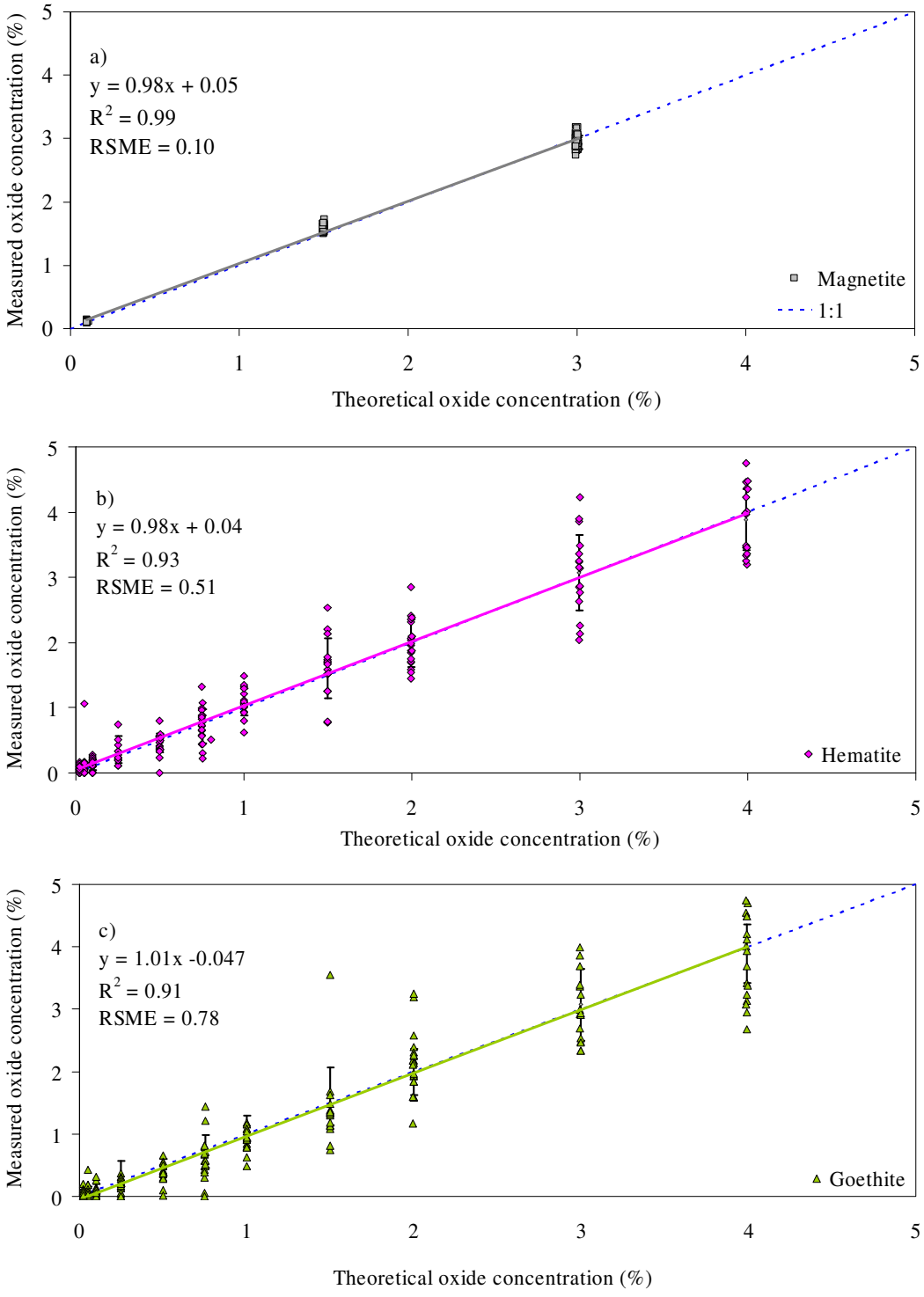

Figure 3.2. Comparison between the corrected and measured concentrations, with the respective regression lines, regression coefficients (R^2) and RSME for (a) magnetite (*M*), (b) hematite (*H*) and (c) goethite (*G*). Error bars indicates standard deviation of the average concentration.

For the rainfall simulation tests, three more pots with a slope of 4 % were prepared in a similar way but with a layer of tagged soil of 0.04 m height. A miniature rain simulator (Ogden *et al*. 1997) was used to simulate rainfall events of an intensity of 80 mm/h with deionised water, during 1.5 h. The resulting runoff and sediment were collected at the plot outlet. The clay and iron particles present in the sediment were determined by picking up a 20 mL sample at .10 m deep at five time intervals (1, 3, 7, 24, 48 and 72 h). Total sediment concentration and iron content were calculated in all the samples.

3.2.3. Sediment tracking

3.2.3.1. Small scale

Rainfall was generated with a portable simulator (Alves *et al*. 2008) with an intensity of 60 mm h^{-1} during more than 1 h on rectangular micro-plots (0.81×0.81 m) under different treatments based on traffic conditions. The treatments consisted of furrows with (+T) and without wheel tracks (–T), at two stages of the cotton cycle, with recent furrows just before sowing (March 2009) and with standing residues before reforming the beds prior to chopping residues (March 2010).

Figure 3.3 shows the recent furrows and the standing cotton residues. Two of the trials were run without any tracer to explore particle size changes of the sediment collected with respect to the original soil using routine methods (Gee and Bauder, 1986).

A soil and magnetite mixture, prepared with the method of Guzmán *et a*l. (2010a) was spread onto the furrows' surface tagging three areas of 2.0 m long, sufficiently separated between each other, in two furrows under different traffic conditions. The magnetite mixture on the furrows' surface was lightly raked to incorporate it into a depth of 0.02 m to obtain a final concentration of 2.4 % of the total dry weight. In March 2010, this procedure was repeated in two different furrows.

Figure 3.3. Experiment plots with recent furrows in March 2009 on the left and mature beds with standing residues on the right.

Figure 3.4 (a) shows the tagging scheme of the furrows with magnetite (M). Once the mixture was incorporated into the soil, the surface of +T furrows was statically consolidated using a metal sheet to apply a uniform pressure. Beds were not tagged either in March 2009 or in March 2010.

No soil samples for bulk density were taken from beds or furrows because in March 2009 the soil was quite loose. The March 2010 bulk density was similar to the value obtained by Boulal (2010) in January 2010 at the top 0.30 m because no soil condition changed significantly during February.

Four soil samples from bed plantings and furrows were taken before and after the rainfall simulations from the top 0.02 m of soil to measure magnetic susceptibility. Additional deeper samples from 0.02 to 0.06 m were also taken to ensure that no tracer reached that depth.

Runoff and sediment were collected during the rainfall simulations to determine total runoff, sediment yield and to measure magnetic susceptibility of the sediment.

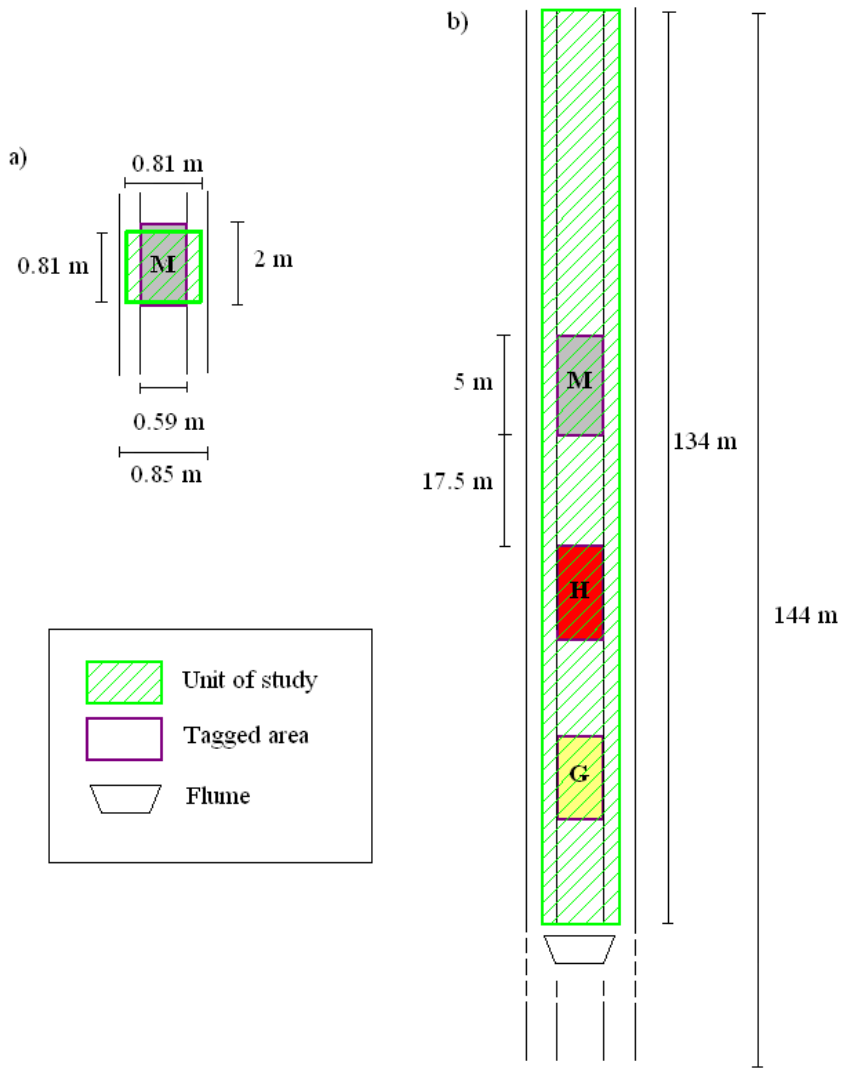

Figure 3.4. Initial locations of the tagged soil mixture segments with magnetite (*M*), hematite (*H*) and goethite (*G*) on the furrows of small scale (a) and hillslope scale plots (b).

The fraction of sediment coming from beds, f_b, and furrows, f_f, was calculated using their respective magnetic susceptibilities before the simulations, χ_b and χ_f, and magnetic susceptibility of the sediment collected, χ_{sed}.

$$\chi_{sed} = \chi_b f_b \left[1 + \frac{\alpha \chi_f}{\chi_b} \left(\frac{1}{f_b} - 1 \right) \right] \qquad (3.4)$$
$$f_f = 1 - f_b$$

The tracer coefficient, α, includes the tagging selectivity of the tracer to soil fine particles, c_s, and the management effect, c_d:

$$\alpha = c_s \cdot c_d \tag{3.5}$$

c_s explains the preferential bound of the tracer for finer soil particles. Blank and tagged soil samples were passed through a sieve column to separate 8 different aggregate sizes from 2000 to 10 µm (2000-1000, 1000-500, 500-250, 250-125, 125-63, 63-45, 45-25 and 25-10 µm). For each untagged aggregate size, their respective clay content was measured using a laser diffraction particle soil analyzer, Beckman Coulter LS-230 based on Guzmán *et al.* 2010b. For each tagged aggregate size, their respective magnetic susceptibility was measured. The mass-normalized relationship between clay content and tracer concentration is plotted in Figure 3.5, with the linear regression line; χ_i and c_i are the magnetic susceptibility and the clay content of each aggregate size, respectively, and χ and c are the weighted average magnetic susceptibility and clay content of the whole soil.

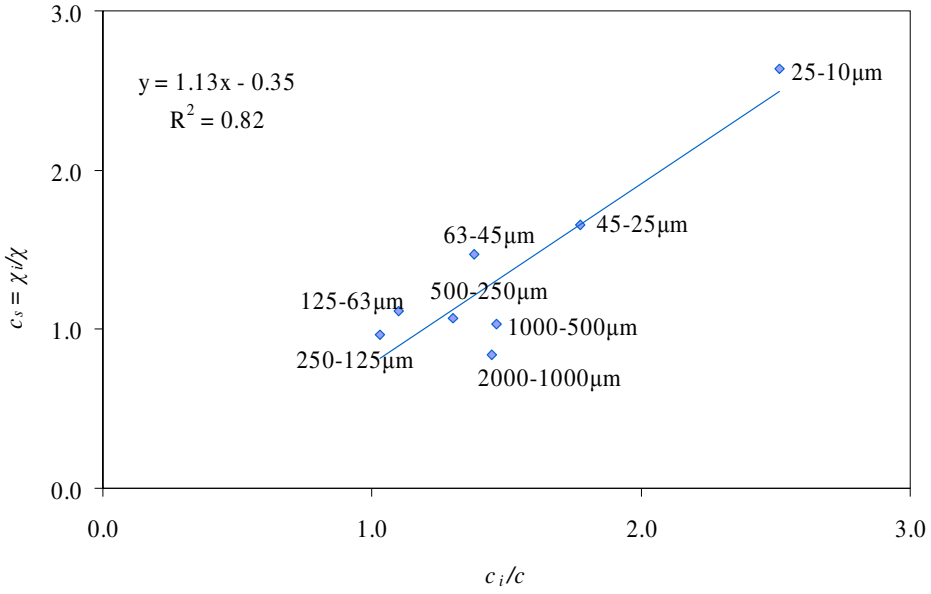

Figure 3.5. Relationship between the mass-normalized clay content and normalized magnetic susceptibility of the 8 different aggregate size intervals.

The coefficient c_d describes the distribution of the tracer through the tagged depth depending on the furrow management: +T or –T. To determine this coefficient, two plastic boxes of 0.03 m^2 were filled with five untagged soil layers of 0.02 m each. The top 0.02 m was filled with a mixture of untagged and tagged soil that was racked until the layer was complete and field experiment concentration was reached. To simulate bulk density of traffic management, the soil surface of one of the boxes was statically consolidated using a metal sheet. After that, soil from both boxes was slightly wetted and air dried. Once the soil was dried, soil samples per each 0.005 m were taken to measure magnetic susceptibility along the tagged soil. Figure 3.6 shows the decreasing exponential trend (which presented the higher regression coefficient) between the magnetic susceptibility at each interval χ_i normalized by the weighted magnetic susceptibility of the whole interval χ, and the height of each interval h_i normalized by the total height of soil h, observed for both treatments.

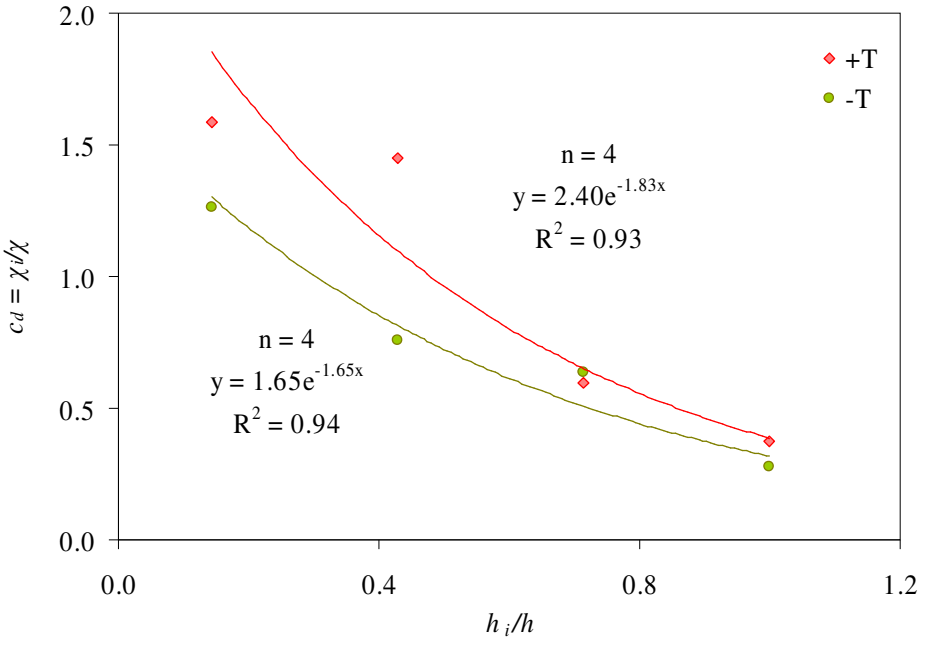

Figure 3.6. Exponential regression line and regression coefficients between normalized magnetic susceptibility and normalized height of tagged soil for the treatments with, +T, and without wheel compaction, –T.

3.2.3.2. Hillslope scale

In July 2009, when the cotton plants covered half the ground area, a rain event of 18 mm/h intensity was simulated using sprinklers (VYR-60) during an 8.5 h period. Four furrows (two +T and two –T) were divided into three equivalent segments 22.5 m long located at 66.5m from the head of the furrows. Each of the segments was divided into a tagged and untagged subsegment 5 m and 17.5 m long, respectively, as shown in Figure 3.4 (b).

Out of a total of ten furrows which conformed the conventional management block, one of them contained an irrigation lateral and another one was used as a control with no tracer, for all the simulations to analyze their textural class, Figure 3.7.

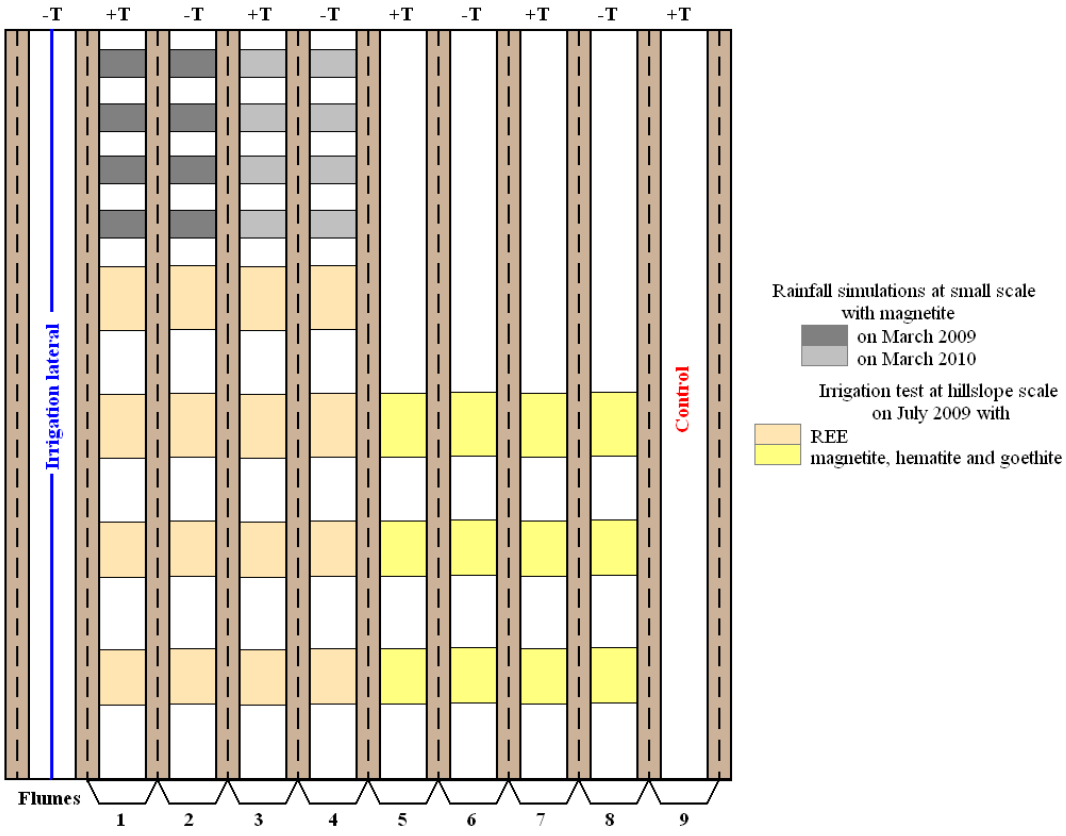

Figure 3.7. Tagging scheme and tracing experiments in the plot.

Of the eight lasting furrows, four of them were tagged with rare earth oxides for a parallel experiment at the irrigation test at hillslope scale in July 2009. As no analytical interferences were expected between rare earth oxides and iron oxides, the upper part of these furrows was tagged with magnetite (two for the rainfall simulation at a small scale in March 2009 and the other two in March 2010, Figure 3.4 (a)). The last four furrows were tagged with the three iron oxides (magnetite, hematite and goethite, Figure 3.4 (b)). With the purpose of comparing the behaviour of rare earth and iron oxide furrows, no more iron oxide was added along the upper 66.5 m in the iron oxide furrows.

Three different mixtures of soil and magnetite, hematite and goethite were prepared as described above to obtain final concentrations, once they were mixed at the field site, of 1.5, 2.5 and 2.5 % of the total dry weight, respectively. These mixtures were spread on the furrow segment surface: magnetite in the farthest upslope position, hematite in the middle, and goethite in the nearest upslope position, Figure 3.4 (b). A blank soil segment 17.5 m long separated consecutive tagged segments. The first top 0.02 m of furrows was tagged. To incorporate the mixture to a depth of 0.02 m, the mixtures were lightly raked, consolidating later the soil surface in trafficked furrow bottoms. There was no tracer on the bed surface in any of the furrows. A reference furrow without any tracer was also included in the rain simulation test to measure the particle size distribution of the collected sediment using the Beckman Coulter LS-230.

From each tagged area, soil was sampled twice at two depth intervals (0-0.02 m and 0.02-0.06 m) to determine the initial tracer concentration. After the simulation, 25 soil samples were taken at the top 0.02 m of soil to determine the final tracer distribution along the furrows. Soil samples from the 0.02-0.06 m depth interval were also taken to check if the tracer reached that depth. Each sample was composed of three subsamples taken in the same horizontal transect of the furrow. Location of sampling transects along furrows were 0.5, 2.5 and 4.5 m in tagged segments and 1, 2.5, 5, 10 and 16 m in untagged segments from the upstream location.

Runoff rate was measured and subsamples collected periodically using long-throated flumes of trapezoidal cross section with a sill width of 0.1 m (Clemmens *et al.* 1984). These flumes were installed 12 m upstream from the outlet of the furrows.

The setup of the sprinkler irrigation test is described in more detail by Boulal *et al.* (2010a). From the collected runoff, sediment concentration was measured and total soil losses estimated. Iron oxide concentrations were analyzed in the recovered sediment through magnetic susceptibility measurements for magnetite and diffuse reflectance spectroscopy for hematite and goethite. Figure 3.8 shows the cotton crop plot at the end of the irrigation test.

Figure 3.8. Cotton crop plot at the end of the irrigation test, with the measurement flumes in the foreground.

As in the case of the small scale simulations, bulk density was not directly measured in the field, considering its value similar to the measurement of Boulal (2010) on June 2009 at the top 0.3 m of the soil because conditions did not change significantly.

Using tracer concentration in soil and sediment corrected by c_d and c_s, a simple mixing model (e.g. Granger *et al.* 1996, Pelletier *et al.* 2007, Rhoton *et al.* 2008) was used to quantify the contribution of each sediment source to the total soil loss. The use of the mixing model also provided a check to equation (3.4).

3.2.4. Erosion model

Given the influence of the bed surface with respect to the collateral half-beds a simple soil erosion model was chosen. Laguna and Giráldez (1993) adapted a model initially proposed by Singh and Regl (1983) to successfully describe the water and sediment yield of an experimental plot under sprinkler-simulated rain. The model consisted of two mass balances, one for sediment and another for water, and one dynamic equation relating water depth and flow rate. The mass balance equation for water, relating the unit flow rate, q, and the water depth, h, to the effective rainfall rate, r_e, gross rainfall minus infiltration rates, varying in space, coordinate x, and time, t, is

$$\frac{\partial h}{\partial t} + \frac{\partial q}{\partial x} = r - i = r_e \tag{3.6}$$

The equation for the mass balance of sediment with a concentration c, and two terms for the sediment production, one due to the rain splash represented by a coefficient, B, and an exponent, m, which can assume the value $m=1$, and other one due to runoff flow shear, represented by another coefficient, ξ, affecting the combined effects of aggregates dislodging, written as a coefficient, k, a power of the water depth to an exponent b, and the sediment deposition, written as the product of sediment concentration by the flow rate, is

$$\frac{\partial}{\partial t}(ch) + \frac{\partial}{\partial x}(qc) = B r_e^{\ m} + h^b \xi (k - c\zeta) \tag{3.7}$$

The equation of the conservation of the momentum for water reduces to a simple potential relationship, adopting the kinematic wave approach, with the coefficient ζ and an exponent, assumed to be $n = b$,

$$q = h^n \zeta \tag{3.8}$$

Equations (3.6), (3.7), and (3.8) were subjected to an initial dry surface, nil water depth at time zero condition, *h(x,0)=0*, and no-flow upstream boundary condition, *h(0,t)=0*, in a surface configuration assimilated to an elongated plane with a width equivalent to the horizontal projection of the half-bed-furrow-half-bed ensemble, and can be solved with the method of characteristics, yielding the solutions for the flow rate, q:

$$q = \begin{cases} r_e^{\,n} t^{\,n} \zeta & t \le t_{cw} = \left(L\zeta^{-1} r_e^{1-n}\right)^{1/n} \\ r_e L & t > t_{cw} \end{cases} \tag{3.9}$$

In this equation t_{cw} is the time of concentration for the water under a rain of continuous and uniform effective intensity, r_e. The length of the furrow is L. The solution for the sediment concentration is:

$$\frac{c}{B} = \begin{cases} k_{B\zeta} + (1-k_{B\zeta}) F_n\left[\left(\xi\zeta r^{n-1} n^{-1}\right)^{1/n} t\right] & t \le t_{cw} \\ k_{B\zeta} + (1-k_{B\zeta})(\xi x)^{-1}\left\{1 - e^{(\mu-\xi x)}\left[1 - \mu F_n\left(\mu n^{-1}\right)\right]\right\} & t_{cw} < t \le t_{cs} \\ k_{B\zeta} + (1-k_{B\zeta}) F_1(\xi x) & t > t_{cs} \end{cases} \tag{3.10}$$

Where t_{cs} is the time for sediment concentration. The function F_n is a generalized version of the Dawson integral (Abramowitz and Stegun 1965, Olver *et al*. 2010):

$$F_n(x) = \frac{1}{x\exp\left(x^n\right)} \int_0^x \exp\left(v^n\right) dv \tag{3.11}$$

The auxiliary variable μ is:

$$\mu = r_e^{\,n-1} \xi\zeta \left[\frac{n}{r_e(n-1)}\left(\frac{r_e x}{\zeta}\right)^{1/n} - \frac{t}{n-1}\right]^n \tag{3.12}$$

Finally the time of concentration for the sediment, t_{cs}, is:

$$t_{cs} = \left(Ln\zeta^{-1} r_e^{1-n}\right)^{1/n} \tag{3.13}$$

The sediment load at any time and place is the product of concentration and the flow rate.

The model parameters: r_e, n, ζ, k, B, ξ, were estimated in two steps. From the observed water hydrographs, r_e was estimated. The value of the parameter n was obtained by solving the nonlinear equation:

$$n^{1/n} = \frac{t_{cs}}{t_{cw}} \tag{3.14}$$

The equation of the time concentration for the water allows the computation of the value of parameter ζ:

$$\zeta = \frac{L}{t_{cw}^{n} r_e^{n-1}} \tag{3.15}$$

In the second step the sediment-related parameters, B, k, and ξ, were estimated using the Rosenbrock algorithm (*e.g.* Press *et al*. 2007) for the optimization of the fit of the equation for the sediment concentration to the observed data.

The goodness of the fit was shown with the help of the Nash and Sutcliffe index, (e.g. Krause *et al*. 2005) which compares the observed, $c_{ob,j}$, and simulated values, $c_{sim,j}$, as:

$$e_{NS} = 1 - \frac{\sum_{j=1}^{n} (c_{ob,j} - c_{sim,j})^2}{\sum_{j=1}^{n} (c_{ob,j} - \bar{c}_{ob})^2} \tag{3.16}$$

Where $\overline{c_{ob}}$ is the average sediment concentration for the observed values.

The erosion model parameters were calibrated using measured data taken during the irrigation test, following the method described above. To explore further the model, some scenarios were simulated varying some of the erosion model parameters considering their physical meaning. Therefore complementary information was provided to understand the sediment dynamics of the system.

3.3. Results and discussion

3.3.1. Preliminary evaluation of the hematite and goethite tracers

The percolation tests did not detect iron oxides in the percolated water from the 0-0.02 m depth interval. Runoff and sediment analysis confirmed no interferences of the oxides to soil movement and a strong binding to soil particles. Figure 3.9 indicates a consistent decrease in the time of soil clay content and iron oxide concentrations for the field site.

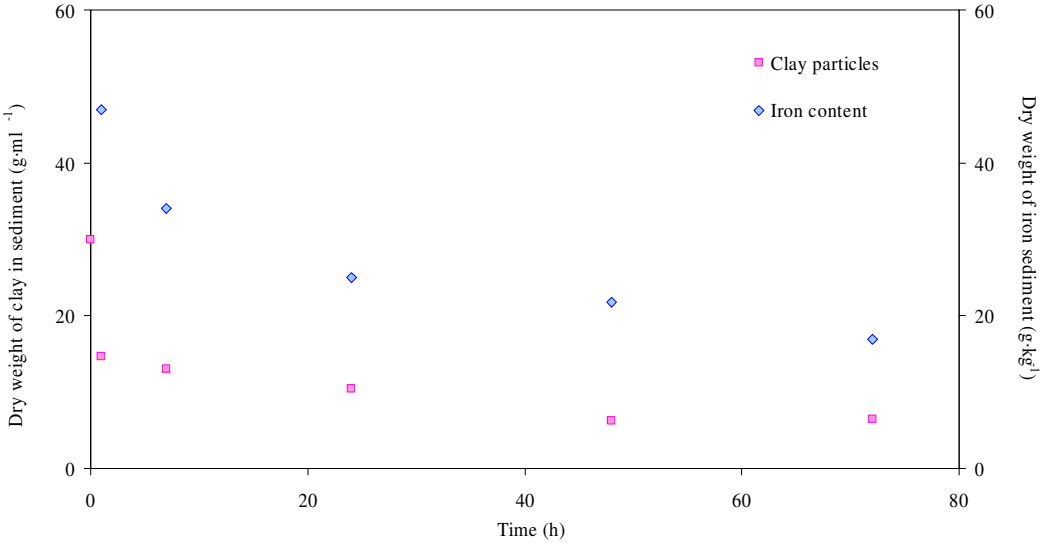

Figure 3.9. Clay size particle and iron oxide contents evolution in the sediments obtained in the rainfall simulation test.

3.3.2. Sediment tracking

3.3.2.1. Small scale

Table 3.1 gathers the average values and standard deviations of water and sediment yield as well as sediment concentration of twelve simulations belonging to tagged furrows.

Bed ground covers	Bare/Furrows just formed (March 2009)			With standing residues (March 2010)			p
Furrow management	+T (n=3)	−T (n=3)	p	+T (n=3)	−T(n =3)	p	
Runoff (mm)	42.3 ± 0.4	39.4 ± 0.2	0.001	39.4 ± 2.6	43.1 ± 3.2	0.190	0.782
Soil losses ($kg \cdot m^{-2}$)	.584 ± .892	.658 ± .056	0.289	.313 ± .168	.318 ± .010	0.964	0.001
Sediment concentration ($kg \cdot m^{-3}$)	12.7 ± 0.6	15.6 ± 0.6	0.004	7.2 ± 2.4	6.7 ± 1.5	0.798	0.000

Table 3.2. Average values and standard deviations for water and sediment yields and of 12 rainfall simulations at small scale. $p<0.05$ indicates significant differences between furrows with, +T, and without wheel compaction, −T, grouped by bed ground covers. A comparison between March 2009 and March 2010 was also carried out without distinguishing between +T and −T furrows shown in the rightmost column.

In March 2010, soil bulk density was 1.43 $Mg \cdot m^{-3}$ at the beds and 1.52 and 1.47 $Mg \cdot m^{-3}$ at +T and −T furrows, respectively. Comparing furrow managements at each bed ground cover, significant differences were observed for runoff and sediment concentration when furrows were just formed. Due to the wheel tracks along furrows +T, soil consolidation was higher, and, consequently, runoff yield was higher than in the otherwise equivalent –T furrows. Nevertheless, sediment yield differences between treatments were not significant. If furrow managements were not taken into account, significant differences were observed and higher values for sediment yield and concentration were measured when furrows were just formed. In this case, the soil was less compacted and average runoff yield was slightly lower (40.9 mm in March 2009 against 41.3 mm in March 2010).

Time to runoff initiation decreased from 9.9 ± 1.1 minutes with bare beds, to 5.2 ± 2.3 minutes when standing residues remained on the beds. This fact can be attributed to the greater consolidation of soil after one year, and to the reduced rainfall interception by cotton residues, Figure 3.3 (on the right).

After the rainfall simulations transversal cuts were made along furrows in March 2009 and March 2010, Figure 3.10. A sediment layer of about 0.01 m depth of untagged particles was deposited onto the tagged soil surface of the furrows in both bed situations: without and with standing residues.

Figure 3.10. Upper soil profile sections after the rainfall simulations test in March 2009 (on the left) and March 2010 (on the right). The black colour of the magnetite particles is apparent in both pictures.

Figure 3.11 summarizes the contribution of each sediment source (bed or furrow) using magnetic susceptibility measurements and equation (3.4). No significant differences were detected between +T and −T furrows in any of the cases, and, therefore, data were analyzed without considering the furrow management.

With recently formed beds with no ground cover, most of the sediment reaching the outlet came from the bed tops and sides, approximately 98%, with very little coming from the furrows. Once the soil was more consolidated and retained by roots and covered by vegetation, in our case standing crop residues on top of the beds, the situation reversed and most of the sediment came from the furrows, approximately 69%. No differences were obtained between the +T and –T treatment in each situation (bare or covered beds) regarding the attribution of sediment source. Quantification of source of sediment obtained using the mixing model, not shown, were similar to those depicted in Figure 3.11.

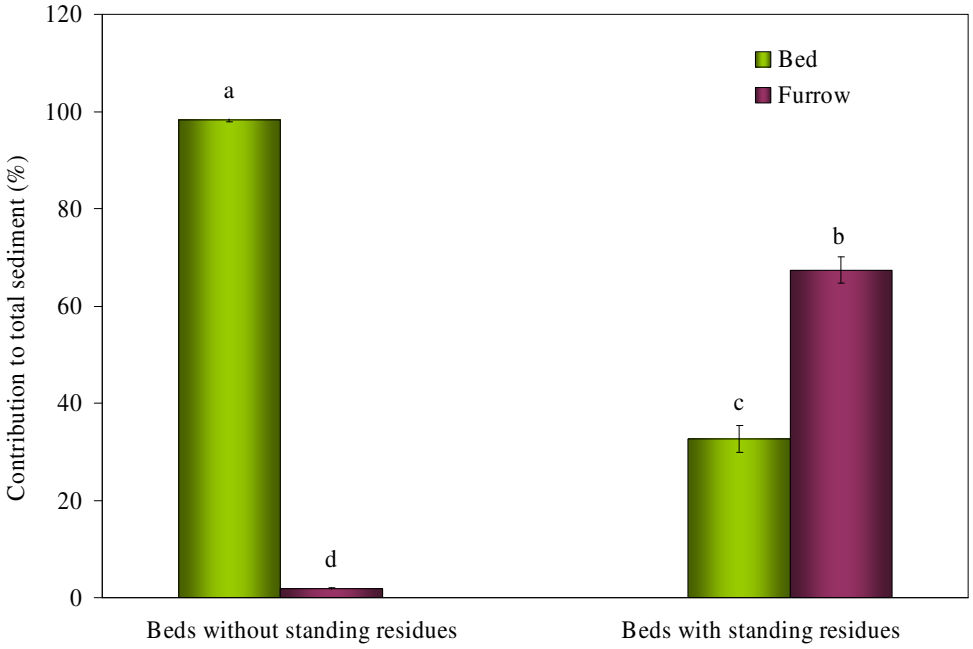

Figure 3.11. Average value and standard deviation of the sediment contribution from beds and furrows distinguishing between bare standing residues covered beds. Letters indicate significant differences for several sediment sources at each bed condition. (Bonferroni test $p<0.05$).

A particle size analysis indicated that clay particle concentration in the sediment increased by an average value of 7 % as compared to original soil. Magnetic susceptibility of sediment was higher compared to the tagged soil before the simulations only when beds were covered by standing residues. This indicated that most of the magnetic susceptibility of the sediment was due to fine particle sizes (whose tracer concentration is higher) coming from tagged soil of the furrows. With bare beds the enrichment of clay particle concentration in sediment was also detected and although magnetic susceptibility of sediment was lower than the original tagged soil, the c_s correction was also applied to the measurements.

3.3.2.2. Hillslope scale

Table 3.2 summarizes the key results of the rainfall simulations at hillslope scale. At this scale there were significant smaller sediment losses compared to the small scale experiments, which could be due to the lower rainfall rates applied, albeit they are comparable with those of large rainfall events in the area.

Time to runoff initiation was the only measurement that presented significant differences between +T and –T furrows this being shorter for furrows supporting heavy traffic. This could be explained by the high soil bulk densities 1.54 $Mg \cdot m^{-3}$ at beds and 1.66 and 1.61 $Mg \cdot m^{-3}$ at +T and –T furrows respectively, in July 2009. Runoff yield and rate were slightly lower in +T furrows, although these differences were not significant, but explicable because of the higher bulk densities of these furrows. On the other hand due to the soil being more consolidated in +T furrows, soil losses were lower compared to –T.

Furrow management	Runoff (mm)	Time to runoff initiation (h)	Runoff rate ($L \cdot min^{-1}$)	Soil losses ($kg \cdot m^{-2}$)	Sediment concentration ($kg \cdot m^{-3}$)
+T	59.5 ± 14.7	1.93 ± .058	16.7 ± 4.1	.079 ± .018	1.4 ± 0.0
-T	25.5 ± 5.0	3.93 ± .472	10.1 ± 3.2	.036 ± .008	1.4 ± 0.0
p	0.091	0.027	0.222	0.204	1.000

Table 3.3. Average values and standard deviations for runoff yield, time to runoff initiation, runoff rate, sediment yield and concentration for +T and –T furrows. $p<0.05$ indicates significant differences between furrow management.

Visual inspection indicated tracer movement and deposition along furrow surfaces downstream of the tagged segments. This appreciation was possible because of the contrast provided by the high visibility of tagged soil (black, red and yellow) and soil without tracer. Figure 3.12 shows an intermediate segment tagged with hematite in one of the furrows after the irrigation test.

Figure 3.12. Tagged soil redistribution after the irrigation test in an intermediate furrow segment tagged with hematite.

The analysis of soil samples (from the top 0.02 m) after the rainfall simulations allowed a quantification of that redistribution, Figure 3.13. This figure shows the average tracer concentration and the standard deviations along the +T and –T furrows after the irrigation test compared to the initial ones. It was observed that the hematite concentration increased in presence of high goethite concentration in the lower segments of the furrows. This can be attributed to the fact that the peak of hematite concentration was lower than the peak of goethite concentration, which masks the maximum of hematite concentration. The ratio $AH_m/(AG_t+AH_m)$was inappreciable, which meant that in soil samples containing both iron oxides, the peak of the highest concentrated oxide can hide the peak of the lowest concentrated oxide. In this case, a background value of hematite of 0.05 % was measured. For this reason, the hematite measurements at the lower segment, initially tagged with a high concentration of goethite (~2.5 %), were discarded in Figure 3.13. A slight decrease in tracer concentration in remaining soil of the tagged areas was also observed

The low soil erosion rates (see Table 3.2), reflect not only some soil detachment but a significant deposition of untagged soil proceeding from untagged areas upstream in the furrows and from the beds. The sediment transported by the stream occurred as a balance between fresh detached soil that is mobilized and the deposition of suspended sediment that was detached upstream.

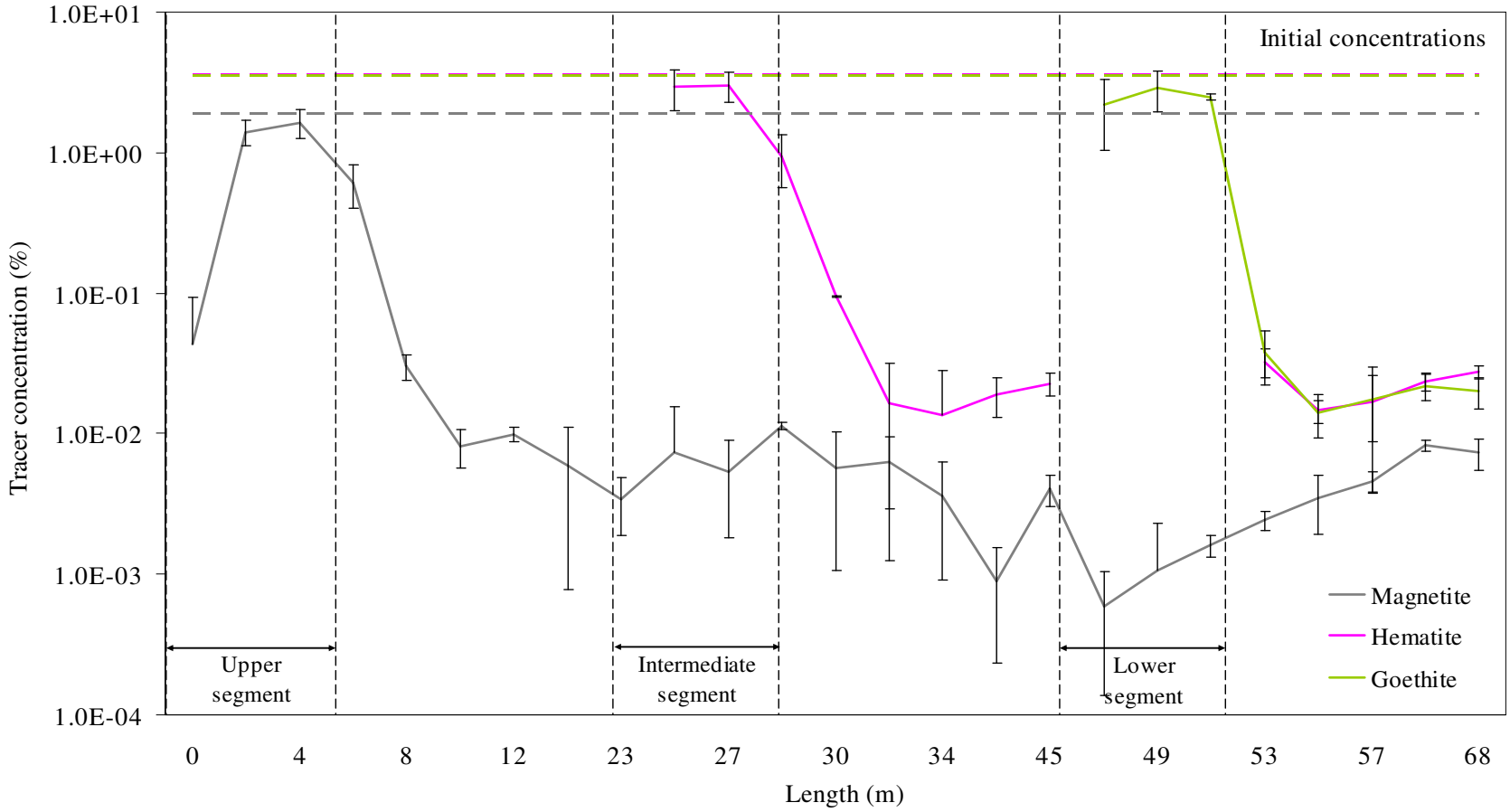

Figure 3.13. Downslope transport of detached tracer (y-axis at a logarithmic scale) deposited at a diminishing rate in a along the furrow.

Figure 3.14 shows one intermediate segment after the irrigation test. In this segment, hematite was the tracer and it was completely coloured before the test. It is observed that although some tracer was lost, blank soil from beds and untagged segments of the furrow were deposited into tagged segments.

Figure 3.14. Intermediate tagged segment with hematite, after the rain simulation test, where tracer losses and deposition of untagged sediments are visible.

Figure 3.15 could correspond to a case of limited transport. This Figure was obtained after the analysis of tracer concentration and the c_d and c_s corrections to determine soil contribution from tagged areas to total sediment for +T and –T furrows.

By fitting a logarithmic function along the furrow to the sediment contribution ratios, the contribution of each furrow segment can be estimated. Using that approach, the furrows could supply 65% of the total sediment and the beds around 35%. These values, regarding relative contribution of furrows and beds to total sediment, are similar to those obtained with the small scale rainfall simulations on the microplots with standing vegetation, see Figure 3.11.

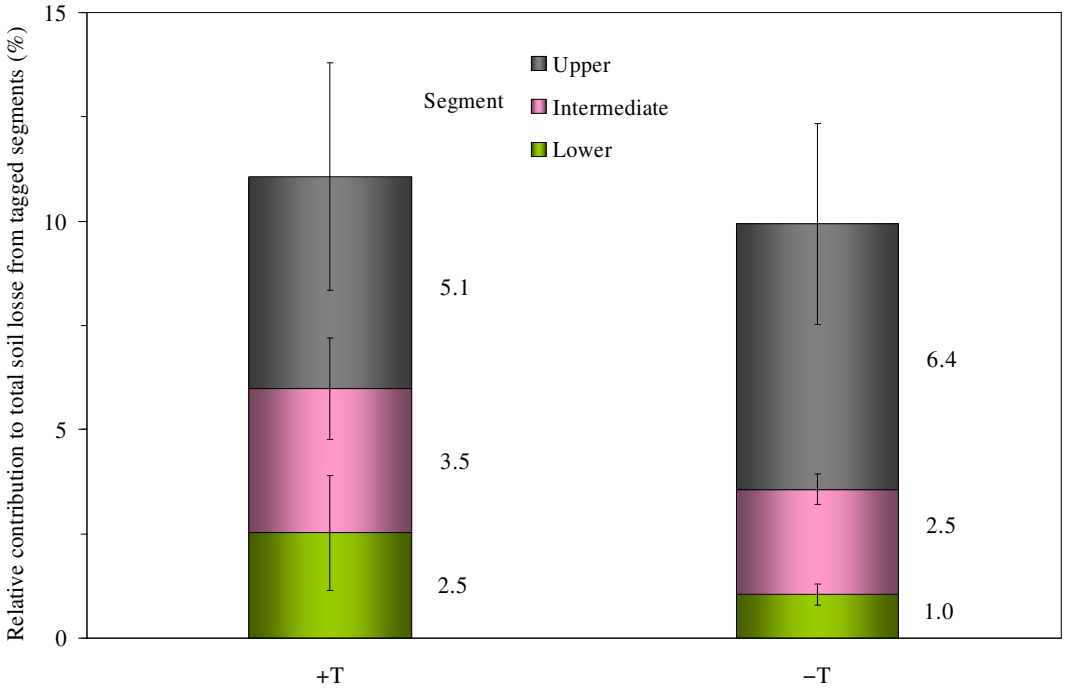

Figure 3.15. Soil contribution from tagged areas to total sediment for +T and –T furrows.

3.3.2.3. Model analysis

The estimated values of the model parameters are written in Table 3.3.

Furrow		q_e (LT^{-1})	c_e (ML^{-3})	t_{ini}	t_{cw} (T)	t_{cs}	n	ζ ($L^{2-n}T^{-1}$)	B (ML^{-3})	k ($ML^{-1-n}T^{-1}$)	ξ (L^{-1})	e_{NS}
+T	1	0.24	1.2	2.07	1.51	2.05	1.44	.569	1.44	.029	.003	.865
	3	0.24	1.3	1.88	2.08	2.70	1.46	.122	1.92	.161	.279	.182
	5	0.34	1.9	1.97	2.55	3.38	1.55	.106	1.80	.133	.129	.879
	7	0.57	1.5	1.62	6.52	7.05	1.08	.007	2.28	.010	.830	.645
–T	2	0.27	1.2	5.51	2.00	7.83	1.31	.032	1.62	.038	.057	.367
	4	0.24	1.3	3.64	3.45	4.37	1.38	.043	1.87	.058	.517	.157
	8	0.41	1.2	5.23	1.37	1.82	1.56	.261	1.32	.293	.021	.864

Table 3.4. Estimated values of the erosion model parameters, and Nash and Sutcliffe efficiencies of the fits of the model to the experiment data for the different furrows.

Furrow 6 was discarded because of the erratic experimental data. The fit of the model to the experiment data is acceptable, although in furrows no. 3, 2 and 4 the efficiency is low. The fit can be observed even for this case in Figure 3.16. The parameter values are reasonable, in the order of the data of Laguna and Giráldez (1993), considering the differences.

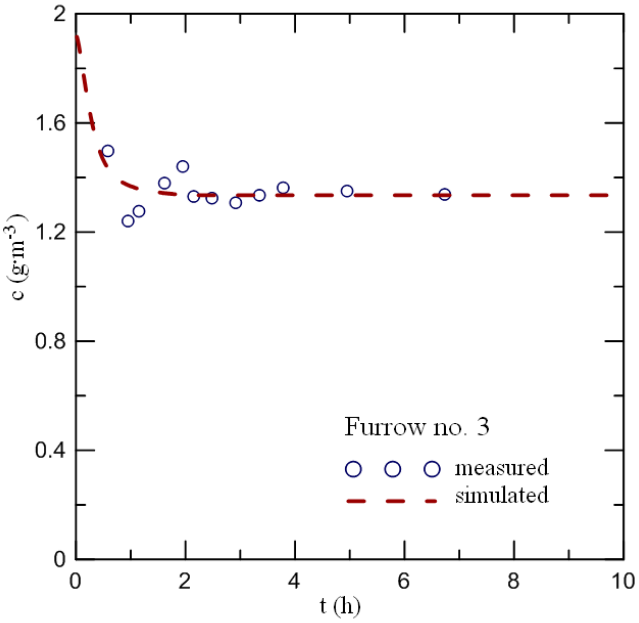

Figure 3.16. Fit of the erosion model, dashed line, to the experiment data open circles in the case of Furrow no. 3, whose Nash and Sutcliffe efficiency is 0.182.

Note that this model implies a final constant value for the concentration which differs with the exponential approach adopted in the previous paragraph. The main problem with the fit is the estimation of the steady water flow rate due to the fluctuations of the gauging instrument. The presence of vegetation and the spatial variability of soil surface and microrelief also reduce the efficiency of the fit as well.

Integrating the product of flow rate and concentration with time at a given position in the furrow yields the sediment carried by the water $Q_s(x)$.

$$Q_s(x) = \int_0^{t_r} q(x,t)c(x,t)dt \qquad (3.17)$$

In equation (3.17) the temporal and spatial dependency of flow rate and sediment concentration has been expressed. The upper limit of the integral, t_r, is the time of rainfall stop, since the recession period is negligible in a long track of soil with vegetation.

The contribution of every segment bounded by the upstream, x_{up}, and downstream coordinates, x_{dw}, is a consequence of equation (3.17), $Q(x_{up}, x_{dw})$,

$$Q_s(x_{up,}, x_{dw}) = Q_s(x_{dw}) - Q_s(x_{up}) \tag{3.18}$$

Finally, the relative contribution of any segment is

$$\frac{Q(x_{up}, x_{dw})}{Q_L} = \frac{Q_s(x_{dw}) - Q_s(x_{up})}{Q_L} \tag{3.19}$$

Table 3.4 compares the prediction of the erosion model with the estimations of sediment contribution with the tracer method and the mixing model.

Furrow	+T			−T		
Segment	Tracer analysis	Erosion model	Mixing model	Tracer analysis	Erosion model	Mixing model
Magnetite	.0508	.0357	.0457	.0636	.0353	.0495
Hematite	.0346	.0337	.0333	.0253	.0295	.0269
Goethite	.0253	.0318	.0317	.0104	.0240	.0229
Sediment yield (kg)	9.03	8.57	-	4.05	4.12	-

Table 3.5. Comparison between the estimated fractions of soil loss from the three segments tagged by the iron oxide indicated in the first column, and by the fitted erosion model, as well as between the observed average soil loss per furrow and the similar magnitude estimated by the erosion mode, for the treatments with, +T, or without traffic, −T.

The model approaches the observations reasonably well, attending to the average total soil loss per furrow. The fractions of soil loss originated in the different segments are somewhat different, even though the estimation of soil loss by the tracers is not an exact estimation. In any case, the model explains the decreasing contribution of the furrow segments as they get closer to the outlet, Figure 3.17.

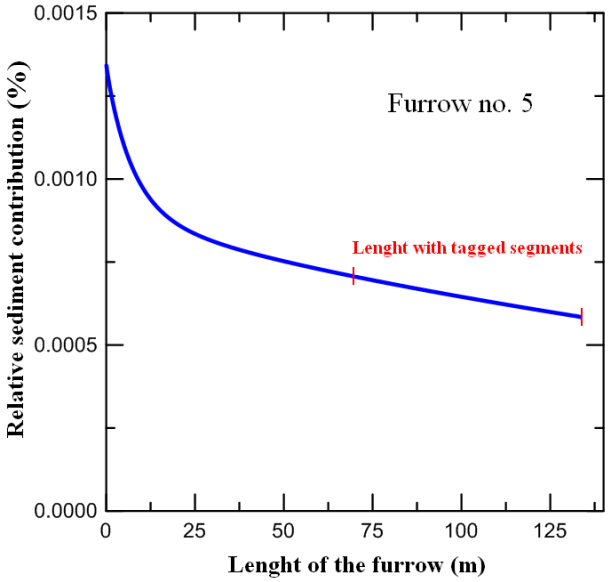

Figure 3.17. Relative contribution to total soil losses along the length of Furrow no. 5. The tagged segments are indicated.

The flow rate increases an the end of the furrow but the sediment concentration does not increase at a parallel rate possibly due to the proximity to the transport capacity conditions. Considering a steady rainfall rate, precludes the description of the almost sudden sediment deposition once the external water supply ends. This contribution is more apparent than relevant in terms of the total sediment yield. In any case it could be incorporated into the next version of the model. A more detailed description of the bed sides could improve the model's results. Nevertheless, the variability of the rainfall application, the interception by the live vegetation and standing stubble, the surface microrelief, and the variable infiltration of water into the soil could explain the differences between the model and the observations. Accepting its limitations the erosion model is a useful tool for the observed erosion processes. The same decreasing contribution trend was also detected by the mixing model.

Figure 3.18 shows the temporal response of the sediment concentration for different values of the model parameters (B, k, ζ and ξ) in Furrow no. 5 maintaining constant the rest of the estimated values in each case.

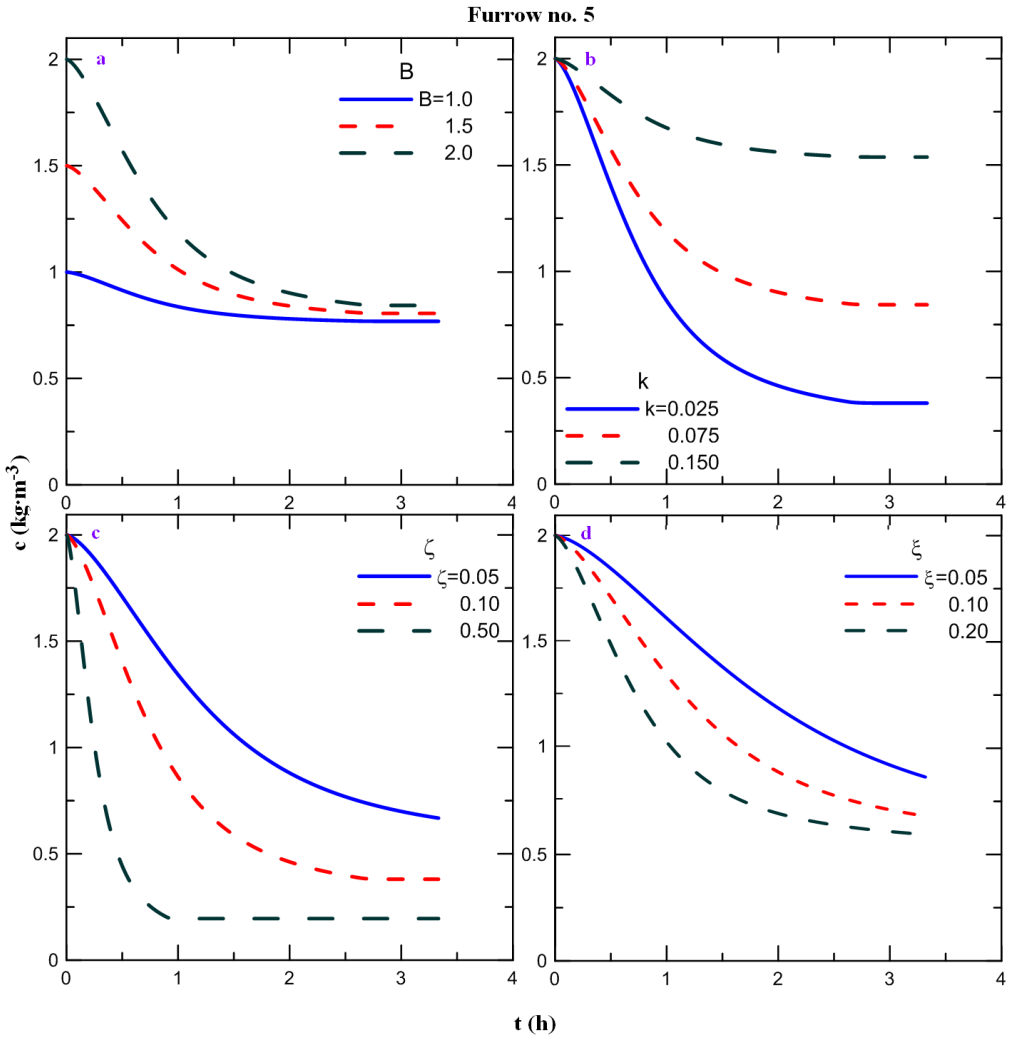

Figure 3.18. Variation of the sediment concentration (c) in function of time for several combinations of the erosion model parameters B, k, ζ and ξ to simulate different scenarios in Furrow no. 5.

Parameter B indicates the energy of the raindrop splash, in Figure 3.18a. As the value of parameter B increases, the sediment concentration that passes through the end of the furrow during the first period, the sediment flushing stage, increases too. Later the sediment concentration tends towards the transport capacity value, once most of the furrow is protected against raindrop splash by the water depth.

Parameter k reflects the shearing effects of surface runoff flow. Therefore as its value gets higher more sediment is mobilized and sediment concentration grows slowly approaching to the transport capacity value, Figure 3.18b. Parameter ζ is the coefficient of the water depth flow rate equation. The parameter ζ is approximately the quotient of the square root of the bed slope and the surface resistance, as the Manning n value. If the value of ζ rises, given the expression for sediment deposition, the sediment will settle down quicker, descending its concentration in the flow, as it can be appreciated in Figure 3.18c. The role of parameter ξ is more difficult to evaluate since it affects the whole contribution of the shearing due to runoff flow. Under the circumstances of the Figure3.18d the deposition rate prevails reducing the sediment concentration as the ξ values are greater.

3.4. Conclusions

Three different iron oxides have been evaluated as sediment tracers at the plot and hillslope scale under different treatments. There are several key points in the use of iron oxides as sediment tracers to consider. First some corrections must be made before interpreting the measurements. Second, once the magnetic susceptibility of sediment is corrected by tracer distribution in soil profile and selectivity transport of finer particle sizes in sediment, interferences caused by the magnetic iron oxide, in hematite and goethite measurements have to be eliminated. Third, due to the use of optical methods in the analysis of hematite and goethite, there are interferences when magnetite is present in the sample. The interference increases with the concentration of the magnetite. These interferences are also detected for goethite and hematite at high and low concentrations respectively, when hematite measurements are overestimated. Fourth, background iron oxide concentrations must be measured to calibrate the technique for each soil.

The combination of sediment tracers and model analysis allowed the interpretation of sediment dynamics in a furrow-bed system. Once the crop is standing, furrows and beds (especially furrows) deliver sediment significantly at a small (1-m) scale.

At a larger scale, the furrow system had net erosion in the upper parts of the furrows and deposition in the lower segments. There is a significant fraction of sediment coming from tagged furrow areas of a decreasing importance as the segment approaches the outlet of the furrow. Some sedimentation was observed in the recession stage of the runoff flow when the transport capacity could not keep the sediment moving towards the outlet.

A simple erosion model helped to explain the observed results. Despite it could be improved, it reproduced the experimental results with relatively high Nash and Sutcliffe efficiencies. In addition, the erosion model allowed the simulation of several scenarios that could help to evaluate and understand the behavior of the system.

3.5. Acknowledgements

This work was funded by Spanish Ministry of Science and Innovation (Projects AGL2006-10927-C03-01, AGL2006-10927-C03-02 and AGL2009-12936-C03-01) and FEDER funds.

3.6. References

Abramowitz, M, Stegun, I.D. 1965. Handbook of mathematical functions. Dover. New York.

Alves, T., Gómez-Macpherson, H., Gómez, J.A. 2008. A portable integrated rainfall and overland flow simulator. Soil Use Manage. 24: 163–170.

Boulal, H. 2010. Cultivos anuales regados sobre lomos permanentes: Introducción y potencial para la conservación de recursos naturales. Ph.D. diss. Dept. of Agronomy, University of Córdoba, Spain.

Boulal, H., Alves, T., Gómez-Macpherson, H., Gómez, J.A. 2007. Efecto del tráfico controlado sobre la infiltración del agua y la erosión del suelo en un sistema de cultivos anuales en lomos permanentes en el sur de España. Estudios de la Zona No Saturada del Suelo Vol. VIII. (available at http://www.zonanosaturada.com/publics/ZNS07/area_3/03.pdf).

Boulal, H., Gómez-Macpherson, H. 2010. Dynamics of Soil Organic Carbon in an innovative irrigated permanent bed system on sloping land in southern Spain. Agric. Ecosyst. Environ. 139: 284–292.

Boulal, H., Gómez-Macpherson, H., Gómez, J.A., Mateos, L. 2010a. Effect of soil management and traffic on soil erosion in irrigated annual crops. Soil Till. Res. 115–116: 62–70.

Boulal, H., Gómez-Macpherson, H., Gómez, J.A., Mateos, L. 2010b. Soil management and traffic effects on infiltration of irrigation water applied using sprinklers. Irrig. Sci. 29: 413–412.

Cañasveras, J.C., Barrón, V., del Campillo, M.C., Torrent, J., Gómez, J.A. 2009. Estimation of aggregate stability indices in Mediterranean soils by diffuse reflectance spectroscopy. Geoderma 158: 78–84.

Clemmens, A.J., Bos, M.G., Reploge, J.A. 1984. Portable RBC flumes for furrows and earthen channels. Trans. ASAE 27: 1016–1022.

Deasy, C, Quinton, J.N. 2010. Use of rare earth oxides as tracers to identify sediment source areas for agricultural hillslopes. Solid Earth Discuss. 2: 195–212. www.solid-earth-discuss.net/2/195/2010/, doi:10.5194/sed-2-195-2010.

Fernández-Gómez, R., Mateos, L., Giráldez, J.V. 2004. Furrow irrigation erosion and management. Irrig. Sci. 23: 123–131.

Gee, G.W., Bauder, J.W. 1986. Particle-size analysis. In: Klute, A. (Ed.), Methods of soil analysis. Part 1: Physical and mineralogical methods. ASA & SSSA, Madison, WI, (Agronomy Monograph no. 9), pp. 383–411.

Granger, D.E., Kirchner, J.W., Finkel, R. 1996. Spatially averaged long-term erosion rates measured from in situ-produced cosmogenic nuclides in alluvial sediment. J. Geol. 104: 249–257.

Guzmán, G., Barrón, V., Gómez, J.A. 2010a. Evaluation of magnetic iron oxides as sediment tracers in water erosion experiments. Catena 82: 126–133.

Guzmán, G., Gómez, J.A., Giráldez, J.V. 2010b. Measurement of particle size distribution of soil and selected aggregate sizes using the hydrometer method and laser diffractometry. EGU General Assembly. Geophys. Res. Abstr. Vol. 12, EGU2010-4422-1.

Guzmán, G., Cañasveras, J.C., Boulal, H., Gómez-McPherson, H., Barrón, V., Gómez, J.A. 2011. Soil redistribution after rainfall events in a furrow-shoulder system at field scale using iron oxides as sediment tracers. Geophys. Res. Abstr. Vol. 13, EGU2011-9711.

Kosmas, C.S., Curi, N., Bryant, R.B., Franzmeier, D.P. 1984. Characterization of iron-oxide minerals by 2nd-derivate visible spectroscopy. Soil Sci. Soc. Am. J. 48: 401–405.

Krause, P., Boyle, P.D., Bäse, F. 2005. Comparison of different efficiency criteria for hydrological model assessment. Adv. Geosci. 5: 89–97.

Laguna, A., Giráldez, J.V. 1993. The description of soil erosion through a kinematic wave model. J. Hydrol. 145: 65–82.

Liebig, M.A., Jones, A.J., Mielke, L.N., Doran, J.W. 1993. Controlled wheel traffic effects on soil properties in ridge tillage. Soil Sci. Soc. Am. J.57: 106–1066.

Mehra, O.P., Jackson, M.L. 1960 Iron oxide removal from soil and clays by a dithionatecitrate system with sodium-bicarbonate buffers. Clay Clay Miner. 5: 317–327.

Mentler, A., Strauss, P., Schomakers, J., Hann, S., Köllensberger, G., Ottner, F. 2009. Organophilic clays as a tracer to determine erosion processes. Geophys. Res. Abstr. Vol. 11, EGU2009-13192. EGU General Assembly 2009.

Ogden, C.B., van Es, H.M., Schindelbeck, R.R. 1997. Miniature rain simulator for field measurement of soil infiltration. Soil Sci. Soc. Am. J. 61: 1041–1043.

Olver, F.W.J., Lozier, D.W., Boisvert, R.F., Clark, C.W. 2010. NIST handbook of mathematical functions. Eds. Cambridge Univ. Press. Cambridge.

Pelletier, J.D., DeLong, S.B., Cline, M.L., Harrington, C.D., Keating, G.N. 2008. Dispersion of channel-sediment contaminants in distributary fluvial systems: Application to fluvial tephra and radionuclide redistribution following a potential volcanic eruption at Yucca Mountain. Geomorph. 94: 226–246.

Polyakov, V.O., Nearing, M.A., Shipitalo, M.J. 2004. Tracking sediment redistribution in a small watershed: implications for agro-landscape evolution. Earth Surf. Proc.Landf. 29: 1275–1291.

Press, W.H., Teukolsky, S.A., Vetterling, W.T., Flannery, B.P. 2007. Numerical recipes. The art of scientific computing. 3rd ed. Cambridge Univ. Press. Cambridge.

Rhoton, F.E., Emmerich, W.E., DiCarlo, D.A., McChesney, D.S., Nearing, M.A., Ritchie, J.C. 2008. Identification of Suspended Sediment Sources Using Soil Characteristics in a Semiarid Watershed. Soil Sci. Soc. Am. J. 72: 1102–1112.

Sellitto, V.M., Fernandes, R.B.A., Barrón, V., Colombo, C. 2009. Comparing two different spectroscopic techniques for the characterization of soil iron oxides: Diffuse versus bi-directional reflectance. Geoderma 149: 2–9.

Singh, V.P., Regl, R.R. 1983. Analytical solutions of the kinematic equations for erosion on a plane. I. Rainfall of indefinite duration. Adv. Water Resour. 6: 2–10.

Soil Survey Staff. 2010. Keys to Soil Taxonomy, 11th ed. United State Department of Agriculture-Natural Resources Conservation Service, Washington, DC, USA.

Tullberg, J.N., Yule, D.F., McGarry, D. 2007. Controlled traffic farming–From research to adoption in Australia. Soil Till. Res. 97: 272–281.

Walling, D.E., He, Q., Blake, W. 1999. Use of ^{7}Be and ^{137}Cs measurements to document short- and medium-term rates of water-induced erosion on agricultural land. Water Resour. Res. 35: 3865–3874.

Xue,Y.Z., Liu, P.L., Yang, M.Y., Ju, T.J. 2004. Study of spatial and temporal processes of soil erosion on sloping land using rare earth elements as tracers. J. Rare Earth 22: 707–713.

Chapter 4. Assessment of soil losses at the plot scale in a rainfed olive orchard using a magnetic iron oxide tracer

Abstract

Soil erosion is a major concern in the management of olive cropped areas in Mediterranean countries, like Spain, due to the in-site and off-site effects on Agriculture and Environment. In order to estimate the soil erosion losses in the field, the use of tracers is very effective. Magnetic iron oxide particles are good tracers to complement, or even replace traditional techniques of soil loss measurement, especially at the small plot scale. The soil movement, or redistribution by water and tillage erosion in an olive orchard, has been estimated in two runoff plots measuring the magnetic susceptibility changes from October 2008 to August 2010. Soil magnetic susceptibility maps, separating the inter-tree rows, tree rows and rill areas influence, were compared once the methods were calibrated in the laboratory and the field. Magnetic iron oxides acting as tracers allowed the estimation of soil losses with a RSME of 0.72 $kg \cdot m^{-2}$. Soil losses were slightly higher in the inter-tree rows than in tree rows, although the splash of the canopy driven gravity drops is very important, due to the average height of olive trees within the plots (4.5 m approximately) and following the classification proposed by Moss and Green (1987) who consider the erosion of the drops that fall from each layer to the soil surface. Magnetite content variations both overland and within the soil profile, selectivity of the tracer for finer soil particles, and soil bulk density changes, due to tillage-compaction and swelling-shrinking processes were the key factors for the precision of the estimation of soil losses. The use of magnetic susceptibility changes in the soil can be a useful method to assess the suitability of different olive orchard management methods and to monitor sediment dynamics in the studied plots.

Key words: iron oxides, soil magnetic susceptibility, magnetic tracers, olive orchard

In preparation as: Guzmán, G., Gómez, J.A., Vanderlinden, K., Giráldez, J.V. Assessment of soil losses at the plot scale in an olive orchard under natural rainfall using a magnetic iron oxide tracer.

4.1. Introduction

About 17% of southern Spain's surface is covered by olive orchards (Gómez *et al*. 2005a). Traditionally, olive orchards were confined to marginal hilly areas with shallow soils (Consejería de Agricultura y Pesca, 2003). More recently, the olive cropped areas have advanced on flatter more fertile soils. In both cases, the adverse topography before, and the traditional weed control strategy based on a reduced tree density and canopy size, leaving the soil bare , make the erosion risk very high (Gómez *et al*. 2003).

Despite the large number of reports dedicated to the study of soil erosion, a significant uncertainty persists in the estimation of actual erosion rates in these areas (Gómez *et al*. 2008; Fleskens and Stroosnijder, 2007). Due to the technical and economic limitations of traditional methods used in erosion measurement, there is a growing interest in the use of new methods including tracking of soil incorporating tracers in experiments performed at different scales and time periods.

Among many sediment tracers, radionuclides such as ^{137}Cs, ^{210}Pb and ^{7}Be, whose respective half-lives, 30.2, 22.3, and 53.2 years allow its use long-term with the first two and short-term with the latter one. Schoorl *et al* (2004) and Gaspar *et al*. (2011) presented olive erosion works with the former radionuclides as tracers. An alternative to radionuclides are rare earth oxides that tag soil aggregates showing a preferential bound for finer particles (Zhang *et al*. 2001) and these have been evaluated in soil erosion studies at plot scale by Polyakov and Nearing (2004), although they have not been tested in different environments like the Mediterranean climate. In addition, to rare earth oxides being difficult to uniformly incorporate into the soil profile, the high cost of the analysis of the sample has reduced its acceptance by researchers in the field.

The magnetic properties of many earth minerals has been taken advantage of in fingerprinting analyses of erosion and sediment delivery in eroding landscapes (Royall, 2001), or more recently by Hatfield and Maher, 2008).

Extending this method to the insertion of external magnetic tracers into the soil constitutes a simpler and cheaper alternative to the rare earth oxide method. Although man-made magnetic tracers, such as rare earth oxides, present some limitations such as the lack of homogeneity when added to a certain soil profile, they allow faster measurements and a lower cost analysis. Hu *et al*. (2011) prepared five magnetic tracers of different sizes and bulk densities (0.99–1.29 $g \cdot cm^{-3}$) and evaluated their potential under simulated rainfall events at laboratory scale finding that only two of them were transported in phase with soil particles. Ventura *et al.* (2001, 2002) also developed a magnetic tracer consisting of magnetized plastic beads of 3.2 mm of mean weight diameter. The tracer performance was evaluated in a hillslope plot under simulated rainfall. The results obtained indicated that the magnetic beads could identify areas of net detachment and deposition without quantifying erosion rates due to the size and density of the tracer. Guzmán *et al*. (2010a) evaluated the use of magnetic iron oxide as a sediment tracer at laboratory scale finding that the oxide was preferentially bound to finer soil particles taken into account in the interpretations of the measurements and that the oxide moved in phase with soil. The magnetic iron oxide also allowed the estimation of soil erosion rates with an accuracy of 0.5 $kg \cdot m^{-2}$.

De Luna *et al*. (2000) observed differences in the behavior of sediment dynamics at plot scale under simulated rainfall events, obtaining higher soil detachment and erosion under olive tree canopies due to the greater kinetic energy under canopies in comparison to open areas. Under natural rainfall events, differences in physical soil properties, infiltration and yield have been found in olive orchards between soil under canopy projections and soil in the rows by Gómez *et al*. (1999) for a 15 years period in two soil managements: conventional tillage and no tillage. Almost all the properties they examined varied with soil location as much as with the method of tillage used. Gómez *et al*. (2002), for twelve rain events, also determined that the areas surrounding the tree trunks were the most relevant in some hydrological processes because of the high concentration of rainfall in the form of stream flow in comparison to other zones of the plots.

For these studies, experimental field measurements are essential to evaluate spatial variability of erosion processes under natural conditions. Magnetic iron oxide variations after rainfall events can be quantified through soil plot mappings. Through these variations it could be possible to detect detachment/erosion sources in olive orchards and monitor sediment redistribution identifying soil movement at the different zones of the plots.

The purposes of this Chapter are *(i) to estimate soil losses coming from intense erosion events measuring variations in their magnetic iron oxide content* and *(ii) to understand sediment dynamics and soil redistribution in olive orchards, identifying potential eroded/deposition areas at short-term.*

4.2. Materials and methods

4.2.1. Field site

The field site experiment was established on a drip-irrigated olive orchard farm La Conchuela (37.53ºN, 4.47ºW) at 147 m above sea level. The olive trees were planted in 1993 (cv. "Arbequino") at 6×7 m spacing, Figure 4.1. The climate in the area is typically Mediterranean, with 80% of the rains concentrated in the Fall and Winter seasons, October-March, (Gómez *et al*. 2009), and a long dry and hot Summer. The main soil type is *Typic Haploxerert* (Soil Survey Staff, 2010) highly plastic when wet, with retraction cracks in dry periods. Table 4.1 shows some characteristics of the field site and soil properties at the top 0.10 m.

4.2.2. Experimental plots

Six closed runoff plots of a rhombic shape with the longest sides parallel to the maximum slope and to the tree lines were initially established in the summer of 2008 (Figure 4.1).

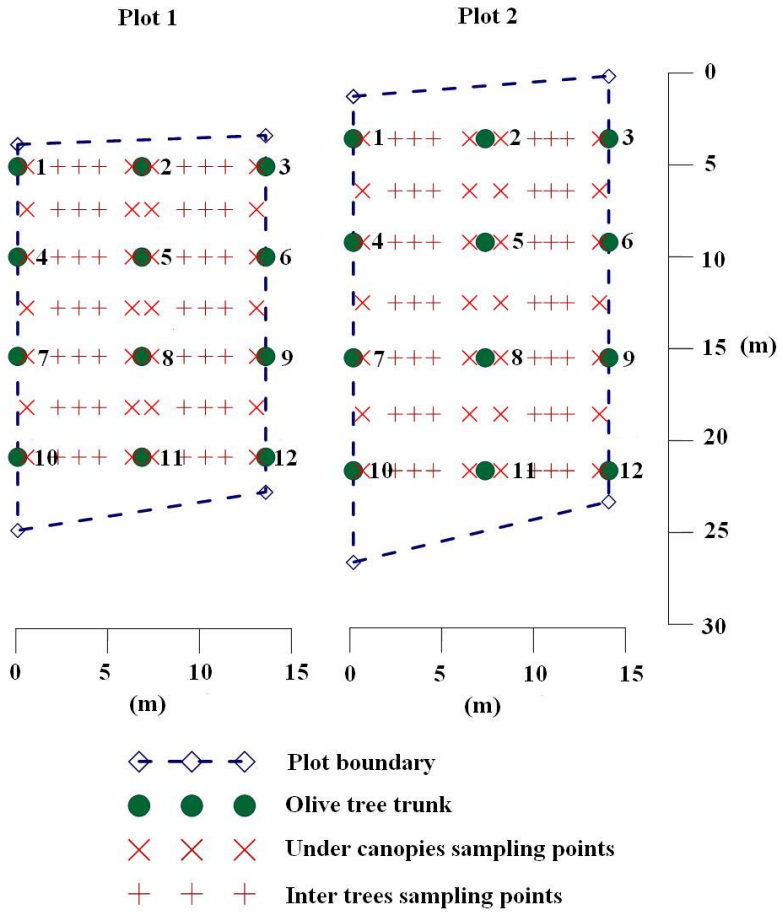

Figure 4.1. Plots scheme showing olive tree position within the plots and soil sampling points under the canopies and inter-tree rows.

Field site characteristics	
Slope (%)	13.4
Soil organic matter (%)	1.24
Clay (%)	48.6
Silt (%)	44.3
Sand (%)	7.1
Background magnetic susceptibility of the soil (10^{-7} $m^3 \cdot kg^{-1}$)	1.21
Magnetic susceptibility of magnetite (10^{-4} $m^3 \cdot kg^{-1}$)	5.29
Average annual rainfall (mm)*	794
Average annual ET_o (mm)*	1225

Table 4.1. Soil properties of La Conchuela experimental catchment. *(From *http://www.uco.es/cgi-ag1vimaf/datos.pl?tipo_estacion=&file=arc_lr.day&estacion=La%20Reina* calculated as the annual average from 1/01/2008 to 31/12/2010 at 'La Reina' agrometeorological station).

Two of these plots were chosen for the magnetic tracer experiment. Plot 1, upslope, was kept under a conventional tillage treatment, consisting of light cultivator passes along the inter-tree rows and herbicide application at the trees' feet. The plot 2, downslope, was kept with a cover crop created by a Fall *Lolium multiflorum* sown in inter-tree strips 3.6 m wide, with a small dose of ammonium nitrate as a starter. Herbicide was applied under the olive canopies. The cover crop is usually killed in the early spring to minimize the competition for water and other nutrients, with olive trees. The October 2008 attempt to establish the cover failed due to a few intense showers just after sowing. Therefore, no management differences were considered between both plots. In April 2010, plots 1 and 2 were plowed again; the cover plant was sown in plot 2. On this occasion, favorable light rains and the application of NPK fertilizer allowed a good plant stand.

The plots were protected against occasional external runoff overflow by a metal sheet wall enclosing three olive tree lines each of them with four trees one in the center and the other two in the respective borders. The mean horizontal canopy projection, estimated by a simple average of several random diameters, was 20 and 26 m^2, for plot 1 and 2, respectively. The canopy covered area was approximately 50 and 55 % of the total plot 1 and plot 2 areas, respectively. Figure 4.1 shows a scheme of the limits of both plots indicating olive tree positions and soil sample points distinguishing between the ones taken from inter-tree and tree rows.

In October 2008, a mixture of magnetic iron oxide and soil particles were spread on the plots. The mixture was prepared with sieved air-dry soil aggregates of 0.06 m size and magnetic iron oxide particles, according to the Zhang *et al*. (2001) method, to increase the background magnetic susceptibility of soil in one magnitude order. Once the mixture was broadcasted onto the soil surface, it was incorporated into the first 0.05 m of the profile with a cultivator to reach a final magnetic iron oxide concentration of 0.25 % of the total dry weight. In the case of plot 2, seeds for cover crop were spread just after the mixture and buried with the cultivator pass.

4.2.3. Runoff and sediment collection

From October 2008 to August 2010, runoff was collected and measured using a system of tipping-bucket gauges with a 5 min resolution. Sediment collected in a barrel located upslope of the tipping buckets was sampled, oven-desiccated and weighted to estimate its average concentration and, by accumulation, total soil losses. One gauge, connected to a data-logger, recorded intensity at 5 min intervals and measured total rain depth. These collection systems are described in more detail by Gómez *et al*. 2009. During that period, the sediment yield from ten representative rainfall-runoff events (from October 2009 to March 2010), were analyzed to determine magnetic susceptibility and magnetite content. The sediment particle size distribution was also analyzed using a Beckman Coulter LS−230 ®, (Guzmán *et al*. 2010b). These measurements were necessary for closing the magnetite mass balance and determining the sediment enrichment ratio of tracer for finer soil particles (Guzmán *et al*. 2010a).

4.2.4. Estimation of soil losses using magnetic iron oxide

Three soil sampling campaigns were carried out in the plots in three different times at the start of the experiment after the tracer incorporation in October 2008; in March 2010, after 17 months; and in August 2010, at the end of the trial. The first (October 2008) and the second (March 2010) campaigns collected 70 soil samples from each plot at different positions, inter-trees and tree rows, and at several depths: 0-0.01 and 0.01-0.08 m. Additional soil samples from the 0.08-0.12 m depth interval were also taken at the same locations to check whether magnetic iron oxide reached the 0.08 m depth. Samples were taken at 1.3 and 1.6 m through the breadth and length of the plot, Figure 4.1. Magnetic susceptibility was measured in the lab using a Bartington MS2 and MS2B equipment. During the second sampling, surface rills were characterized measuring their length and width at different sections estimating their depth and shape with detailed photographs. Soil magnetic susceptibility of the rills was measured *in situ* using a Bartington MS2 and MS2D field probe. Soil samples for bulk density and soil moisture were taken at two different depth intervals, 0-0.05 and 0.05-0.10 m in both samplings.

The third sampling (August 2010) consisted of a mapping of the plots using the field probe, as an average of four readings at the same locations of the first and second samplings. Soil moisture was measured in each location using a TDR at the 0-0.15 m depth interval. Soil samples for bulk density were not taken because *a priori*, soil probe calibration was thought to be set up comparing magnetic susceptibility measurements. For this reason, soil bulk density of inter-tree rows at the top 0.05 m was considered the one determined by Gómez *et al*. (2009). For tree rows, bulk density was assumed to be the same as that measured in March because no variation in soil conditions, during the March-August period, was appreciated in these zones. All the samplings under the canopies required the removal of the fallen leaves resting on the soil surface for a proper contact between field probe and soil surface. No rills were observed in any of the plots during the August sampling due to the erasing effect of the tillage pass and no large rainfall events during the March-August period.

Figure 4.2 shows the three plot conditions at the three samplings: October 2008 (a) at the tagging, March 2010 (b) with rills, April 2010 (c) after the tillage pass and August 2010 (d) at the end of the experiment.

Figure 4.2. View of the plots at the three samplings: October 2008 (a), March 2010 (b), April 2010 (c) and August 2010 (d).

The comparison between soil magnetite content was computed considering the mass of soil in the sampling layer (*e.g.* Kachanoski and de Jong 1984). The magnetic susceptibility of the soil sample, χ_s, with a mass m_s, composed of a mass of untagged soil and magnetite, m_b, and m_m, respectively, $m_s=m_b+m_m$, and respective magnetic susceptibilities, χ_b, and χ_m, is,

$$\chi_s = \chi_b + \frac{m_m}{m_s}(\chi_m - \chi_b) \tag{4.1}$$

The subindex $_b$ refers to the blank condition of the untagged soil. The ratio m_m/m_s is the mass concentration of magnetite in soil.

The mass of soil lost per unit area, E, was estimated through the change in magnetite content at each plot during the experiment period, $(m_{m0}-m_{mf})/m_{m0}$,

$$E = \left(1 - \frac{m_{mf}}{m_{mo}}\right)\frac{\rho_{b0} z_s}{\alpha} \tag{4.2}$$

The initial bulk density of the soil was ρ_{b0}, the depth of the sample volume z_s. The correction factor, α, is the product of two coefficients: one is a selectivity coefficient that represents the affinity of the magnetic tracer to the finer soil particles, c_s, (Guzmán *et al*. 2010a); the other coefficient, c_d explains a higher tracer concentration when tagged soil is mixed with blank soil.

The former coefficient was determined through a mixing test in the laboratory, described in Section 3.2.3.1. The exponential trend line of Figure 4.3 is an average of the decreasing trend lines shown in Figure 3.6 for furrows +T and −T, where χ_i is the magnetic susceptibility at each interval normalized by the weighted magnetic susceptibility of the whole interval χ, and the height of each interval h_i normalized by the total height of tagged soil h.

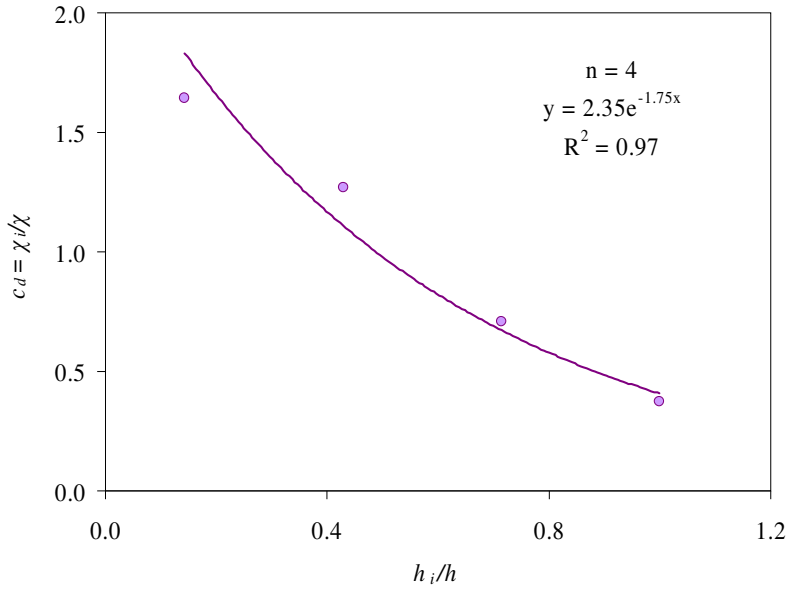

Figure 4.3. Exponential regression line between normalized magnetic susceptibility and height of tagged soil in a laboratory mixing test. The regression coefficient is also indicated.

Using the magnetic susceptibility changes at the different plot zones, and their corresponding soil loss, namely, tree rows, E_{tr}, with area A_{tr}; inter-tree rows, E_{itr}, with area A_{itr}; and, when present, rills, E_r, with approximate area A_r, it is possible to integrate them with a simple equation, to reach the total soil loss E_t from the total area of the plot, A.

$$E_t = \sum_{i=tr,itr,r} \frac{A_i}{A} E_i \qquad (4.3)$$

4.2.5. Soil redistribution in plots

The tillage pass carried out within the March-August 2010 period (April 2010) by the farmer permitted an analysis of the soil redistribution process with the help of the magnetic tracer.

4.2.6. Field probe calibration

As Dearing (1999) pointed out, for some field situations where homogeneity of the measured volumes does not present significant differences, it is possible to obtain an empirical relationship between mass (MS2B) and volume susceptibilities (MS2D). For this purpose, during the third mapping, fifteen soil samples at 0-0.01, 0.01-0.08 and 0.08-0.12 m depth intervals were taken in some of the sites where the probe was placed as a function of the homogeneity of the soil surface and the representativeness of the measurements: from background up to the highest readings. As the field probe reaches a soil depth higher than 0.06 m, where sensitivity of the signal is approximately 10 % (Dearing, 1999), soil samples from the 0-0.08 m interval were used to determine magnetite content, checking with the deepest ones that no magnetite was present in them. Figure 4.4 shows the observed relation between field probe volume susceptibility (MS2D) and magnetite content determined in the lab through mass magnetic susceptibility (MS2B).

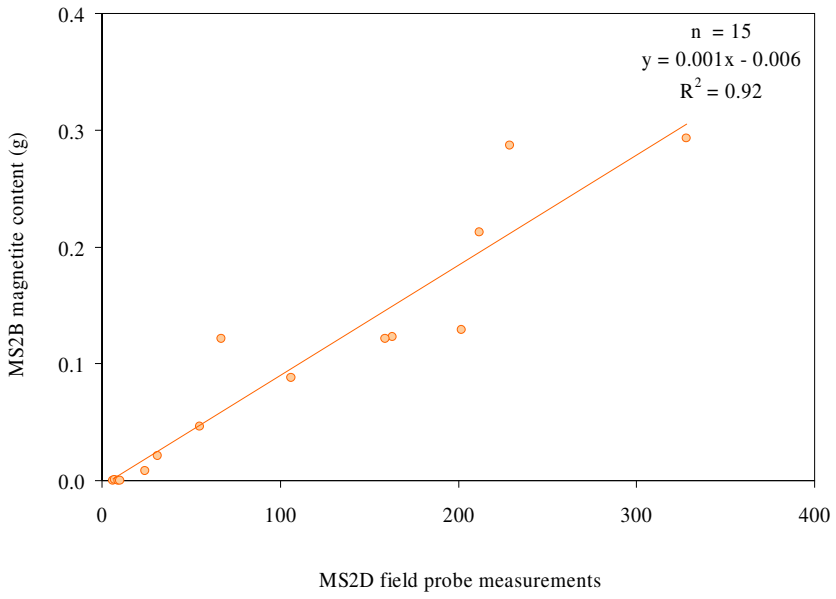

Figure 4.4. Relation between MS2D field probe measurements and the magnetite content of soil samples obtained through MS2B laboratory measurements from the same locations where probe measurements were done (n = 15).

For the field probe calibration, it was assumed that no significant soil losses occurred from the second to the third sampling. Magnetite content determined by the relation between MS2D and MS2B, Figure 4.4 at the third sampling had to be slightly lower or approximately the same as the one measured at the second sampling.

4.3. Results and discussion

4.3.1. Runoff and sediment collection

Precipitation, total soil losses and runoff generated of the successive rainfall events were recorded from October 2008 to August 2010 in the plots, Figures 4.5 and 4.6.

From October 2008 to March 2010 rainfall events produced runoff flows but not sediments. This could be attributed to the low energy of both raindrops and surface runoff flow, in otherwise consolidated soil. Rainfall events in the winter of 2010 generated 99 % of the total soil losses and 91 % of total runoff in both plots because these events signified more than 50 % of the total rainfall measured from October 2008 to August 2010. Despite the failure of the cover crop in plot 2, both runoff and soil losses were generally lower in this plot in all the cases.

Total magnetic susceptibility of sediment was calculated as the weighted average of the respective values corresponding to the total soil loss in each of the ten events analyzed. The total susceptibility was almost 7.5 % higher than the initial susceptibility of tagged soil due to the preferential adsorption of tracer in fine particles and the increase in clay particles in sediment.

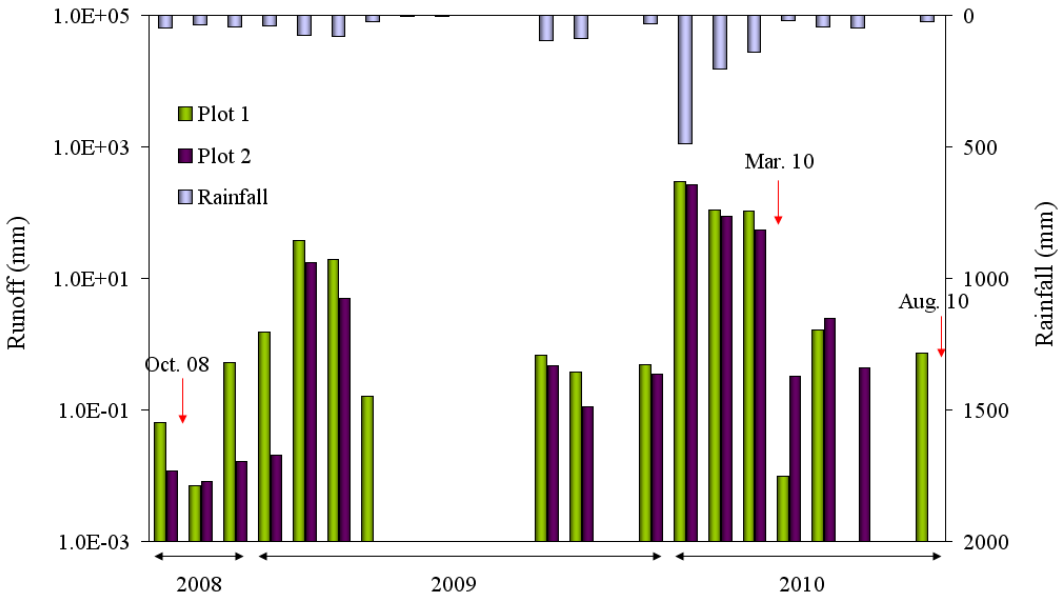

Figure 4.5. Monthly precipitation and runoff volumes observed in plots 1 and 2 from October 2008 to August 2010. The left axis represents runoff at a logarithmic scale and the right one, upside down in an arithmetic scale, corresponds to rainfall.

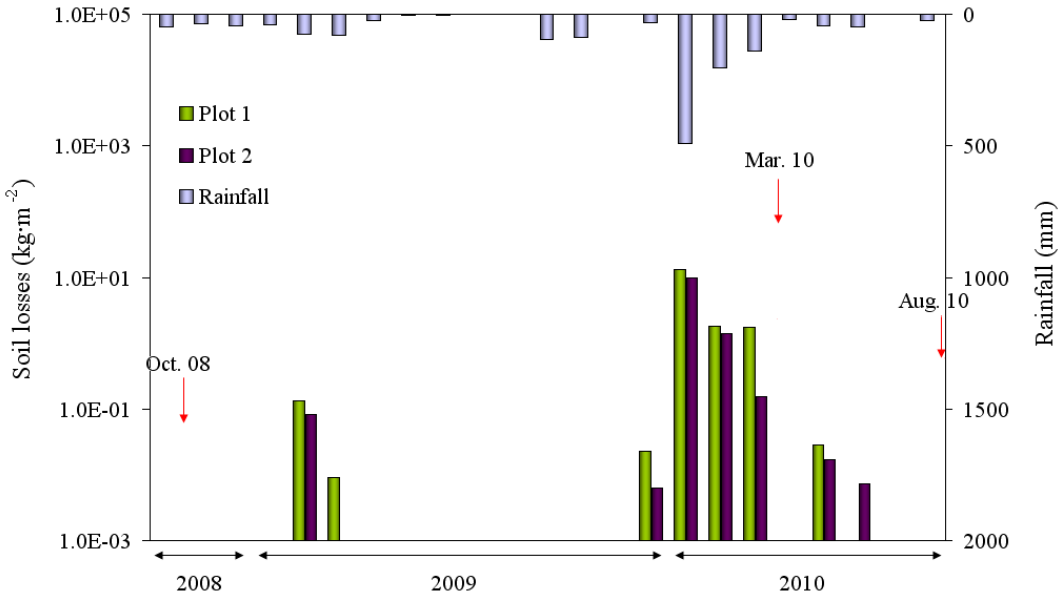

Figure 4.6. Monthly precipitation and soil losses observed in plots 1 and 2 from October 2008 to August 2010. The left axis represents soil losses at a logarithmic scale and the right one, upside-down with arithmetic scale, corresponds to rainfall, as in Figure 4.5.

4.3.2. Estimation of soil losses using magnetic iron oxide

Figure 4.7, shows the magnetite content just after tagging the top 8 cm of soil at the plots (October 2008). As mentioned in previous Chapters, the incorporation of the magnetic iron oxide into the soil profile uniformly is one of its main limitations although in this case, differences in magnetite content did not present important differences when comparing sampling points.

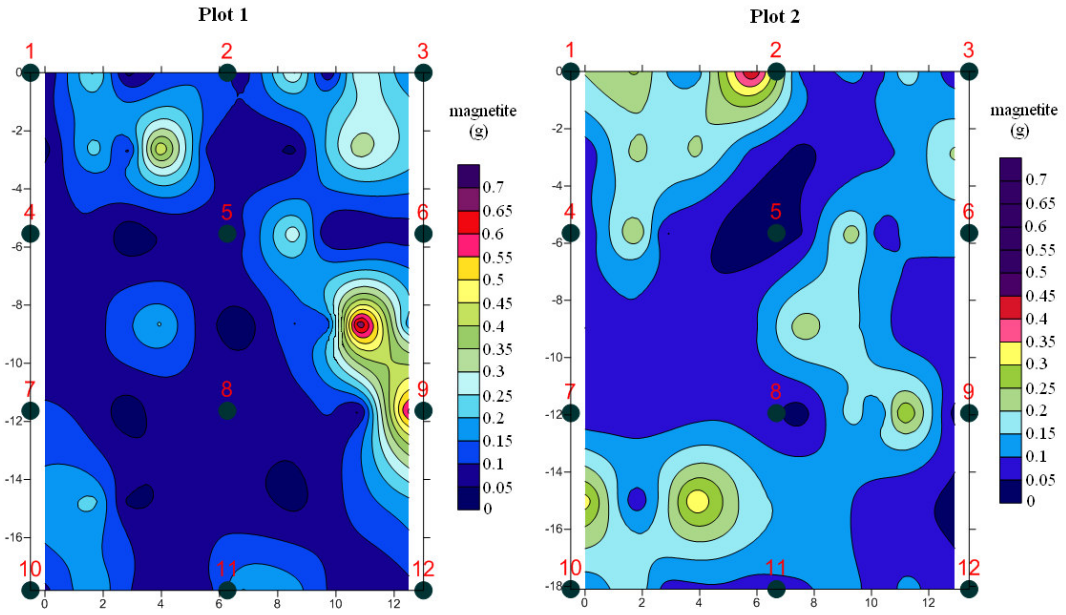

Figure 4.7. Magnetite distribution at the top 8 cm after tagging the plots in October 2008. Numbers from 1 to 12 indicate olive trees position.

Table 4.2 presents the average and standard deviations of the bulk density and soil moisture contents of the three samplings separating tree rows and inter-tree rows. Bulk density and soil moisture content were found out at the three different samplings: October 2008 when plots were just tagged, March 2010 with well developed rills and August 2010 at the end of the experiment.

	Zones	Bulk density ($Mg \cdot m^{-3}$)			
		Oct. 08	Mar. 10	Aug. 10	p
Plot 1	Inter- tree rows	1.45 ± .18	1.51 ± .07	1.38 ± .02	0.328
	Tree rows	1.48 ± .06	1.42 ± .15	1.42 ± .15	0.770
	p	0.760	0.342	0.640	-
Plot 2	Inter- tree rows	1.58 ± .11	1.57 ± .02	1.38 ± .02	0.003
	Tree rows	1.48 ± .08	1.41 ± .15	1.41 ± .15	0.723
	p	0.182	0.080	0.710	-
	Zones	Soil moisture ($m^3 \cdot m^{-3}$)			
		Oct. 08	Mar. 10	Aug. 10	p
Plot 1	Inter- tree rows	.16 ± .02	.21 ± .00	.09 ± .01	0.000
	Tree rows	.14 ± .03	.21 ± .02	.18 ± .01	0.009
	p	0.520	0.915	0.000	-
Plot 2	Inter- tree rows	.16 ± .03	.20 ± .00	.13 ± .00	0.001
	Tree rows	.13 ± .01	.21 ± .01	.19 ± .02	0.000
	p	0.064	0.110	0.000	-

Table 4.2. Average bulk density and soil moisture contents and their standard deviations at the three samplings, separating between tree rows and inter-tree rows for both plots. $p<0.05$ indicate significant differences between samplings (rows) and zones (columns).

In August, significant differences were found in soil moisture between zones probably because soil surface was removed during April enhancing water evaporation in the rows. A comparison of soil moisture content between samplings detected significant differences in the inter-tree and tree rows in all the cases because of the changes in the soil. For bulk density, these differences were not significant in most of the cases because it remained almost constant in the October-March period.

Figure 4.8 compares measured and estimated soil losses from October 2008 to March 2010 and from October 2008 to August 2010. It also shows the correlation between them, the regression coefficient and the root square mean error ($kg \cdot m^{-2}$) for n = 4 in at the studied plots using the average values for bulk density shown in Table 4.2. Since no significant differences existed for bulk densities at each sampling distinguishing between inter-tree areas and tree rows, c_s and c_d for both plots, average values were used to estimate soil losses. To do this in March 2010, rills were considered in both plots because, where they were not taken into account, lost soil was underestimated by 1.5 %.

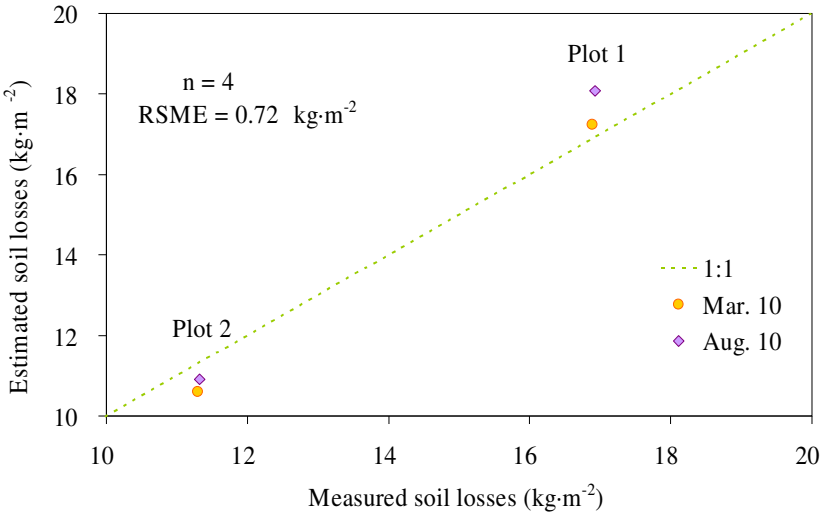

Figure 4.8. Measured and estimated soil losses and RSME for the two plots at the two samplings (Mar. 10 and Aug. 10), n = 4.

Figure 4.9 represents the soil loss rates in both plots distinguishing between inter-tree rows *(itr)*, tree rows *(tr)* and rills *(r)* in March 2010 and between inter-tree rows *(itr)* and tree rows *(tr)* in August 2010.

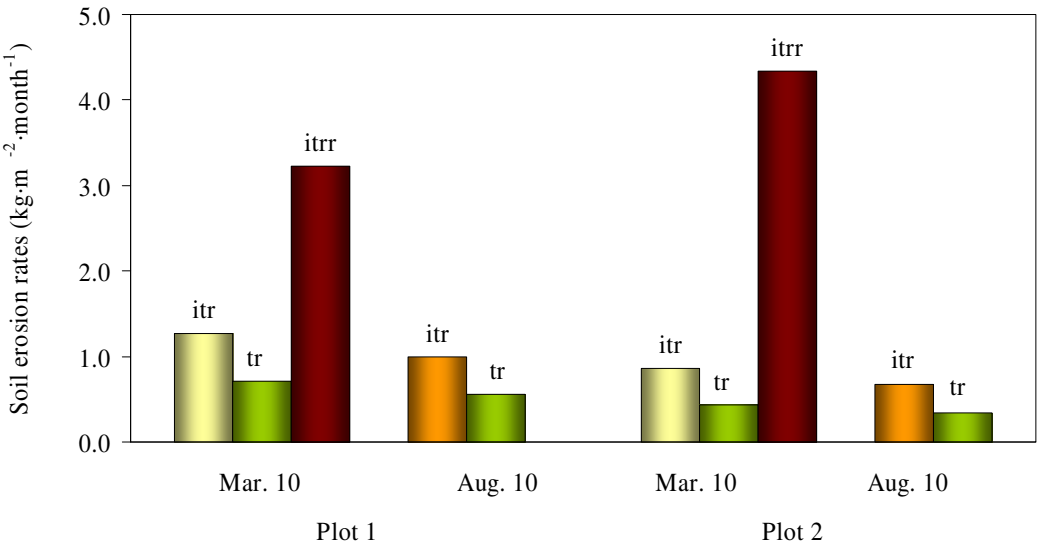

Figure 4.9. Soil erosion rates for each area in the plots at the two samplings (Mar. 10 and Aug. 10) distinguishing between inter-tree rows (*itr*), tree rows (*tr*) and rills (*r*).

Although there were no significant differences in bulk density in the different areas in the plots at each sampling, inter-tree row erosion rates were slightly higher compared to tree row erosion rates due to soil beneath trees being covered by the olive canopies and tree leaves that protected the soil surface. Soil erosion rates in August were lower compared to the ones calculated in March because no important soil losses were observed in the five months between them. Rill erosion rates were higher and significantly different because in these areas most of the tagged profile was lost, and, therefore, differences in magnetite content were noticeable between October and March in these areas.

Figure 4.10 shows the soil losses of inter-tree rows, tree rows and rills (March 2010) and inter-tree and tree rows (August 2010) referring the erosion rates to their corresponding area in the plots.

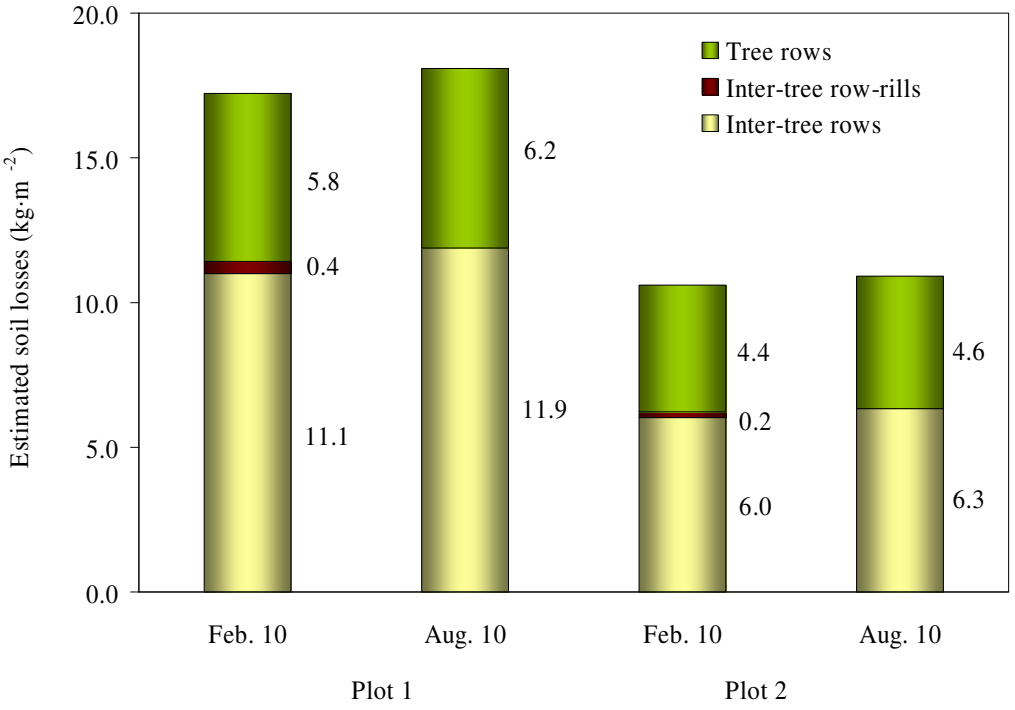

Figure 4.10. Estimated soil losses differentiating between tree rows, inter-tree rows and rills at the two samplings (Mar. 10 and Aug. 10) for both plots.

Although soil losses from tree rows were the lowest ones in all the cases, the contribution of these areas to total soil losses was considerably high. This was explained because of the greater volume, and therefore covered area, of the canopies in the plots. Soil losses of rills were the highest in the plots but their contribution was the lowest because they signified only 1% of the total area in the plots. The sum of inter-tree rows and rills contributions in March were similar to those observed in August, which indicated a relatively good calibration of the field probe measurements. However, the estimated soil losses of tree rows and inter-tree rows in August (referred to October) are slightly higher than in March due to the soil lost during the March-August period.

While for c_s and c_d the response of the errors followed an increasing linear trend line, the response against magnetite content variations decreased. A decreasing linear trend line was also detected for bulk density in March, where no plowing was done in the plots, and, therefore, the bulk density of inter-tree rows in the sampling was higher than the ones in the inter-tree rows in August. In August, the best fit corresponded to a parabola. Errors in the underdetermination of bulk density, especially in the wet period, resulted in large errors in the determination of soil loss rates.

The dispersion of the magnetite mass data is represented in the box and whisker plots of Figure 4.11. The erosion period, October 2010-March 2010, reduced the magnetite mass range at the tree rows (*tr*) and in the inter-tree rows (*itr*) in both plots. The rills' magnetite masses are lower in both plots too. The changes in the less erosive, subsequent period, March-August 2010, are due to the redistribution effect of the tillage, homogenizing the data, or reducing the range of magnetite masses.

Table 4.3 compares the mean values for the magnetite mass in the three samplings.

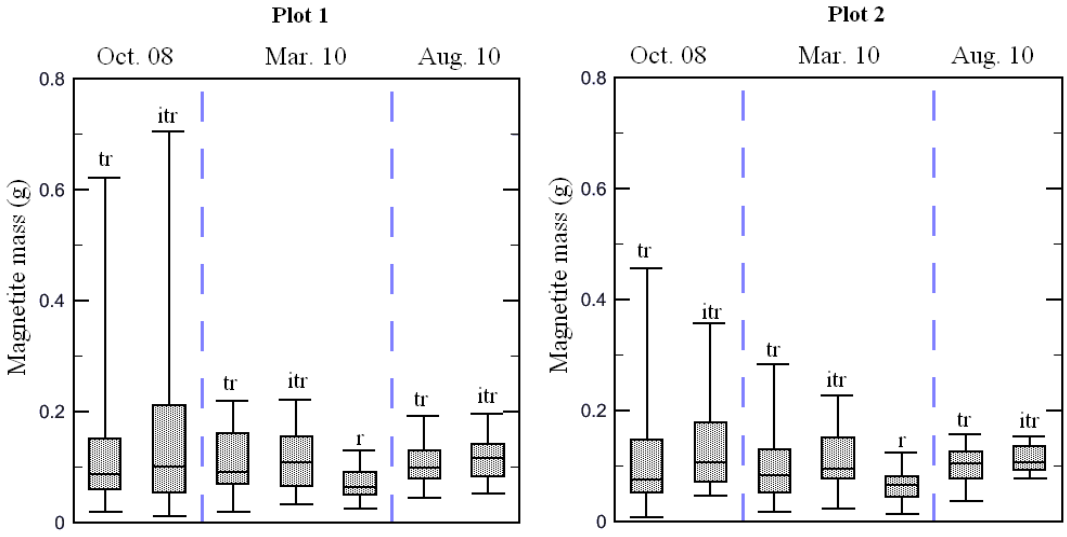

Figure 4.11. Box and whisker plots of the magnetite masses in both plots. The middle horizontal bar inside the box represents the median, the extreme bars of the box, are the first, below, and the third, above, quartiles. The extreme bars correspond to the minimum and maximum values, respectively. *tr*, *itr* and *r* corresponds to tree rows, inter-tree rows and rills respectively.

Plot	Magnetite mass (g)	Tree rows			Inter-tree rows			Rills
		Oct.08	Mar.10	Aug.10	Oct.08	Mar.10	Aug.10	Oct.08
1	Average	0.118	0.105	0.104	0.147	0.117	0.116	0.071
	CV	0.944	0.572	0.320	0.930	0.458	0.318	0.447
2	Average	0.109	0.102	0.101	0.131	0.113	0.113	0.063
	CV	0.914	0.663	0.329	0.572	0.484	0.218	0.464

Table 4.3. Mean values (*g*) and coefficient of variation (*CV*), of the magnetite masses in the plots, dates and areas are indicated.

Figure 4.12 shows the variation in magnetite content in plots 1 and 2 at the top 8 cm of soil profile, calculated as the difference of magnetite mass measured in March 2010 and the magnetite mass measured in October 2008.

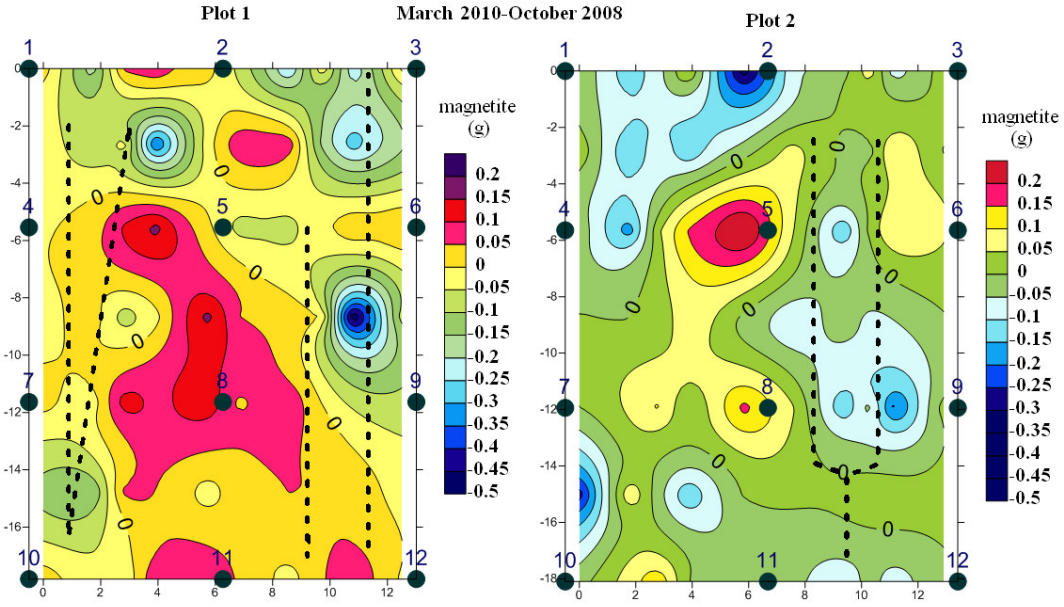

Figure 4.12. Magnetite content variation at the second sampling (March 2010) referred to the tagging of both plots (October 2008). Numbers from 1 to 12 represent olive trees location.

A decrease in magnetite mass (or negative values), indicate eroded areas, where tagged soil has been lost or redistributed after 17 months. On the contrary, values greater than zero indicate an increase in magnetite content or tagged soil at the sampling point. Although no clear trend of eroded/deposition areas in the plots is detected, there is an increase in magnetite content in the central tree row in both plots, especially noticeable in plot 1. The dashed line schematizes the shape and represents the position of the rills. It seems that through determining magnetite variation in the plots it is possible to identify significant losses of tagged soil profile in these specific areas. Magnetite mass maps on August, showed a more uniform redistribution of tagged soil at both plots, especially in the inter-tree rows, due to the tillage pass effectuated on April.

4.4. Conclusions

Magnetic iron oxide tracers constitute a useful tool for the estimation of soil losses after rainfall events under controlled rainfall conditions (Guzmán *et al*. 2010a).

In this study magnetite was used to estimate soil losses in olive orchard runoff plots through the variation of its concentration in the short-term (17 and 22 months).

There were several key factors in this approach that must be considered for the correct estimation of eroded soil, especially in a vertic soil with variable moisture content. For the comparison of magnetite content between samplings and the estimation of soil losses and magnetic susceptibility this must be corrected by bulk density. Due to changes in soil conditions between different samplings, it was necessary to measure or estimate adequately bulk density when soil samples were taken. Magnetic susceptibility or magnetite concentration, are inversely proportional to soil profile consolidation. Therefore, for a constant sampling depth, the magnetite content (or tagged soil) in the sampler is different as a function of the bulk density.

Field probe measurements offered a rapid way to measure volume magnetic susceptibility but if it is necessary to compare it with laboratory measurements, which determine mass magnetic susceptibility, it is essential to plot an empirical curve that relates both methods. Bulk density will strongly affect the magnetic susceptibility measurements in both methods, and therefore magnetic iron oxide content, being necessary to define a sampling depth for laboratory samples, deep enough to match probe depth.

As magnetite content decreases exponentially with depth, and as preferential transport of fine soil particles by water erosion is found, estimated eroded soil is overestimated. To solve this it is necessary to correct the estimation of soil loss by the selectivity and the distribution coefficients. Magnetic iron oxide not only allowed the estimation of total soil losses but also the quantification of the contribution of each area inside the plots.

Soil loss rates were lower in the tree rows than in the inter-tree rows, but their contribution must be considered because covered areas in the plots were around 50%. Rills in the plots were areas where almost all tagged soil was lost, and although these zones did not signify any great areas inside the plots, they must be considered to close magnetite and soil mass balance.

As mentioned above, the key factors in the errors of soil loss rate estimation were: selectivity and distribution coefficients, magnetite content in soil and bulk density. In all the cases, errors in the determination of these factors gave linear responses against error in soil loss rate estimation (increasing for both coefficients and decreasing for magnetite content). The response was not always linear for bulk density, being significantly sensitive for underestimations of this soil parameter.

The comparison of magnetite content between samplings offered useful information about soil movement and redistribution of soil as well as the identification of eroded/deposition areas in the plots.

4.5. Acknowledgements

Part of this study was supported by Projects P08-AGR-03925 (Andalusian Government) and AGL2009-12936-C03-01 (Spanish Ministry of Science and Innovation), RESEL (Spanish Ministry for Science and Environment) and FEDER funds. These supports are gratefully acknowledged. We are also very grateful to Francisco Natera, owner of 'La Conchuela farm', and his staff for their continuous support to the runoff plots experiments.

4.6. References

Consejería de Agricultura y Pesca, Junta de Andalucía. 2003. El olivar andaluz. Servicio de Publicaciones y Divulgación. Sevilla.

de Luna, E., Laguna, A., Giráldez, J.V. 2000. The role of olive trees in rainfall erosivity and runoff and sediment yield in the soil beneath. Hydrol. Earth Syst. Sci. 4: 141–153.

Dearing, J.A. 1999. Environmental magnetic susceptibility. Using the Bartington MS2 System, 2nd Ed. Chi Publishing, England.

Fleskens, L., Stroosnijder, L. 2007. Is soil erosion in olive groves as bad as often claimed? Geoderma 141: 260–271.

Gaspar, L., Navas, A., Walling, D.E., Machín, J., Gómez Arozamena, J. 2011. Using 137Cs and 210Pbex to assess soil redistribution on slopes at different temporal scales. Catena, doi: 10.1016/j.catena.2011.01.004.

Gómez, J.A., Sobrinho, T.A., Giráldez, J.V., Fereres, E. 2009. Soil management effects on runoff, erosion and soil properties in an olive grove of Southern Spain. Soil Till. Res. 102: 5–13.

Gómez, J.A., Giráldez, J.V., Vanwalleghem, T. 2008. Comments on "Is soil erosion in olive groves as bad as often claimed?" by L. Fleskens and L. Stroosnijder. Geoderma 147: 93–95.

Gómez, J.A., Giráldez, J.V., Fereres, E. 2005a. Water erosion in olive orchards in Andalusia (Southern Spain): a review. European Geosciences Union. Geophys. Res. Abstr. vol. 7, 08406.

Gómez, J.A., Vanderlinden, K., Nearing, M.A. 2005b. Spatial variability of surface roughness and hydraulic conductivity after disk tillage: implications for runoff variability. J. Hydrol. 311: 143–156.

Gómez, J.A., Battany, M., Renschler, C.S., Fereres, E. 2003. Evaluating the impact of soil management on soil loss in olive orchards. Soil Use Manag. 19: 127–134.

Gómez, J.A., Vanderlinden, K., Giráldez, J.V., Fereres, E. 2002. Rainfall concentration under olive trees. Agric. Water Manag. 55: 53–70.

Gómez, J.A., Giráldez, J.V., Pastor, M., Fereres, E. 1999. Effects of tillage method on soil physical properties, infiltration and yield in an olive orchard. Soil Till. Res. 52: 167–175.

Guzmán, G., Cañasveras, J.C., Boulal, H., Gómez-Macpherson, H., Barrón, V., Gómez, J.A. 2011. Soil redistribution after rainfall events in a furrow-shoulder system at field scale using iron oxides as sediment tracers. EGU General Assembly. Geophys. Res. Abstr.s vol. 13, EGU2011-9711.

Guzmán, G., Barrón, V., Gómez, J.A. 2010a. Evaluation of magnetic iron oxides as sediment tracers in water erosion experiments. Catena 82: 126–133.

Guzmán, G., Gómez, J.A., Giráldez, J.V. 2010b. Measurement of particle size distribution of soil and selected aggregate sizes using the hydrometer method and laser diffractometry. EGU General Assembly. Geophys. Res. Abstr. vol. 12, EGU2010-4422-1.

Hatfield, R.G., Maher, B. 2008. Suspended sediment characterization and tracing using a magnetic fingerprinting technique: Bassenthwaite Lake, Cumbria, UK. Holocene. 18: 105–115.

Hu, G.Q., Dong, Y.J., Wang, H., Qiu, X.K., Wang, Y.H. 2011. Laboratory testing of magnetic tracers for soil erosion measurement. Pedosphere 21: 328–338.

Isaaks, E.H., Srivastava, R.M. 1989. An introduction to applied geostatistics. Oxford University Press. Oxford.

Kachanoski, R.G., de Jong, E. 1984. Predicting temporal rlationship between soil Cesium 137 and erosion rate. J. Environ. Qual. 13: 301–304.

Kimoto, A., Nearing, M.A., Zhang, X.C., Powell, D.M. 2006. Applicability of rare earth element oxides as sediment tracers for coarse-textured soils. Catena 65: 214–221.

Moss, A.J., Green, T. W. Erosive Effects of the Large Water Drops (Gravity Drops) that Fall from Plants. Aust. J. Soil Res. 25: 9–20.

Polyakov, V.O., Nearing, M.A. 2004. Rare earth element oxides for tracing sediment movement. Catena 55: 255–276.

Royall, D. 2001 Use of mineral magnetic measurements to investigate soil erosion and sediment delivery in a small agricultural catchment in limestone terrain. Catena 46: 15–34.

Schoorl, J. M., Boix Fayos, C., de Meijer, R.J., van der Graaf, E.R., Veldkamp, A. 2004. The ^{137}Cs technique applied to steep Mediterranean slopes (Part I): the effects of lithology, slope morphology and land use. Catena 57: 15–34.

Soil Survey Staff. 2010. Keys to Soil Taxonomy, 11th ed. United State Department of Agriculture-Natural Resources Conservation Service, Washington, DC.

Ventura, E., Nearing, M.A., Amore, E., Norton, L.D. 2002. The study of detachment and deposition on a hillslope using a magnetic tracer. Catena 48: 149–161.

Ventura, E., Nearing, M.A., Norton, L.D. 2001. Developing a magnetic tracer to study soil erosion. Catena 43: 277–291.

Villalobos, F.J., Testi, L., Hidalgo, J., Pastor, M., Orgaz, F. 2006. Modelling potential growth and yield of olive (Olea europaea L.) canopies. Eur. J. Agron. 24: 296–303.

Zhang, X.C., Friedrich, J.M., Nearing, M.A., Norton, L.D. 2001. Potential use of rare earth oxides as tracers for soil erosion and aggregation studies. Soil Sci. Soc. Am. J. 65: 1508–1515.

Chapter 5. General discussion and conclusions

5.1. General discussion

The aim of this thesis was to develop an innovative group of sediment tracers based on iron oxides and use them at a hillslope scale to understand soil redistribution and sediment dynamics after water erosion experiments under different crops and soil managements.

The review carried out in Chapter 1 distinguishes five groups of sediment tracers: Radionuclides, Rare earths, Fingerprinting, Magnetics and Others, the first group being the most extended. They include a wide range of materials, substances and soil properties already established, offering different information, applicability and uses. Despite these existing differences among all the tracing techniques, they present some common issues such as the homogeneous incorporation of the tracer into the soil profile. Moreover, all of them present uncertainties and assumptions that must be considered to provide reliable quantitative results. As none of the described tracers fulfils all the requirements for being an ideal sediment tracer, new approaches are being developed.

The magnetic iron oxide evaluation at laboratory scale described in Chapter 2 provided the results of the utilization of iron oxides as sediment tracers. Magnetite characterization through the pipette method and dry sieving concluded that the magnetic iron oxide was a silt size iron powder able to tag soil aggregates in a dry way and uniformly except for the finer sizes whose binding affinity was higher. As the analysis cost is relatively quick, affordable and non-destructive, a large number of soil samples could be analyzed to determine this selectivity that would allow the reliable interpretation of the results obtained. The iron oxides are strongly bound to soil aggregates without significantly changing soil aggregate structure, and are not leached by infiltrating water as this was checked with the percolation test short term.

The strong binding to soil aggregates and the lack of vertical movement by the effect of water long the soil profile was also corroborated at the short-term hillslope scale. In Chapter 4, soil samples were taken at different depths at 17 months after the beginning of the test and no significant magnetite content was found in untagged soil originally due to pedogenic processes or bioturbation.

The main limitation of the use of iron oxide is its incorporation into the soil profile. The preparation of a mixture of sieved soil and iron oxide, the subsequent dry-wet cycles and the incorporation of the mixture into the soil profile is a key point to improving the use of magnetite as a tracer and extend its use in soils which cannot be disturbed. New application methods of the tracers would also facilitate their use at larger scales.

To obtain a reliable estimation of soil losses and soil movement after rainfall events or mechanical soil management, it is essential to consider some key factors in the use of these oxides such as: the preferential bound/binding to finer soil particles, the higher concentration of tracers at tagged soil surface or the bulk density effect at the samplings for magnetic susceptibility measurements. It is also important to note that, depending on the iron oxide concentrations, the sample analysis presents some greater interference as the magnetite content increases. When the goethite concentration is relatively high in comparison to the hematite concentration, hematite measurements is overestimated by 0.05 % (Chapter 3).

The accuracy of the iron oxide as an erosion rate estimator was demonstrated through the rainfall simulation test at a small scale (Chapter 2), and under natural rainfall at a hillslope scale (Chapter 4) with an accuracy of within 0.5-0.7 $kg \cdot m^{-2,}$ respectively. This accuracy did not differ significantly despite the different natures of the experiment conditions, which indicated the consistence of the iron oxides as suitable sediment tracers.

One desirable property of sediment tracers is the possibility of their combination with other tracers and techniques in order to identify the different sources of sediments. Combining iron oxides and the erosion model allowed the evaluation of the conventionally tilled bed planting system, providing helpful information about the sediment dynamics and erosion processes for these particular conditions (Chapter 3).

In Chapter 3, the additional use of a simple soil erosion model was a useful tool for the reproduction and understanding of the observed erosion processes accepting its limitations. It provided complementary information to understand sediment dynamics in the system and simulate different scenarios.

As magnetic iron oxide offers the possibility of non-destructive measurements of magnetic susceptibility, the mapping of the soil surface allowed the identification of detachment and deposition areas and their matching with absolute values obtained via the tracer mass balance.

In Chapter 4 total soil losses of the studied plots were estimated differentiating between inter-tree rows, rills and tree rows. Although the erosion rate of tree rows was lower than that determined for the inter-tree rows, these areas contribute significantly to total soil losses because of the large covered area in the plots. Despite the small area of the rills inside the plots, they contributed significantly to total soil losses. Through the representation of relative magnetite content maps of the plots' soil surface, it would be possible to detect soil movement after large rainfall events and its redistribution after soil tillage.

The proposed technique would be especially suitable for evaluating relatively large soil losses or, in combination with soil loss measurements, for identifying the relative weight of different erosion losses by splash and overland flow and under different crops and soil managements (Chapters 3 and 4).

5.2. Conclusions

- Sediment tracers are useful tools as a complement to traditional soil erosion measurements. Despite all the existing tracers already established, new substances are being developed because none of the established approaches fulfils all the requirements for being an ideal sediment tracer.

- The potential of magnetic iron oxide as a new sediment tracer was validated through water erosion experiments under controlled conditions at a laboratory scale. For a reliable estimation of soil losses, results must be interpreted considering the preferential bound of the iron oxides for finer soil particle sizes.

- The combined use of iron oxides (magnetite, hematite and goethite) offered essential information about water and sediment movement in a conventionally tilled bed planting system under different crop and traffic conditions in simulated rainfall events. The use of an erosion model was a complementary approach to understand and extrapolate the experimental data on soil erosion in different scenarios.

- Laboratory and field magnetic susceptibility measurements were set up successfully. Variations in magnetic iron oxide, allowed the estimation of soil losses under natural rainfall events short-term and soil redistribution after tillage, differentiating between zones in olive orchard plots. For reliable results, magnetic iron oxide must be calculated considering the bulk density effect on magnetic susceptibility measurements.